SISSA **ISAS**

SCUOLA INTERNAZIONALE SUPERIORI DI STUDI AVANZATI
INTERNATIONAL SCHOOL FOR ADVANCED STUDIES

Progenitors for long and short gamma-ray bursts

Thesis submitted for the degree of
Doctor Philosophiæ

CANDIDATE:
Daniele Malesani

SUPERVISORS:
Prof. Guido Chincarini
Prof. Annalisa Celotti

October 2006

To myself

Contents

Acknowledgemnts

When I read acknowledgments in a thesis, and find such sentences as "I would like to thank my parents, my tutors, my friends, my colleagues...", I have always thought this is just a formal text. Well. That's not true. I really feel the need to thank many persons, which have supported me during the years of the Phd — not always easy times.

First, I have to thank Lucia. Without her, I would have likely quit my PhD program long ago. She probably doesn't know, but her support has been an effective guide for me. Life has been a lot brighter when she was around.

Second. Many people. Annalisa, my supervisor in Trieste. I think she learnt the meaning of the word "patience" by dealing with me, and really supported me beyond reason. Professor Chincarini deserves an equal mention, both for hosting me at the Osservatorio Astronomico di Merate, where I actually spent a large part of my PhD time, and for always trusting and encouraging me. Many colleagues - now become friends - helped me to work. Among many, I can't forget Massimo, Gianpiero, and Stefano, albeit they always want to beat me (probably that's why I can't forget them). Thanks to them, I had many opportunities to write papers, attend conferences, and deal with new and hot issues in the field. Last, I would also like to thank the referees of my thesis, Johan Fynbo and Luigi Piro, which read it and helped me improving it a lot.

I don't want to let my parents in second place. They always helped me when needed, and always gave me the freedom to do what I liked more (an important point for a clueless researcher). This has always been so, and has gone on also now that I am leaving Italy for a while.

Now the friends. My life has been split between two places, Trieste and Merate. In both I could find valuable people tolerating me, and with them I spent good time. A special thought goes to Fab(b)io, Viviana, Francesca,

Bruno, Mattia, Fabio, Joaquín. They made me feel at home also in Trieste, a city distant from any other place in the World. The list in Merate is even longer, so that I will mention only few: Paolo, Rodolfo, Daniela, Giorgia. Together with many others, I really enjoyed the life in the "foresteria". Usually people either love or hate Merate. I luckily belong to the former class. Last, a special thought goes to my university mates, with whom I spent beautiful times, and in particular to Giovanni, Pietro, Toni, Alessandra.

Many people are missing here, and anyway come to my mind: I have not forgotten them. I hope we will still have chances to be together in the future.

Plan of the thesis

During the course of my PhD thesis, I have been involved in the study of gamma-ray burst (GRB) afterglows, most on the observational side. Gamma-ray burst are powerful explosions occurring in the far Universe, and come together with long-lasting emission, observed from the radio to the X-ray bands (the afterglows). Two kinds of GRBs exist, based upon their duration: long and short.

In this thesis, I have studied several observational aspects of GRBs. The work has been done during very exciting years for the GRB research, subject to fast and intense developement. The confirmation of the association between long GRBs and SNe and the localization of short GRB afterglows have been two of the main results. My thesis could touch both these results.

The first part of the thesis deals with the connection between long-duration GRBs and core-collapse SNe. I will present evidence that the two phenomena are closely associated. After a brief introduction about the gamma-ray burst phenomenon (Chapter 1), I will introduce in Chapter 2 the case of GRB 031203. This burst provides one of the best examples available showing a clear association with a SN, based on both photometric and spectroscopic data. The properties of both the GRB and the SN will be discussed. In particular, I will show that the SN belongs to the class of "hypernovae", a group of very energetic core-collapse SNe.

GRB 031203 was a very peculiar event, distinct from the bulk of GRBs observed to date. In Chapters 4 and 5 I will present two GRBs with "regular" properties. I will show that these bursts, too, have a firm SN association (based upon spectroscopic evidence). Remarkably, the two SNe are not identical: one was a hypernova, while the other was not. Both events show differences with respect to other GRB-associated SNe, implying that some degree of diversity (possibly tied to geometric effects) is present among GRB-associated SNe.

Chapter 6 introduces a recent, enigmatic case: GRB 060614. For this event, very deep limits on an associated SN were set. This unambiguously allows to rule out a hypernova origin for this GRB. GRB 060614 is one of the strongest cases which show the heterogeneity of the GRB/SN population.

The second part of my thesis (Chapter 7) deals with short-duration gamma-ray bursts. These objects do not explode in SN events, and their origin is still subject of debate. I will present observation of the first optical afterglow ever discovered for a short GRB, together with the identification and characterization of its host galaxy. I will summarize the available observations on short gamma-ray burst in order to find hints for their progenitors. Present data are consistent with these burst being originated by merging binary systems, but this hypothesis needs still much more testing to be accepted beyond doubt.

Last, Chapter 8 stands alone, presenting X-ray and optical observations of GRB 050326. I will show this is a dark GRB (that is, the ratio of optical to X-ray emission is lower than a critical value). I will discuss the possible reasons for such faintness, namely that the burst was significantly obscured by dust (by more than 5 magnitudes) or that it was at high redshift ($z \gtrsim 5$). The latter hypothesis is favored if we pretend that this burst obeys the Ghirlanda relation.

In Chapter 9, I will try to draw some conclusions about the progenitors of long and short gamma-ray bursts, presenting the status of what we already know and what we still need to understand.

Selected publications

This thesis is largely based upon the following works:

1. Della Valle, M., **Malesani, D.**, Benetti, S., et al. 2003, A&A, 406, L33: *Evidence for supernova signatures in the spectrum of the late-time bump of the optical afterglow of GRB 021211.*

2. **Malesani, D.**, Tagliaferri, G., Chincarini, G., et al. 2004, ApJ, 609, L5: *SN 2003lw and GRB 031203: a bright supernova for a faint gamma-ray burst.*

3. Della Valle, M., **Malesani, D.**, Bloom, J. S., et al. 2006, ApJ, 642, L103: *Hypernova signatures in the late rebrightening of GRB 050525A.*

4. Covino, S., **Malesani, D.**, Israel, G. L., et al. 2006, A&A, 447, L5: *Optical emission from GRB 050709: a short/hard GRB in a star forming galaxy.*

5. Mazzali, P. A., Deng, J., Pian, E., **Malesani, D.**, et al. 2006, ApJ, 645, 1323: *Models for the type-Ic hypernova SN 2003lw associated with GRB 031203.*

6. Moretti, A., De Luca, A., **Malesani, D.**, et al. 2006, A&A, 451, 777: *Swift and XMM-Newton observations of the dark GRB 050326.*

7. Amati, L., Della Valle, M., Frontera, F., **Malesani, D.**, Guidorzi, C., Montanari, E., & Pian, E. 2006, A&A, submitted: *Implications of the consistency of GRB 060218/SN 2006aj with the $E_{\rm p}$ – $E_{\rm iso}$ correlation.*

8. Della Valle, M., Chincarini, G., Panagia, N., Tagliaferri, G., **Malesani, D.**, et al. 2006, Nature, submitted: *GRB 060614: an enigmatic long-duration gamma-ray burst not due to a hypernova.*

Chapter 1

Gamma-ray bursts: a review

1.1 Observational properties

Gamma-ray bursts (GRBs) were discovered in the late Sixties (Klebesadel et al. 1973) by military satellites devoted to detecting nuclear explosions in the space. They are brief, intense flashes of soft gamma radiation, coming from random directions in the space. In the course of the years, several space-born missions have studied these enigmatic objects, among which GINGA, *Beppo*SAX, HETE-II and INTEGRAL. The most comprehensive sample was collected by the BATSE instrument onboard the Compton Gamma-Ray Observatory (e.g. Fishman & Meegan 1995), including more than 3000 events. Currently, most of the space observations are carried out by the *Swift* observatory, a spacecraft entirely devoted to GRB science. In addition to the gamma-ray detector, *Swift* carries two narrow-field instruments to observe at optical and X-ray wavelengths. At least from an operational point of view, there are two main phases of the gamma-ray burst phenomenon: the prompt emission (occurring at gamma-ray energies, and lasting at most few minutes), and the afterglow (a long-lasting, multiwavelength emission which follows the main GRB). Last, a supernova (SN) is often seen to dominate the optical emission at late epocs (10–20 days), at least in the class of long-duration GRBs.

1.1.1 Prompt emission

GRB emission lasts betwen tenths and tens of seconds (for a general review on the prompt emission properties, see Fishman & Meegan 1995). GRBs

show very different temporal structures. Some have smooth, broad profiles, while others have large variability on timescales much shorter than the overall duration (Fig. 1.1, left). Some have a weak precursor followed by a quiescent period. In constrast to the comples temporal behaviour, GRB spectra are relatively simple. In the vast majority of cases, they are well described by a broken power law (Band et al. 1993). Thus, they are characterized by three fundamental parameters: the peak energy (at which most of the energy is radiatied), and the two power-law slopes, at low at high energy. Typically, the peak energy is located in the soft gamma-ray/hard X-ray interval 100–1000 keV (e.g. Preece et al. 2000). High-energy emission (in the MeV-GeV range) has been reported for a few cases (e.g. Hurley et al. 1995; Gonzalez et al. 2003). Recently, mostly thanks to the *Beppo*SAX and HETE-II satellites, a class of softer events peaking at lower energy (2–50 keV) has been discovered, consisting of the so-called X-ray rich GRBs and X-ray flashes (XRFs; Heise et al. 2003; Lamb et al. 2004; Sakamoto et al. 2004). The present evidence indicates that XRFs are likely a low-energy extensions of classical GRBs (Sakamoto et al. 2005). In fact, apart from the lower peak energy, the both classes have similar spectra and temporal profiles. Moreover, they all lie on the $E_{\rm peak}$ vs $E_{\rm iso}$ relation (Amati et al. 2002). Burst spectra show significant temporal evolution. The general trend is from hard to soft, but in case of multi-peaked events the patterns are more complicate (Ford et al. 1995). Both the peak energy and the spectral slopes change during the burst (Ghirlanda et al. 2002). GRB pulses at low energy usually lag behind the emission at higher frequency.

An important classification can be made for GRBs, mostly based on their temporal properties. The distribution of burst durations, as measured by the BATSE instrument, is clearly bimodal, with a gap at about 2 s (Kouveliotou et al. 1993). The two classes are called, respectively, short and long GRBs. As observed by BATSE, the short events comprise $\sim 1/4$ of the total. *Swift* looks less sensitive to short GRBs, due to the different spectral response, and only $\sim 1/10$ of events are short. In the BATSE sample, such bimodality is confirmed by spectral properties: shorter bursts are the average harder (Fig. 1.1, right). However, it is not clear whether the spectral classification is real or caused by an instrumental bias. Another distinct feature of short bursts is that they have negligible (sometimes negative) spectral lags (Norris et al. 2001).

The main problem in the study of gamma-ray bursts has always been the lack of precise localization due to the poor spatial resolution of gamma-ray

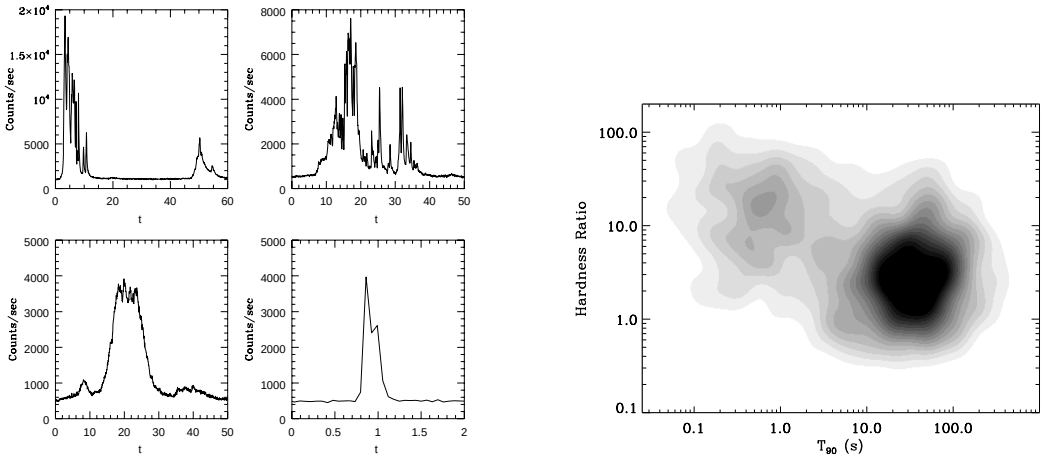

Figure 1.1: Left: examples of gamma-ray light curves, as observed by BATSE. Note the different morphologies: some profiles are smooth, other are spiky (light curves taken from the BATSE web site). Variability can be present on timescales much shorter than the bursrt duration. Some quiescent intervals are also apparent. Right: distribution of BATSE bursts in the plane duration versus hardness ratio. T_90 is the time within which 90% of the photons are collected. Short and long bursts are distinguished both spectrally and temporally. Figure adapted from Lazzati et al. (2001).

detectors. Only in the last decade have instruments become sensitive enough to provide accurate positions to GRBs, allowing meaningful searches at long wavelengths. The breakthrough in the GRB research happened about a decade ago, with the discovery of long-lasting X-ray, radio, and optical counterparts (afterglows) to long-duration GRBs (Costa et al. 1997; van Paradijs et al. 1997; Frail et al. 1997). Afterglows for short GRBs were discovered only in the past year (e.g. Gehrels et al. 2005; Fox et al. 2005b; Covino et al. 2006; Hjorth et al. 2005a) so that our understanding of these events is comparably smaller. I defer a full discussion of short GRBs and their afterglows to chapter 5.

1.1.2 Afterglows

The first X-ray and optical counterpart of a long-duration GRB was discovered in 1997, thanks to the *Beppo*SAX satellite. In the following years, several afterglows could be discovered and studied (now more than 100 are

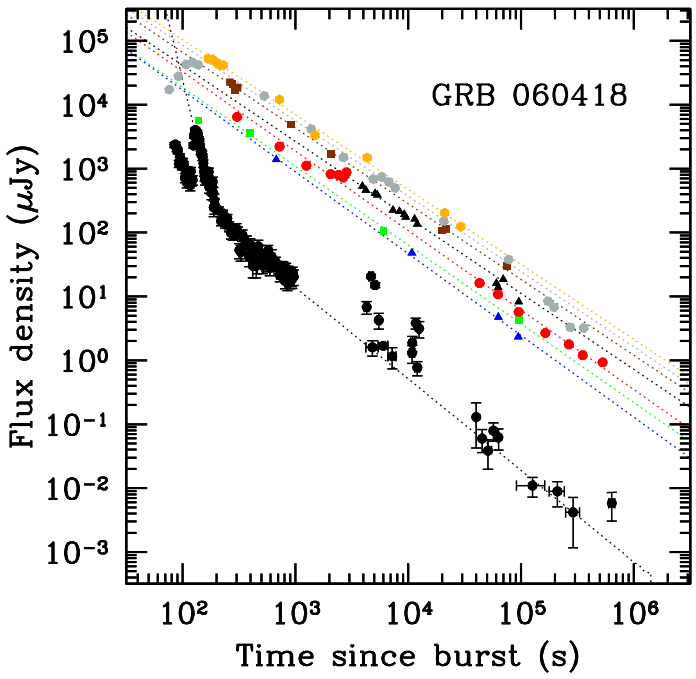

Figure 1.2: X-ray (circles) and optical (other symbols) light curves of the afterglow of GRB 060418. Several flares are apparent at X-ray wavelengths. In the optical the early rise is likely due to the beginning of the afterglow.

known; see van Paradijs et al. 2000 for an observational review). Afterglows show emission over a very broad spectral range, from radio to X-rays. They can be studied on very different timescales, from few seconds after the burst up to a year or more. Overall, their flux shows a steady decay with a power-law time dependance. One or more breaks are usually observed in the well studied cases, where the decay rate changes. In addition, there are examples of irregular light curves, where superimposed on the general decay there is short-term variability, and in some bumps and rebrightenings emerge. This has been demonstrated both in the X-ray (where powerful flares are often present in the early-time decay; e.g. Piro et al. 2005; Burrows et al. 2005b; see Fig. 1.2) and optical (where variability is usually less pronounced; e.g. Galama et al. 1998a; Lipkin et al. 2004) ranges. The early-time afterglow (the first hour after the GRB) has indeed displayed a rich variety of physical processes. The X-ray Telescope (XRT) onboard *Swift* has recently provided

a large sample of X-ray light curves, showing the emergence of a "canonical" behaviour (Chincarini et al. 2005; Nousek et al. 2006). In the first $\sim$ 100–500 s, there is a phase of steep decay (Tagliaferri et al. 2005a), which subsequently becomes very shallow (sometimes almost constant) to steepen again around $\sim$ 1 000-10 000 s. Flares are often superimposed on this general decay. At optical wavelengths, the light curves are more diversified. In some cases, the early decay simply prosecutes unbroken up to a day or longer (e.g. Quimby et al. 2005). Sometimes, on the contrary, it is initally flat (or even rising; e.g. Fox et al. 2003a) and subsequently steepens. In a few cases, at early time the emission is dominated by the so-called optical flash (Akerlof et al. 1999), a rapid-decaying component which rapidly fades. Last, in some cases the optical emission appears somehow correlated with the prompt one, and shows irregular variability (Blake et al. 2005; Vestrand et al. 2005). Radio light curves are initially rising (the radio spectrum is heavily self-absorbed), and peak a few days after the GRB. Radio emission is the most powerful at late times, and can be observed for a very long time (e.g. Frail et al. 2000). At early times, when the source is small, flickering in the radio data is often apparent, due to interstellar scintillation.

Afterglow spectra are usually composed by a set of power-law segments, separated by several break frequencies. Such frequencies shift in time, and may cross the observed bands (although no conclusive evidence for this has been ever presented). Almost all GRBs were detected at X-ray energies (De Pasquale et al. 2005; O'Brien et al. 2006). Searches in the optical have been more tricky, leading to a varying percentage of dark GRBs (as large as $\sim$ 50%; e.g. Fynbo et al. 2001; Lazzati et al. 2002; Berger et al. 2002). While instrumental and observational effects are clearly involved in the determination of such fraction, the recent large number of dark GRBs as observed in the *Swift* era has been a surprise (Roming et al. 2005b). Likely dust extinction coupled with an average large redshift contributes to suppressing the optical flux, albeit intrinsic effects may also play a role (De Pasquale et al. 2003; Roming et al. 2005b).

The optical afterglow light is (slightly) polarized (Covino et al. 1999; Wijers et al. 1999; Greiner et al. 2003). Linear polarization at the level of $\sim$ a few percent has been detected in several cases, showing variability in both its intensity and position angle (Barth et al. 2003; Lazzati et al. 2004). This indicates that some asymmetry must be present in the emitting region.

1.2 GRBs as cosmological objects

The discovery of optical counterparts, further to bringing new elements in the GRB picture, have also allowed two major advances. First, the accurate position which can be achieved at these frequencies has allowed to individuate that GRBs are hosted inside galaxies (e.g Sahu et al. 1997). Second, and perhaps even more important, optical spectra have allowed to measure redshifts for these objects (e.g. Metzger et al. 1997). This has finally settled the issue about the distance of GRBs. It turns out that GRBs are truly cosmological events, with an average redshift of $\langle z \rangle = 1.8$ (Fig. 1.3). The *Swift* sample has an even larger median value ($\langle z \rangle = 2.8$; Jakobsson et al. 2006). The current record-holder is GRB 050904 at $z = 6.295$ (Kawai et al. 2006; Tagliaferri et al. 2005b; Haislip et al. 2006), and there are several examples at $z = 4$–5. There is also a low-redshift tail ($z \lesssim 0.1$), still comprising very few, peculiar objects. These bursts are quite faint, and they would easily escape detection at larger distances. Actually, they may easily outnumber the more powerful, rarer GRBs harboring at higher redshift (Guetta et al. 2004; Liang et al. 2006; Della Valle 2006a). Current estimates of the GRB rates amount to ~ 1 event Gpc^{-3} yr^{-1} (e.g. Schmidt 1999), but they depend critically on the degree of collimation presented by GRBs.

The determination of GRB distances has allowed to set the energy scale of these events. The observed gamma-ray energies range from 10^{48} to more than 10^{54} erg. However, this emission is not isotropic, and the beaming-corrected estimates are lower, of the order of 10^{50} erg (Frail et al. 2001). Such large values, further to constraining GRB models, make them very powerful probes of the far Universe. Their high power can easily outshine other astronomical objects, including AGN (Watson et al. 2006b). Spectra of afterglows carry important information on the gas and dust composition at high redshift (Fig. 1.4). Gamma rays are also little affected by dust extinction, so their detection may be able to probe obscured ennvironments as well. If GRBs are associated to the death of massive stars, as seems to be the case (see below), they represent a powerful tracer of the cosmic star formation history up to the far Universe. Last, several methods have been proposed to adopt GRBs to measure the geometry of the Universe (see Ghirlanda et al. 2006 for a review).

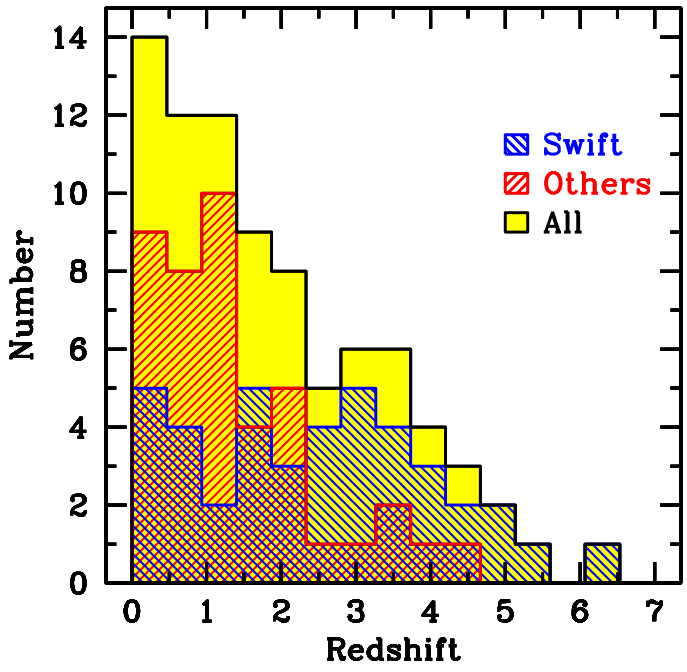

Figure 1.3: Redshift distribution of GRBs, putting in evidence the *Swift* sample (redshifts were taken from the Jochen Greiner GRB web page).

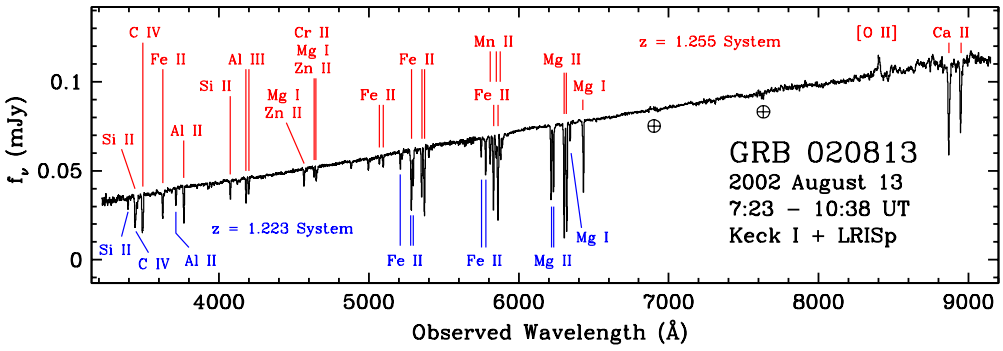

Figure 1.4: Optical spectrum of GRB 020813, taken with the Keck telescope (Barth et al. 2003). Several absorption features are apparent, grouped at two different redshifts. The larger on is the burst redshift (as confirmed by the O II line in emission from the host galaxy). The brightness of afterglows has allowed acquiring spectra with large signal-to-noise ratio.

1.3 Theoretical models

The observational material presented in the above sections allows to draw some inferences to explain the GRB phenomonon. In the years, this has led to a sort of "standard" model, which provides a framework capable to explain most of the observed features. In particular, it accounts for both the prompt and afterglow emission (the latter being actually a *prediction*; Mészáros & Rees 1997). It should be said, however, that several issues are far from settled. For excellent reviews, see Piran (1999), Zhang & Mészáros (2004), and Mészáros (2006).

The observed energies, coupled with the short variability timescales and the nonthermal spectra, provide the main ingredient. Causal arguments imply that the GRB emission region needs to be small ($R \lesssim \delta t/c$), and the large resulting photon densities would imply an optical depth to pair production exceedingly large ($\tau \sim 10^{13}$; Piran & Shemi 1993). In such context, the energy would be released as a thermal spectrum, with an unreasonably low efficiency. The solution to this riddle is to invoke relativistic motion. If the explosion region is expanding relativistically (with Lorentz factor $\Gamma \gg 1$), several effects come into play, and the optical depth in the comoving frame is significantly reduced (by a factor $\sim \Gamma^4$; Lithwick & Sari 2001). Assuming $\Gamma \gtrsim 100$, a low optical depth can achieved. Such relativistic motion is basic to any model of gamma-ray bursts. Remarkably, direct observations have confirmed relativistic motion by observing superluminal expansion in GRB 970508 (Frail et al. 1997) and GRB 030329 (Taylor et al. 2004).

The standard solution to escape the compactness problem leads to the so-called fireball model. A large amount of energy (in the form of a photon/pair relativistic plasma) is "polluted" with a small quantity of baryons. The plasma expands relativistically, but, due to the high optical depth, it is very radiatively inefficient. As the expansion goes on, the internal energy is gradually transferred to protons, in the form of bulk kinetic energy. The energy can be thus transported out to large radii, where the opacity is low enough so that nonthermal spectra can be radiated. However, there is the need to re-convert the bulk into internal energy. This can be achieved through the generation of shocks. Two kinds of shocks can be envisaged:

- external shocks (Mészáros & Rees 1993): the whole fireball may interact with some surronding material, and decelerate against it;
- internal shocks (Rees & Mészáros 1994): different portions of the fluid

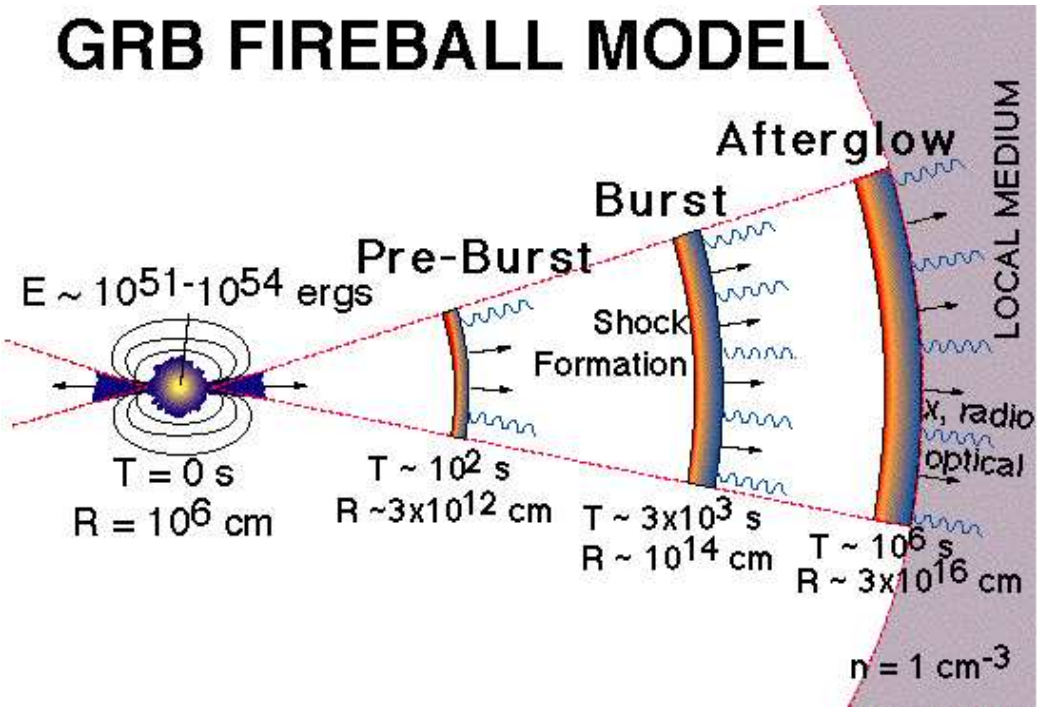

Figure 1.5: Cartoon representing the different phases of the GRB standard model, from the fireball generation to the external shock dissipation.

with slightly different velocity can collide between themselves.

External shocks are expected to provide smooth temporal profiles, contrary to what observed in several examples (Fig. 1.1, left). External shocks may be a viable solution if the central engine expels several shells of matter (multiple fireballs). However, each shell is expected to interact with the external medium at a progressively later time. A widening of the pulses over the course of the burst is thus expected. This behaviour has not been observed (Fenimore et al. 1999a). Internal shocks are currently the preferred solution, since interaction between several shells may occur always at the same radius. If the initial separation between shells is Δ, the interaction radius is of the order of $\sim \Gamma^2\Delta$. For large enough Γ, at the interaction radius the optical depth is low and radiation can escape. This leads to a constraint $\Gamma \gtrsim 100$, in accordance with the value derived from the compactness argument. In the internal shock scenario, the burst duration corresponds to the lifetime of the central engine. It is not clear by means of which mechanism the internal

energy is radiated. One promising candidate is synchrotron emission, which however suffers some problems (namely, the fast electron cooling, which is required to yield high radiative efficiency, would imply spectra softer than observed; Ghisellini et al. 2000). Other possibilities have been outlined (e.g Liang 1997; Medvedev 2000; Pe'er et al. 2006), but there is no general consensus on this issue.

Alternative mechanisms have been proposed to power the gamma-ray emission. Much attention has been attracted from magnetically-dominated models (see Lyutikov et al. 2006 for a review). Such models envisage a dynamical role for the magnetic field, which is supposed to carry a significant fraction of the energy. Energy may be dissipated through reconnection processes. These models avoid the need to transform the internal energy into bulk energy and then going back. A large magnetization might also explain the lack of an optical flash, which is expected to be ubiquitous in the fireball model (Zhang & Kobayashi 2005). However, it is not clear if such large magnetic field exist and, above all, if they can be transported out to large radii. The ultimate test for the two models may be to observe (or not observe) polarization in the early stages of the afterglows, since in magnetic models a large, ordered magnetic field is expected, which should give rise to highly polarized synchrotron radiation (Lazzati et al. 2004).

In both scenarios, after the prompt emission, the fireball still carries a significant fraction of its initial energy. At a critical radius (which depends on both the fireball and circumburst medium properties), it starts decelerating due to the interaction with the surrounding material. Further kinetic energy is dissipated into internal energy, and, possibly, radiation. This emission (actually coming from an external shock) is believed to power the afterglow (Mészáros & Rees 1997). Impacting against the external medium, a shock is also expected to heat the fireball, leading to a fast-decaying component (reverse shock) which can power the optical flash. A relatively simple theory predicts light curves and spectra with properties consistent with the observed ones (Sari et al. 1998; Panaitescu & Kumar 2000). During the afterglow phase, synchrotron radiation is widely believed to be the main emission mechanism. Significant Compton emission can be also radiated (Sari & Esin 2001), but it should lie above the usually observed spectral windows (though see e.g. Harrison et al. 2001; Corsi & Piro 2006). By modeling the afterglow spectra and light curves, the basic explosion parameters can be determined. The fireball (isotropic equivalent) energy is found to be of the order of 10^{51}–10^{54} erg, and the fraction of the energy carried but the relativistic electrons

and the magnetic field is larger than the simplest expectations (of the order of 0.1–10%). Last, the surrounding medium is usually modelled with a uniform radial profile, and particle density of the order 0.1–10 cm^{-3} (e.g. Panaitescu & Kumar 2001a; Yost et al. 2003).

The steep light curves displayed by several afterglows at late times (mostly in the optical and radio bands) have been explained as due to a jetted outflow (Rhoads 1999; Sari et al. 1999). At early time, due to the relativistic aberration, only a small fraction of the shell surface (of the order of $1/\Gamma^2$) is visible to the observer. This means that there is no difference between a jetted or spherical configuration, as long as Γ is large enough. When it drops below the critical value $\sim 1/\vartheta$ (where ϑ is the jet opening angle), the aspherical geometry can be seen, and this results in a steeper decay. The break time allows estimating ϑ. A jetted emission also helps alleviating the large energy requirements inferred assuming spherical geometry. For example, the isotropic-equivalent energy released by GRB 990123 was 2.5×10^{54} erg, equivalent to $\sim$ one solar mass converted into radiation, a requirment hard to satisfy in any model. After beaming correction, the observed energies are lower, of the order of $\sim 10^{51}$ erg, just a fraction of the kinetic energy of a supernova explosion. Remarkably, the beaming-corrected energies show a lower scatter than the isotropic values (Frail et al. 2001). Moreover, a very tight correlation has been found between the gamma-ray energies (after beaming correction) and the peak frequency of the GRB prompt spectrum (Ghirlanda et al. 2004). This lends some credibility both on the afterglow model (used to infer the opening angle) and to the jet hypotesis. It should be said, however, that very few *Swift* bursts have shown a convincing jet signature (Panaitescu et al. 2006a), so that the whole issue will require further investigation.

1.4 Progenitors

The fireball model, outlined above provides a very general scenario for explaining the GRB phenomenon. This is possible since the outcome is largely independent of the initial conditions. Simply releasing a large amount of energy in a small volume leads to the fireball formation, which evolution does not keep track of the details of the initial explosion. While this implies that the model can be applied under wide ranges of conditions (for example, it works for both short and long GRBs), the physical engine which triggers

the explosion remains unveiled, and difficult to constrain. There are several constraints which which such engine must satistfy.

- Compactness: the small scales implied by the rapid variability of many (but not all) GRB light curves require small emission radii. Radii lower than $\sim 10\,000$ km are implied.
- Energetics: GRBs can release large amounts of energy. Taken into account the nonspherical geometry, current estimations indicate up to $\sim 3 \times 10^{51}$ erg in electromagnetic form.
- Relativistic motion: with such large luminosities, relativistic motion is unavoidable to cope with the compactness problem. Any GRB progenitor model must be capable to launch matter close to the speed of light.
- Rate: the number of GRBs is very small, just a small fraction of that of SNe. Thus, very special conditions are needed to give rise to a GRB.
- Environments: the host galaxies of long and short GRBs suggest an association with young stars for the former, and with populations of diverse age for the latter.

Such constraints lead to the need for a central engine tied to a compact object, most likely a stellar-mass black hole or a neutron star. Typical examples are collapsing cores of massive stars (Woosley 1993; Paczyński 1998), collapsing neutron stars (Usov et al. 1992; Vietri & Stella 1998), and binary compact object systems undergoing merger (Eichler et al. 1989; Belczyński et al. 2002).

In the years, evidence has been accumulating that most long-duration GRBs are tied to the death of massive stars. The origin of short events is more uncertain, albeit there is growing, indirect evidence indicating that they may originate in binary compact objects merging systems. I now briefly describe the basics of the association between long-duration GRBs and core-collapse SNe, while short bursts will be treated later.

The first line of evidence pointing towards a connection between long-duration GRBs and star formation comes from the study of their host galaxies and environments. GRB hosts show distinct traces of active star formation. Their colors are bluer than average (Le Floc'h et al. 2003), indicating the

presence of hot, massive stars. They show prominent nebular emission lines (Djorgovski et al. 1998; Prochaska et al. 2004). They show, on the average, very large equivalent Lyα widths (Fynbo et al. 2003). Spectral modeling indicates large specific star formation rates (Christensen et al. 2004). However, present data also indicate significant differences with other star-forming systems. Notably, GRB host galaxis have on the average only weak submm and infrared emission (Tanvir et al. 2004; Le Floc'h et al. 2006), though there are possibly exceptions (Berger et al. 2003a). They usually have low metallicities (e.g. Stanek et al. 2006; Fruchter et al. 2006), and possibly low dust content. It is not yet fully clear whether such difference is due to some observational bias, or is a consequence of some fundemental requirement for GRB progenitors. For example, up to now most information comes from optically-bright GRBs (i.e. GRBs which had an optical afterglow), while little is known about optically-dark events (which may be preferentially hosted by dusty and more metallic systems). On the other hand, if GRBs are produced by exploding, massive stars, low metallicity is required to launch the relativistic jets (see below; MacFadyen & Woosley 1999).

Further clues for an association between GRBs and star formation come from the spatial offset distribution of bursts with respect to their host galaxy centers. Such distribution is similar to that of the ultraviolet light, again indicative of an association with young stars (Bloom et al. 2002a). On a completely different side, absorption line studies of afterglow spectra have revealed ions in unusual excited states (such as Si II*, C II*, and Fe II*), which require the presence of an intense radiation field and/or very large gas densities (Berger et al. 2006; Prochaska et al. 2006). A puzzling point concerns the lack of clear wind signatures in the density profile of the surrounding medium as inferred from afterglow modeling (see e.g. Ramirez-Ruiz et al. 2005a; Eldridge et al. 2006).

All the evidence presented above strongly argue for an association between long-duration GRBs and star formation. This allows selecting some promising progenitor candidates. Core-collapse supernovae (SNe), magnetars, and collapsing neutron stars are in principle suitable candidates. Also a fraction of binary compact object systems may undergo merging in relatively short times. However, observations now strongly favor a direct association between core-collapse SNe and GRBs.

1.5 Long GRBs and core-collapse supernovae

A GRB/SN association has been theoretically explored for years (even before the actual discovery of GRBs; Colgate et al. 1968). Woosley (1993) proposed that a collapsing star might launch, under certain circumstances, relativistic jets capable to power a gamma-ray burst. The current version of the collapsar model (MacFadyen & Woosley 1999) predicts that a massive star ($\sim$ 20–40 $M_{\odot}$) endowed with fast enough rotation could form an accretion disk encircling the new-born black hole. Such accretion would power the jet emission, in a way similar to AGN or Galactic X-ray binaries. The necessary conditions for the production of a GRB are three. First, the star needs to form a black hole after collapse, so that a large star mass is required. Second, the star needs to have lost its external hydrogen envelope, otherwise the jets would not be able to erupt out of the star surface. Thus, a Wolf-Rayet star is implied as progenitor, and a type-Ic (or -Ib) SN is expected to accompany the burst. Last, the stellar core needs to be fast rotating, otherwise the matter would not form an accretion disk, but directly infall onto the black hole. Satisfying these two requirements simultaneously is not simple, since the mass loss needed to remove the external envelope is expected to carry also a significant amount of angular momentum, leading to a slow-rotating core. To solve this problem, binarity has been often invoked (Fryer & Heger 2005; Petrovic et al. 2005). Recently a solution has been proposed using single, fast-rotating stars (Yoon & Langer 2005; Woosley & Heger 2006). The formation of an extended, slowly rotating envelope can be avoided if complete chemical mixing is achieved. In this case, mass is expelled with smaller angular momentum loss. However, in any case, large metallicites are strongly disfavored, since they imply a higher mass (and angular momentum) loss.

The first, indirect evidence for a GRB/SN connection was relatively weak. Cross-correlation between closeby SNe and GRBs from the BATSE catalog led to some dubious associations (e.g. Wang & Wheeler 1998; Woosley et al. 1998; Germany et al. 2000; Rigon et al. 2003). The major problem was the large size of BATSE error boxes (a few degrees). Recently Bosnjak et al. (2006) have discovered a set of correlated SN/GRB pairs. Interestingly enough, among these events there is a number of type-Ic SNe larger than expected from a random distribution, lending some credibility to the associations, at least in a statistical approach. There are further suggestions indicating a massive star origin. For example, X-ray spectra of several GRB afterglows showed features in emission, often due to Fe (Antonelli et al. 2000;

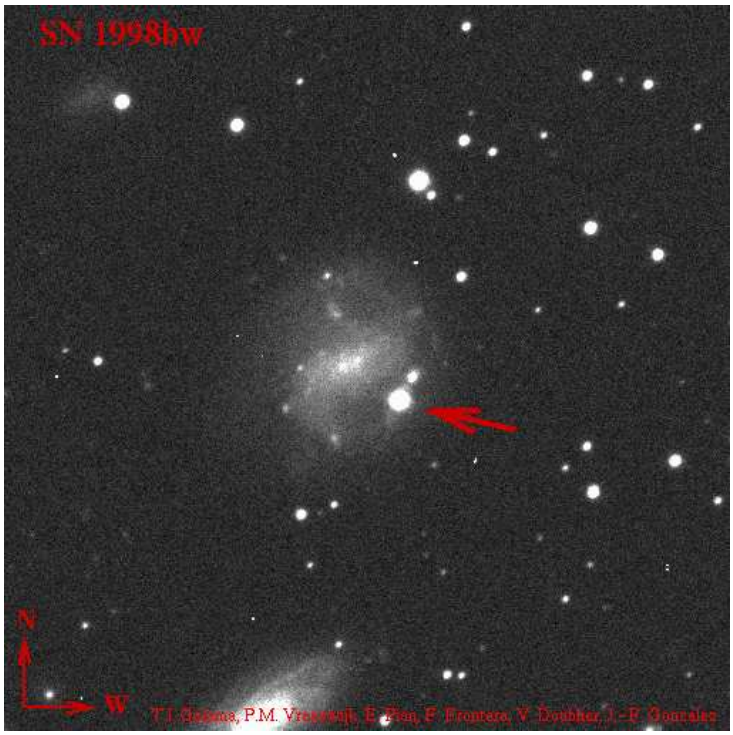

Figure 1.6: The beautiful host galaxy of GRB 980425. The arrows pinpoints the emission from the associated SN 1998bw.

Piro et al. 2000, e.g.). To explain such features, a large amount of Fe is required (of the order of $\sim$ 0.1–1 $M_\odot$; Vietri et al. 2001), as produced in SN explosions. However, it should be said that no such line has ever been observed by *Swift*. Optical spectra also provide hints for a SN origin. At high resolution, absorption lines are sometimes observed to be split in several components, separated by a few thousands km s^{-1}. The most simple solution is that they are due to absorbing clumps in a high-velocity wind such that of a Wolf-Rayet star (e.g. Schaefer et al. 2003; Fiore et al. 2005).

In 1998, *Beppo*SAX discovered GRB 980425 (Pian et al. 2000). Inside the error circle (much smaller than the BATSE ones), a very peculiar supernova was discovered, SN 1998bw (Galama et al. 1998b), at redshift $z = 0.0085$ (Fig. 1.6). The a-posteriori chance association probability was quite low ($\sim 10^{-4}$). This SN was a peculiar event, belonging to the class of type-Ic SNe (possibly becoming more similar to a type-Ib at late phases; Patat et al. 2001). First, it was exceptionally bright, with a peak magnitude

$M_V = -19.1$. Second, the spectra showed very broad features, initially difficult to interpret, and later explained as due to very large outflow velocities (of the order of 30 000 km s^{-1}). Modeling the SN properties, a large kinetic energy was inferred (larger than 10^{52} erg; Iwamoto et al. 1998). Nebular spectra showed indication for asymmetries in the explosion (Maeda et al. 2002). Radio observations showed this SN to be exceptionally bright also at these frequencies, and required the presence of ejecta accelerated at mildly relativistic velocities (Kulkarni et al. 1998). This event was termed a "hypernova". At such low redshift, however, if the GRB was physically associated with the SN, also the GRB properties were quite strange. First, the burst energy was significantly smaller ($\sim 10^{48}$ erg) than that observed in the other cases. Second, it lacked an optical afterglow (or at least, it was significantly fainter than usual). The X-ray afterglow was also peculiar, since it had a very slow decay (slope $\alpha = 0.2$; Pian et al. 2000; Kouveliotou et al. 2004), much different from usual cases (which have $\alpha \sim 1$). This event, thus, was looking as a very peculiar SN, accompained by mildly relativistic ejecta capable to power faint prompt, radio, and X-ray emission. While it showed that core-collapse SNe may power GRBs, it was not clear whether such association was valid also for cosmological, powerful events.

In the following years, it was noted that some afterglow light curves showed a flattening, or even a rebrightening, at about 15–30 days after the GRB (e.g. Bloom et al. 1999, 2002b; Reichart 1999; Stanek et al. 2005). Zeh et al. (2004) have recently performed a fit to a sample of afterglows with $z < 1$, finding a bump in all the events with a light curve sampled well enough. Such bumps could be due, in principle, to the emergence of a SN, akin to SN 1998bw. Since SN light curves peak at about that epoch, they might outshine the afterglow which had declined significantly by that time. Different alternatives, such as dust echos (Esin & Blandford 2000), were in principle possible, even if colors were not indicative of this possibility (such bumps are quite red, while blue light is preferentially scattered). However, the only way to confirm the nature of such events was to undertake a spectroscopic analysis of the bumps (Della Valle et al. 2006b).

The breakthrough event was GRB 030329, a classical, long-duration GRB at low redshift ($z = 0.1685$). The proximity of this case allowed a very detailed photometric and spectroscopic study of the aftergow light curve, leading to the spectacular discovery of a SN very similar to SN 1998bw (Hjorth et al. 2003; Stanek et al. 2003; Kawabata et al. 2003), which was named SN 2003dh (Fig. 1.7). Like SN 1998bw, SN 2003dh was a hypernova, with

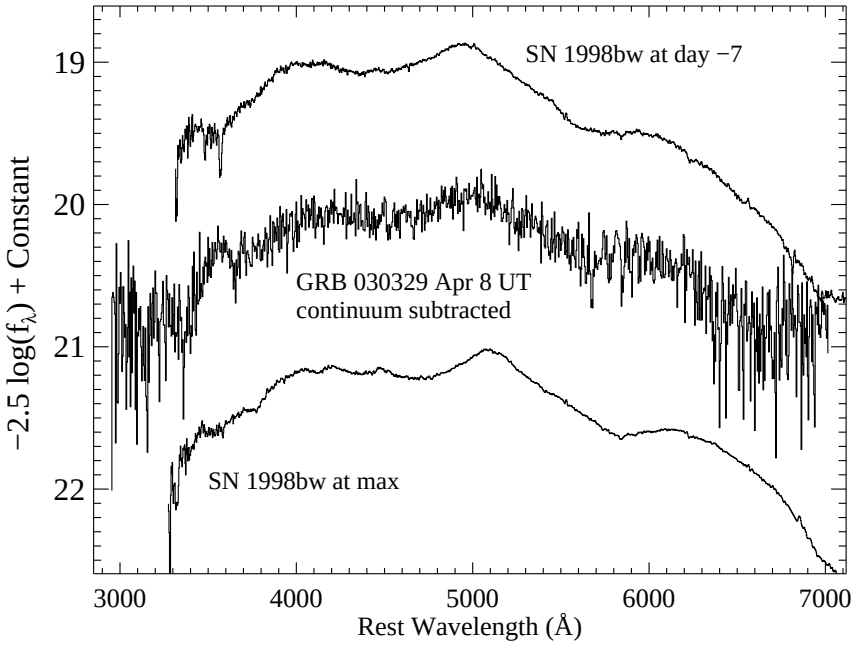

Figure 1.7: Spectrum of the afterglow of GRB 030329 when the SN was already dominating (2003 April 4). The spectrum shows clear resemblance with that of SN 1998bw at a comparable epoch. From Stanek et al. (2003).

a comparable magnitude (to within half a magnitude) and similar kinetic energy. Since the properties of GRB 030329 were overall similar to those of cosmological GRBs (in terms of energetics, existence of a powerful afterglow, and temporal properties) this left little doubt that at least a fraction of long-duration GRBs are produced during the death of massive stars.

In the following years, much effort has been devoted to exploring in detail the SN/GRB connection. Other remarkable examples have been discovered (e.g. GRB 031203/SN 2003lw and GRB 060218/SN 2006aj; Malesani et al. 2004; Pian et al. 2006). The emerging picture looks complex. The best-studied cases show SNe with properties remarkably similar, all being hypernovae with large peak luminosity ($M_V \sim -19$), high expansion velocity, and correspondingly large explosion energy. Other examples showed somehow different properties. For example, Garnavich et al. (2003) showed that the SN associated with GRB 011121 was bluer than SN 1998bw (possibly

resembling a type-IIn SN). HST observations showed that any SN associated with XRF 040701 (Soderberg et al. 2005) had to be significantly fainter than SN 1998bw (although the light curve was poorly sampled). Last, very recently, much surprise has arisen due to the discovery of a nearby GRB (GRB 060614), also at low redshift ($z = 0.125$). Photometric monitoring by several groups (Gal-Yam et al. 2006; Fynbo et al. 2006; Della Valle et al. 2006d) has shown no apparent SN down to quite stringent limits. While it is not possible to exclude a SN origin for this object, this case (together with GRB 060505) is currently the best example showing that some diversity must be present among GRB progenitors.

Chapter 2

SN 2003lw and GRB 031203: A Bright Supernova for a Faint Gamma-ray Burst

In late 2003, the status of the SN/GRB connection looked, on one hand, quite simple. Long-duration GRBs could be produced by the death of massive stars, as spectacularly demonstrated by the SN 2003dh/GRB 030329 association. The existence of late-time bumps in several afterglow allowed to speculate that such association was general. However, due to their faintness, the quality of bumps data was not outstanding. Only two associations had been proven beyond doubt (SN 1998bw/GRB 980425 and SN 2003dh/GRB 030329), and studied in detail. Puzzingly, despite the two SNe looked almost identical, the gamma-ray events were significantly different. Further data were needed. I describe here observations of another clear case of SN/GRB associations. This material has been published by Malesani et al. (2004).

GRB 031203 was discovered by the INTEGRAL satellite on 2003 Dec 3.91769 UT (Götz et al. 2003), with a duration of ~ 30 s and a peak flux of 1.3×10^{-7} erg cm^{-2} s^{-1} ($20 - 200$ keV; Mereghetti & Götz 2003a). The precise and fast dissemination of the GRB coordinates (*Swift* had still to fly) by the INTEGRAL burst alert system (Mereghetti et al. 2003b) allowed an effective search for the afterglow. We also immediately activated our ToO program at ESO, starting NIR observations at the NTT 7 hours after the GRB (Zerbi et al. 2003). Rapid XMM-Newton follow-up showed the presence of a bright, fading X-ray source (Santos-Lleo & Calderon 2003). at the coordinates $\alpha_{\rm J2000} = 08^{\rm h}02^{\rm m}30\overset{\rm s}{.}19$, $\delta_{\rm J2000} = -39°51'04\overset{''}{.}5$, with an estimate

1-σ error of $0\farcs7$ (Watson et al. 2004). A radio afterglow was also discovered (Frail 2003) at a position consistent with the XMM error box. A compact galaxy, located at a consistent position,

was proposed to be the GRB host galaxy by Prochaska et al. (2003). The redshift was $z = 0.1055 \pm 0.0001$ (Prochaska et al. 2003, 2004), making GRB 031203 one of the closest burst ever detected. The proximity of this event made it a good candidate for searching a supernova component in its light curve, even if its location towards the Galactic plane (Galactic coordinates $l = 255\fdg74$, $b = -4\fdg80$) made optical observations tricky. However, the Galactic dust clouds towards the GRB direction allowed the formation of a scattered, expanding X-ray halo (Vaughan et al. 2004) due to the reflection of the burst and/or early afterglow light. This allowed an (indirect) measurement of the X-ray flux at the earliest stages after the burst onset.

Given the low redshift of this event, the isotropic-equivalent burst energy is extremely low[1], $E_{\rm iso} \sim 10^{50}$ erg (30–400 keV; Sazonov et al. 2004), below the standard reservoir $\sim 10^{51}$ erg of normal GRBs (Frail et al. 2001; Bloom et al. 2003a). At that time, the only known bursts with such low energy were GRB 980425 (Galama et al. 1998b) and XRF 020903 (Sakamoto et al. 2004). Today, only GRB 060218 (Campana et al. 2006) and GRB 060505 (Fynbo et al. 2006) have joined this set (considering only long-duration GRBs).

Based on photometric monitoring of the host galaxy, several groups have reported evidence for a SN associated with GRB 031203 (Bersier et al. 2004; Thomsen et al. 2004; Cobb et al. 2004; Gal-Yam et al. 2004). After the ultimate confirmation, coming from spectroscopic observations and reported by the MISTICI collaboration (Tagliaferri et al. 2004), the IAU named this event SN 2003lw.

2.1 Observations and data reduction

Photometry. We observed the field of GRB 031203 starting $\approx$ 7 h after the trigger, to search for the near-infrared (NIR) afterglow, using SofI on the ESO-NTT at La Silla (Chile). Subsequent imaging with ISAAC on the ESO-VLT showed the presence of a varying source coincident with the putative host galaxy of GRB 031203: the total flux had dimmed in the J, H and K

[1] The "concordance" cosmology with $H_0 = 71$ km s^{-1} Mpc^{-1}, $\Omega_{\rm m} = 0.27$, $\Omega_\Lambda = 0.73$ (WMAP results; Spergel et al. 2003) is adopted throughout this thesis. At $z = 0.1055$ the luminosity distance is $D = 477$ Mpc and the distance modulus is $\mu = 38.42$ mag.

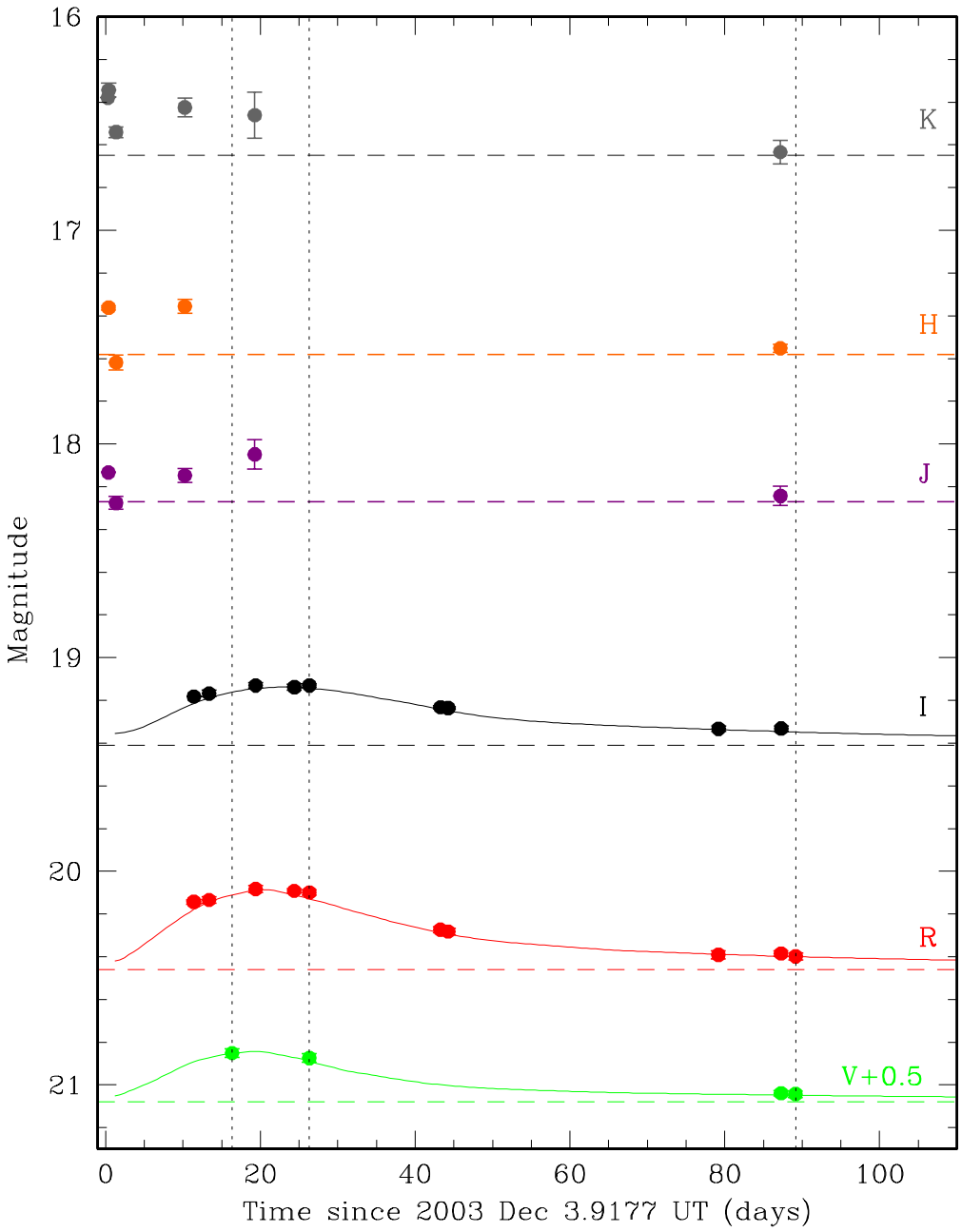

Figure 2.1: Optical and NIR light curves of GRB 031203 (dots), including the contribution from the host galaxy. Error bars indicate the amount of relative errors only (Table 2.1). The solid curves show the evolution of SN 1998bw (Galama et al. 1998b; McKenzie & Schaefer 2000), rescaled at $z = 0.1055$, stretched by a factor 1.1, extinguished with $E_{B-V} = 1.1$ and brightened by 0.5 mag. Dashed lines indicate the fitted host galaxy contribution. Vertical dotted lines mark the epochs of our spectra.

filters by a few tenths of a magnitude (see Fig. 2.1). We therefore started a campaign to monitor the optical/NIR light curve of the event, searching for a SN rebrightening. The observation log is presented in Table 2.1.

Image reduction was performed following the standard procedures, using the `Eclipse` package (Devillard 1997). Aperture photometry was performed with `Gaia`. The results were checked performing image subtraction with `ISIS` (Alard 2000). To avoid saturation from the bright, nearby star, U0450_05672411 ($R \sim 10.2$), the exposure time was always kept short. In same exposures, occulting bars were placed to cover the bright star (showing that the effect was negligible). Optical and NIR photometry were calibrated against Landolt standard stars and the 2MASS, respectively. To focus on the issue of variability, in Table 2.1 we list just the relative photometry with respect to a reference epoch. We should also note that the host galaxy spectrum is dominated by prominent emission lines (Fig. 2.5). This may lead to relatively large offsets when comparing results between different instruments, owing to unavoidable small differences in the filter profiles and CCD efficiencies.

Spectroscopy. Moderate-resolution spectra (FWHM $\approx$ 10 Å) were taken with the VLT on 2003 Dec. 20 (FORS 2), 2003 Dec. 30 (FORS 1), and 2004 Mar. 01 (FORS 1). Spectral analysis was performed in the standard way. Flux calibration was achieved by observing spectrophotometric stars LTT 3864 and Feige 56. After comparing synthetic magnitudes calculated from our spectra with the photometry, we introduced a correction to account for light loss outside the slit. To ensure a sound relative calibration between the spectra, we also checked that the fluxes of the host galaxy emission lines did not vary among the different exposures. After this process, we introduced a correction of 16% to the spectrum of Dec. 30. This number also provides an estimate of the intrinsic error in the absolute flux calibration. For a detailed discussion of the GRB 031203 host properties, we refer to Prochaska et al. (2004) and Margutti et al. (2006).

2.2 Results

In Fig. 2.1 we show the light curves of GRB 031203. Early-time NIR photometry shows a dimming in all bands between the first and second night after the GRB. This is confirmed by PSF-matched image subtraction (Fig. 2.2). We believe that we have seen the NIR afterglow of GRB 031203. The magni-

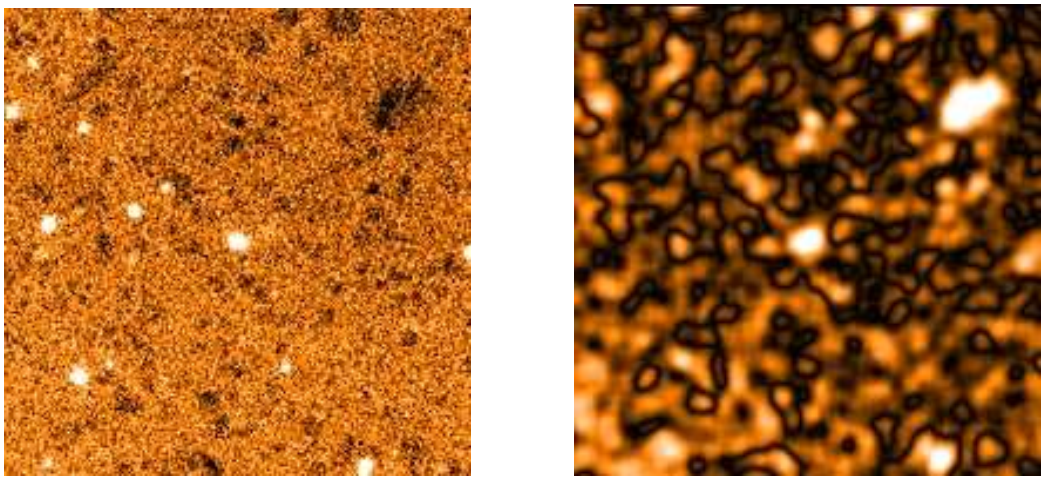

Figure 2.2: *Left*: the field of GRB 031203 in the H band on Dec 3.3 UT. The object right in the center is the sum of the afterglow and host contribution. *Right*: result of the PSF-matched subtraction of the host galaxy contribution (taken from late images) from the image on the left. There is a clear variation of the object coincident with the host galaxy of GRB 031203, showing that the afterglow was indeed contributing to the total flux. Note that the other spots in the subtraction image are due to flat-field defects. Similar results are obtained in the J and K filters.

tudes are $J = 20.60 \pm 0.09$, $H = 19.05 \pm 0.07$, $K = 17.56 \pm 0.05$ (9 hours after the GRB), obtained by subtracting the host contribution. Cobb et al. (2004) have I-band observations at similar epochs, and do not report evidence for variability. However, extrapolation to the visible region yields $I \sim 23.4$, quite a faint value when compared to the host luminosity $I \approx 19.4$. Little contribution from the afterglow is seen in our measurement of Dec. 5 (32 hours after the GRB), implying a quick decay between the two nights ($F(t) \propto t^{-\alpha}$, with $\alpha \gtrsim 2$).

In Fig. 2.3, we compare the spectrum in the NIR and X-ray regions (X-ray data from Watson et al. 2004). A discontinuity is apparent, indicating a different origin for the emission in the two bands. The X-ray component has a much harder spectrum, and a slower decay ($\alpha = 0.55 \pm 0.05$). Interestingly, Watson et al. (2004) infer a fast decay of the early-time X-ray afterglow, consistent with our NIR value ($\alpha \gtrsim 1.7$). In the standard model of afterglows (e.g. Sari et al. 1998), a fast decay is consistent with a soft spectrum bluewards of the peak frequency. A dust extinction larger than assumed

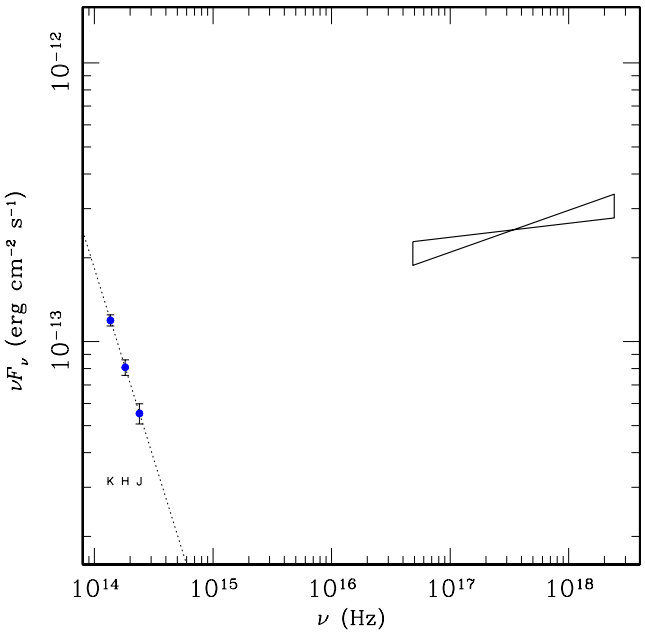

Figure 2.3: Spectral energy distribution of the afterglow of GRB 031203 on 2003 Dec. 4.3 UT (9 hours after the trigger). The NIR values are calculated from our data by subtracting the host contribution and assuming $E_{B-V} = 1.1$. The NIR spectral index is $\beta = 2.36 \pm 0.02$ ($F_\nu \propto \nu^{-\beta}$). The X-ray spectrum is from Watson et al. (2004), reported at $t = 9$ h using the X-ray decay slope.

may be responsible for the red spectrum. This would imply, however, that the peak magnitude of SN 2003lw (see below) would be exceptionally bright, so that dust suppression is unlikely. It is not simple to explain such steep component in the framework of standard afterglows. Recently, observations of GRB 060218 have shown a steep-spectrum component similar to the NIR emission of GRB 031203 (Soderberg et al. 2006a). Such component was in excess to the "standard" afterglow emission, and has been tentatively interpreted as due to the central engine activity (see also Fan et al. 2006). Since both GRB 031203 and GRB 060218 had very low afterglow luminosity, this component might be hidden in more energetic events.

A few days after the GRB, a rebrightening is apparent in all optical/NIR bands. The rebrightening amounts to $\approx 30\%$ of the total flux, and is coincident with the center of the host galaxy to within $0\farcs1$ (≈ 200 pc at $z = 0.1055$). For comparison, we show in Fig. 2.1 the VRI light curves of SN 1998bw

(Galama et al. 1998b; McKenzie & Schaefer 2000), placed at $z = 0.1055$ and dereddened with $E_{B-V} = 1.1$ (see below). Interpolation of the $UBVRI$ data was performed in order to estimate the fluxes of SN 1998bw at the frequencies corresponding to the observed bands. Even after correcting for cosmological time dilation, the light curve of SN 2003lw is broader than that of SN 1998bw, and requires an additional stretching factor of ≈ 0.9 to match the observed R and I observations. Near the peak, the light curve is rather flat, resembling the hypernova SN 1997ef (Iwamoto et al. 2000) more than SN 1998bw. This feature may be present in other GRB-associated SNe (Della Valle et al. 2006b). The R-band maximum is reached on approximately 2003 Dec. 24 (~ 18 comoving days after the GRB). We note that the details of the light curve shape are sensitive to the removal of the host contribution, which is the dominating light contributor. This may explain the different finding of Cobb et al. (2004), who find a longer rise, and Thomsen et al. (2004), who need no stretch. We note, however, that the SN 1998bw template (after the stretching and brightening procedure), fits our data remarkably well. Assuming a light curve shape similar to SN 1998bw, which had a rise time of 16 days in the V band, our data suggest an explosion time nearly simultaneous with the GRB. Type-Ic SNe usually reach V-band maximum in $\sim$ 12–20 days, the brightest events showing a slower evolution (see e.g. Fig. 2 of Mazzali et al. 2002).

A precise determination of the absolute magnitude of the SN is made difficult by the uncertain, and significant, extinction. From our spectra (see also Prochaska et al. 2004) we constrain the average combined Galactic and host extinction to be $E_{B-V} \approx 1.1$ based on the Balmer ratios of the host galaxy. Given the good spatial coincidence of the SN with the center of the host, such value is our best estimate for the SN extinction. We also adopt a Galactic extinction law (Cardelli et al. 1989) with $R_V = 3.1$. It is not known how such dust is distributed between the Milky Way and the host galaxy. The measured E_{B-V} is consistent with that inferred from Galactic maps (Schlegel et al. 1998). However, for such large values of the extinction, FIR-based maps are known to have significant errors. In particular, the correction factor estimated by Dutra et al. (2003) would imply a value $E_{B-V} \approx 0.7$ for this line of sight, letting significant dust in the GRB host. In any case, given the low redshift of the GRB, the dust correction is similar either assuming all the dust at $z = 0$ or dividing it among the two galaxies. Also adopting a different extinction law for the GRB host (in particular, adopting an SMC-like curve) leads to a difference lower than 0.1 mag. An extinction with $E_{B-V} \approx 1.1$ mag is also favored by spectral modeling (Mazzali et al. 2006;

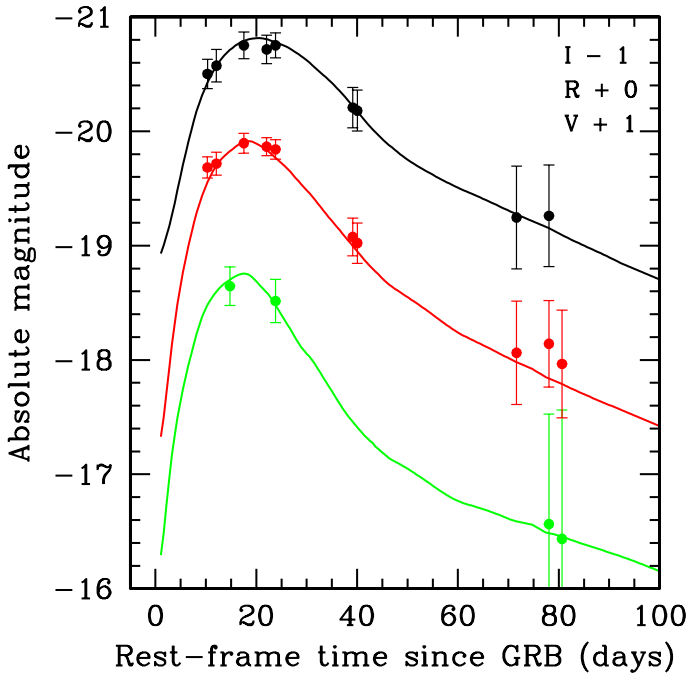

Figure 2.4: Light curves of SN 2003lw in the V, R, and I filters (observed frame), after removal of the host galaxy contribution and assuming $E(B-V) = 1.1$. The solid lines show the light curves of SN 1998bw, reported at $z = 0.1055$, brightened by 0.5 mag, and time-expanded by a factor 1.1.

see also Sect. 2.3).

Figure 2.4 shows the light curves in absolute magnitudes of SN 2003lw, compared with those of SN 1998bw. With the assumed reddening, SN 2003lw appears brighter than SN 1998bw by 0.5 mag in all the V, R, and I bands. The two SNe had therefore very similar colors. The absolute magnitudes of SN 2003lw are $M_V = -19.75 \pm 0.15$, $M_R = -19.9 \pm 0.08$, and $M_I = -19.80 \pm 0.12$. Thomsen et al. (2004), using I-band data, also found that SN 2003lw was brighter than SN 1998bw by ~ 0.55 mag, in full agreement with our result. Cobb et al. (2004), however, found a comparable luminosity for the two SNe; this discrepancy is entirely due to the lower extinction they assume.

Fig. 2.5 shows our spectra of the host galaxy of GRB 031203, taken when the SN was close to maximum light and at a later epoch. The broad undulations due to the emergence of the SN are clearly apparent in the December

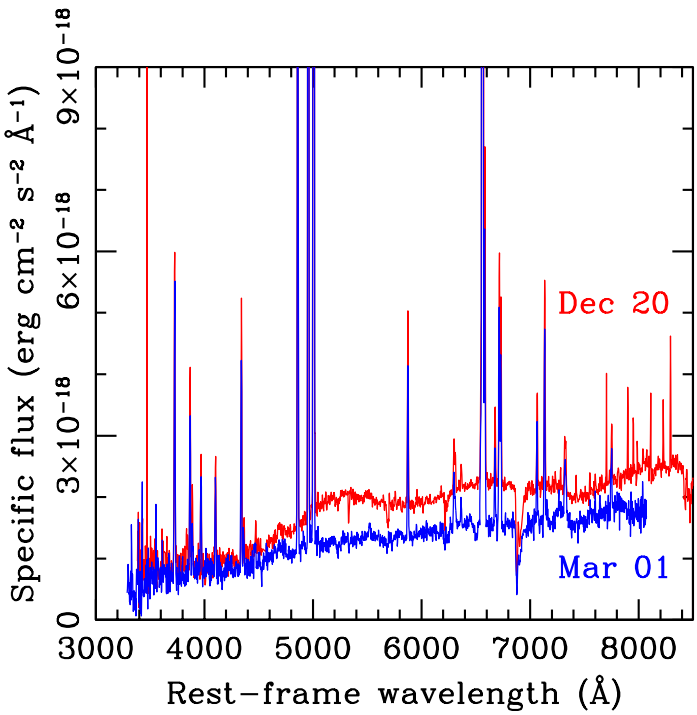

Figure 2.5: Spectra of the host galaxy of GRB 031203 taken when SN 2003lw was close to maximum and at a late time, when it provided a negligible contribution.

spectrum. As confirmed by the photometry, the SN provided only a negligible contribution to the total light in March. By subtracting the late-time host spectrum, we were able to isolate the net SN contribution.

Fig. 2.6 shows the spectra of the rebrightening on 2003 Dec. 20 and Dec. 30 (14 and 23 rest-frame days after the GRB), after subtracting the spectrum taken on 2004 Mar. 1 (81 rest-frame days after the GRB). The spectra of SN 2003lw are remarkably similar to those of SN 1998bw obtained at comparable epochs (shown as dotted lines in Fig. 2.6; from Patat et al. 2001). Both SNe show very broad absorption features, indicating large expansion velocities. We thus tentatively classify SN 2003lw as a hypernova. The main absorptions are identified in Fig. 2.6 as in SN 1998bw, following Iwamoto et al. (1998). The velocity of the Si II line in SN 2003lw is apparently smaller than in SN 1998bw. The broad peaks near 5300 Å and 6600 Å are probably the emission components of P-Cygni profiles due to the blending of several lines. There is evolution between the two epochs: the

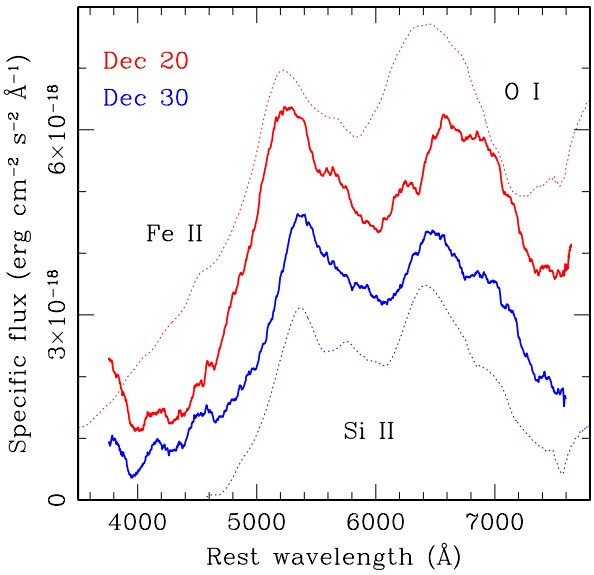

Figure 2.6: Spectra of SN 2003lw, taken on 2003 Dec. 20 and Dec. 30 (solid lines), smoothed with a boxcar filter 250 Å wide. Dotted lines show the spectra of SN 1998bw (from Patat et al. 2001), taken on 1998 May 9 and May 19 (13.5 and 23.5 days after the GRB, or 2 days before and 7 days after the V-band maximum), extinguished with $E_{B-V} = 1.1$ and a Galactic exinction law. The spectra of SN 1998bw were vertically displaced for presentation purpose.

bluer bump is observed at longer wavelengths in the second spectrum, and is slighty narrower. Moreover, the shape of the redder peak is different in the two epochs. Both peaks appear at redder wavelengths than in SN 1998bw. Detailed modeling of the spectra has been provided by Mazzali et al. (2006).

2.3 Models of SN 2003lw

Based on the data presented above, and including also the NIR observations by Gal-Yam et al. (2004), Mazzali et al. (2006) have modeled the light curves and spectra of SN 2003lw, in order to infer the properties of the SN and of the progenitor star. Further, the spectral coverage was extended into the red, in order to better constrain the extinction. From the available optical/NIR

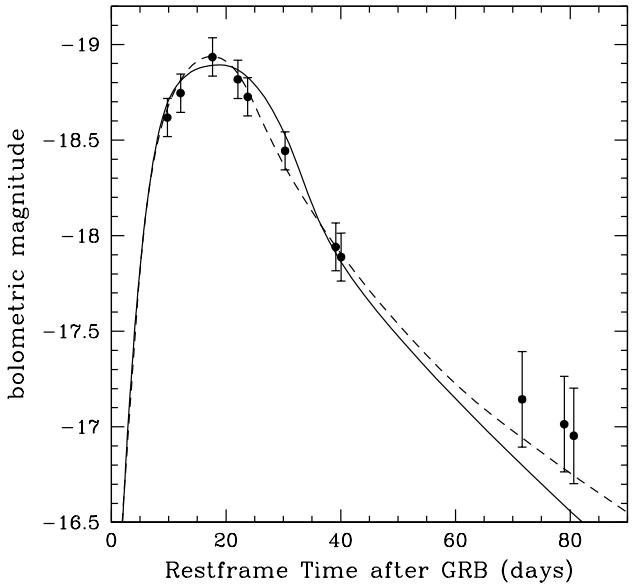

Figure 2.7: Bolometric light curve of SN 2003lw. The solid and the dotted lines show two different models, which are able to fit well the early and late epochs, respectively. The need for two different models is likely due to some intrinsic asymmetry in the SN ejecta. Both models, however, yield similar explosion parameters. From Mazzali et al. (2006).

data, the bolometric light curve of SN 2003lw was computed, and compared with that of SN 1998bw. As for the light curves in the individual passbands, also the bolometric curves are similar, provided that a brightening (by $\sim$ 0.3 mag) and a time expansion is applied (Fig. 2.7). This was expected, since the colors of the two SNe are similar. The modeling was based on the code initially developed by Iwamoto et al. (2000). Given the similarity of SN 1998bw and SN 2003lw, models adopted for the former SN were rescaled to match the properties of the latter. In particular, the peak timescale scales as $\tau \propto \kappa^{1/2} M_{\rm ej}^{3/4} E^{-1/4}$, where κ is the opacity, $M_{\rm ej}$ the ejected mass, and E the expansion energy. Since SN 2003lw evolved slower than SN 1998bw by a factor 1.1, an increase in the mass (and hence in the energy) by a factor 1.2 provides the necessary temporal expansion. To match the larger brightness of this SN, the amount of ^{56}Ni was increased. This led to the estimates $M_{\rm ej} \approx 12.5\ M_\odot$ and $E = 5 \times 10^{52}$ erg. A total ^{56}Ni mass of 0.54 $M_\odot$ was necessary to reproduce the brightness of SN 2003lw. With the adopted ejected mass, a massive progenitor star is implied, with $M \sim 40$–$50\ M_\odot$.

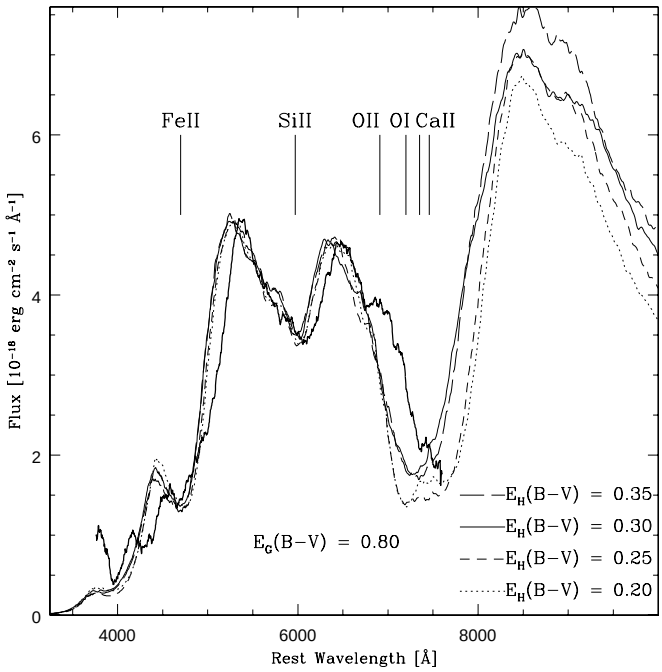

Figure 2.8: Spectrum of SN 2003lw on 2005 Dec. 20, together with hypernova models. Different linestyle indicates different values of the local reddening as indicated in the legend.

Spectral models were performed with the code developed by Mazzali et al. (1993). The spectra were computed assuming a Galactic extinction $E_{B-V} = 0.8$ mag (as prescribed by Dutra et al. 2003) and varying the host E_{B-V} between 0.2 and 0.35 mag. All models successfully reproduce the observed spectra in the B and V regions. The line profiles imply a photospheric velocity $v_{\rm ph} \approx 19\,000$ km s^{-1}. There is however some difference in the red part (Fig. 2.8). Low values of E_{B-V} would require very strong absorption features from calcium and oxygen in the SN ejecta, thus implying exceedingly large oxygen abundances. Therefore, larger E_{B-V} values provide a better match. The favored value has $E_{B-V} = 0.25$–0.3 mag.

2.4 Conclusions

The discovery of GRB 031203, and of the associated SN 2003lw provided an important step towards the understanding of the SN/GRB connection. By modeling the X-ray dust echo, Watson et al. (2004) concluded that GRB 031203 was an X-ray flash (XRF); however, the prompt emission data make this hypotesis tricky (Sazonov et al. 2004), since the spectrum at gamma-ray energies is hard (see Ghisellini et al. 2006 for possible solutions to this riddle). More likely, the soft emission component revealed by the dust echo was due to a powerful X-ray (Watson et al. 2006c) flare as observed in a few afterglows by *Swift* (Burrows et al. 2005b; Falcone et al. 2006) and *Beppo*SAX (Piro et al. 1998, 2005). GRB 031203, like SN 1998bw (Pian et al. 2000), seems therefore to violate the correlation between the isotropic-equivalent gamma-ray energy $E_{\rm iso}$ and the peak spectral energy $E_{\rm p}$ (Amati et al. 2002; Lamb et al. 2004). In fact, assuming $E_{\rm iso} \sim 1.5{\times}10^{50}$ erg (Sazonov et al. 2004), the Amati et al. (2002) relation would imply $E_{\rm p} \sim 10$ keV, a value indicating an XRF nature for GRB 031203. This is in contrast with what observed by INTEGRAL, which imply $E_{\rm p} \gtrsim 190$ keV (90% confidence level).

The afterglow of GRB 031203 was very weak, the faintest ever detected in the optical/NIR. Extrapolation in the R band yields a luminosity ~ 200 times fainter than one of the dimmest afterglow discovered so far (GRB 021211: Fox et al. 2003b; Pandey et al. 2003a). The detection of the SN optical light implies that the reason of such faintness was not an extreme dust obscuration. Also given the low redshift of the event, this example shows that some optical afterglows may escape detection just because they are faint (e.g. Fynbo et al. 2001; De Pasquale et al. 2003).

GRB 031203, together with GRB 980425 at $z = 0.085$, was a very dim event, perhaps a jet observed far from its axis (e.g. Maeda et al. 2002; Yamazaki et al. 2003). Being so faint, they would have been likely missed at cosmological distances. Since the volume they sample is much smaller than that probed by classical, distant GRBs with $\langle z \rangle \approx 1$, the rate of these events could be much larger (Guetta et al. 2004). Indeed, also following the discovery of a few new faint, nearby GRBs (GRB 060218: Campana et al. 2006; GRB 060614, GRB 060605: Fynbo et al. (2006)), it looks that dim GRBs may outnumber bright events, even with a great uncertainty due to the poorly constrained beaming correction (e.g. Liang et al. 2006; Della Valle 2006a).

GRB 031203 was quite similar to GRB 980425, even if overall more power-

ful (Soderberg et al. 2004a). Both events consisted in a single, underenergetic pulse. Their afterglows were very faint or absent in the optical, and showed a very slow decline in the X rays (Pian et al. 2000; Watson et al. 2004). Last, they were both accompained by a powerful hypernova. We defer a more extended discussion about this event to Chapter 8.

Mean date (UT)	Seeing ($''$)	Instrument	Filter	Magnitude
2003 Dec 20.247	0.6	FORS2	V	-0.023±0.020
2003 Dec 30.250	0.5	FORS1	V	20.37±0.050*
2004 Feb 29.193	0.7	FORS1	V	0.165±0.012
2004 Mar 02.064	0.7	FORS1	V	0.169±0.015
2003 Dec 15.314	0.6	FORS1	R	20.14±0.030*
2003 Dec 17.284	0.7	FORS1	R	-0.009±0.016
2003 Dec 23.295	0.5	FORS1	R	-0.060±0.016
2003 Dec 28.296	0.6	FORS1	R	-0.051±0.010
2003 Dec 30.241	0.5	FORS1	R	-0.044±0.013
2004 Jan 16.171	0.8	FORS1	R	0.130±0.013
2004 Jan 17.185	0.5	FORS1	R	0.139±0.014
2004 Feb 21.101	0.7	FORS1	R	0.248±0.019
2004 Feb 29.198	0.7	FORS1	R	0.242±0.012
2004 Mar 02.069	0.6	FORS1	R	0.255±0.016
2003 Dec 15.321	0.5	FORS1	I	19.18±0.030*
2003 Dec 17.291	0.6	FORS1	I	-0.014±0.015
2003 Dec 23.300	0.4	FORS1	I	-0.052±0.013
2003 Dec 28.301	0.6	FORS1	I	-0.044±0.015
2003 Dec 30.245	0.4	FORS1	I	-0.052±0.009
2004 Jan 16.177	0.6	FORS1	I	0.050±0.008
2004 Jan 17.179	0.6	FORS1	I	0.054±0.007
2004 Feb 21.107	0.5	FORS1	I	0.151±0.013
2004 Feb 29.203	0.8	FORS1	I	0.150±0.013
2003 Dec 03.288	0.9	SofI	J	18.13±0.034*
2003 Dec 04.258	0.5	ISAAC	J	0.143±0.030
2003 Dec 14.140	1.1	SofI	J	0.014±0.032
2003 Dec 23.191	1.0	SofI	J	-0.084±0.069
2004 Feb 28.111	0.5	ISAAC	J	0.110±0.045
2003 Dec 03.300	0.9	SofI	H	17.36±0.042*
2003 Dec 04.271	0.5	ISAAC	H	0.257±0.035
2003 Dec 13.148	0.9	SofI	H	-0.006±0.033
2004 Feb 28.104	0.5	ISAAC	H	0.190±0.019
2003 Dec 03.204	0.9	SofI	K	16.38±0.036*
2003 Dec 03.312	0.8	SofI	K	-0.036±0.033
2003 Dec 04.267	0.5	ISAAC	K	0.161±0.025
2003 Dec 13.154	0.8	SofI	K	0.046±0.044
2003 Dec 22.188	1.0	SofI	K	0.082±0.107
2004 Mar 28.095	0.5	ISAAC	K	0.255±0.055

Table 2.1: Summary of photometric observations of GRB 031203. Absolute photometric calibration was achieved for the epochs marked with asterisks. For the other epochs, relative photometry is provided in order not to propagate the calibration error.

Chapter 3

Supernova signatures in the spectrum of the GRB 021211 afterglow

As shown in the previous chapter, there is no doubt that some GRBs are associated with core-collapse SNe. However, a detailed and good-quality knowledge is limited to a small number of nearby events. Three out of four GRBs with a firm association are moreover quite peculiar, distinct from the bulk of cosmological GRBs. There is thus the need to look for SN signatures in a wider sample of events. Furthermore, the SN properties associated with regular GRBs must be studied in some detail. This task is possible through the study of late-time bumps, which often appear as rebrightenings in the optical light curves of afterglows 20–30 days after the GRB (e.g. Bloom et al. 1999; Zeh et al. 2004). This task, unluckily, is exceedingly difficult, due to the faintness of the bumps. At moderate redshifts ($z \approx 0.5$–1), the bumps peak at magnitude $R \sim 24$–25. Thus, only large telescopes can afford to observe such objects. Moreover, the host galaxy usually contributes a large fraction of the observed light, further complicating the task of getting clean spectra. Despite these difficulties, bumps have been observed in several cases. Zeh et al. (2004) have shown that all GRBs in their sample with $z < 1$ have an associated bump (but see Price et al. 2003), which can be fit, within the large uncertanties, with template light-curves based on core-collapse SNe. This evidence is based upon photometric data. Spectroscopic analysis has proved much more difficult to achieve. Alternative explanation for the late-time bumps have been proposed, such as dust echoes (Esin & Blandford 2000),

thermal re-emission of the afterglow light (Waxman & Draine 2000), off-axis emission (Butler et al. 2005). In principle, color analysis can help to discern among the various models (e.g. Reichart 2001), but the ultimate answer can only come from spectroscopic studies. Indeed, SNe are charachterized by unique features, namely broad lines with P-Cygni profiles and widths of $\sim 10^4$ km s^{-1}.

Up to date, only a handful bumps have been observed spectroscopically. Garnavich et al. (2003) obtained spectra of GRB 0111121 at $z = 0.36$, for which photometric monitoring with HST (Bloom et al. 2002b) clearly revealed the emergence of a bump. Fynbo et al. (2004) performed the same operation for XRF 030723. In both cases, however, no clear SN features were singled out. For GRB 011121, the spectrum turned out bluer than for SN 1998bw (thus suggesting a resemblance with a type-IIn SN). For XRF 030723, the lack of features might be explained by very large expansion velocities (Tominaga et al. 2004) (thus hinting to a hypernova; but see Butler et al. 2005 for a different interpretation of the rebrightening). Soderberg et al. (2005) presented a spectrum of the late-time excess of XRF 020903 at $z = 0.225$, which also resembled that of a hypernova. Last, spectra were obtained for GRB 050525A at $z = 0.606$ (Della Valle et al. 2006b; see next chapter). In this chapter spectroscopic evidence for a SN associated with GRB 021211 is presented. This material has been published by Della Valle et al. (2003a).

3.1 GRB 021211.

GRB 021211 was detected on 2002 Dec 12 by the HETE-II satellite at 11:18:34 UT (Crew et al. 2002). The γ-ray fluence was $(0.96 \pm 0.29) \times 10^{-6}$ erg cm^{-2} in the 7–30 keV band and $(1.98 \pm 0.15) \times 10^{-6}$ erg cm^{-2} in the 30–400 keV band (Crew et al. 2003). The GRB was therefore classified as X-ray rich. Given the redshift $z = 1.006$ of this event (Vreeswijk et al. 2006), the inferred (isotropic) energy was $E_{\rm iso} = (6 \pm 0.5) \times 10^{51}$ erg, at the low end of the energy distribution of GRBs (Frail et al. 2001). Owing to the rapid distribution of coordinates, an optical afterglow was rapidly discovered by Fox & Price (2002), just 20 minutes after the GRB onset, as a pointlike source with magnitude $R = 18.29 \pm 0.02$ at coordinates $\alpha = 08^{\rm h}08^{\rm m}59\overset{\rm s}{.}9$, $\delta = +06^\circ 43' 37\overset{''}{.}5$ (J2000; Fox et al. 2003b). Moreover, the automatic telescopes RAPTOR (Woźniak et al. 2002), KAIT (Li et al. 2003), and Super–LOTIS (Park et al.

2002), imaged the error box a few minutes after the GRB. These observations allowed to monitor the early light curve of the afterglow, which could be described by a broken powerlaw with a flattening at $t \approx 10$ min (Li et al. 2003). This resembled the behavior of the optical flash of GRB 990123 (Akerlof et al. 1999), but was quite different from several other events observed in the earliest epochs. As a matter of fact, these two GRBs have provided the only clear examples of an optical flash even after the launch of *Swift* and the detection of several early afterglows (with the possible case of GRB 050904; Boër et al. 2006).

The striking feature of the optical afterglow of GRB 021211 was however its extreme faintness. Compared to other events at similar epochs and redshifts, this afterglow was dimmer by ~ 3 magnitudes in the R-band (see e.g. Fox et al. 2003b; Nardini et al. 2006). The afterglow was dimmer by ~ 3 magnitudes in the R-band with respect to the average (at least at the time of its explosion; e.g. Fox et al. 2003b). This could in principle be due to heavy extinction within the host. However, Fox et al. (2003b) report a broad-band color $B - K = 3.9$ (on Dec 11.6 UT), well within the range of GRB afterglows (Šimon et al. 2001). This indicates that GRB 021211 suffered small extinction. Moreover, this burst was also underluminous in all observed wavebands: only upper limits were reported in the radio (Fox et al. 2003b; Rol & Strom 2002), submillimeter (Fox et al. 2003b; Hoge et al. 2002), and TeV (McEnery 2002) regions. Unfortunately, no follow-up X-ray observations could be performed. The intrinsic faintness of the optical afterglow made this object a good target for looking a SN component.

3.2 Photometry.

Late-time observations were secured at the ESO VLT–UT4 (Yepun) equipped with the FORS 2 instrument, in the R band, during the period 2003 January – March 2003 (see Table 3.1).

The conversion to absolute flux was obtained by using both standard calibration and a secondary sequence calibrated, on Feb 28, with a Landolt standard field (SA98), to account for the observations obtained under non-photometric conditions. Aperture photometry was executed with the packages `apphot` and `photcal` within IRAF, by choosing aperture radii from 0.5 to 3″, then correcting to infinity with the values found for the standards and using the `DAOGROW` algorithm. The measurements on the various aper-

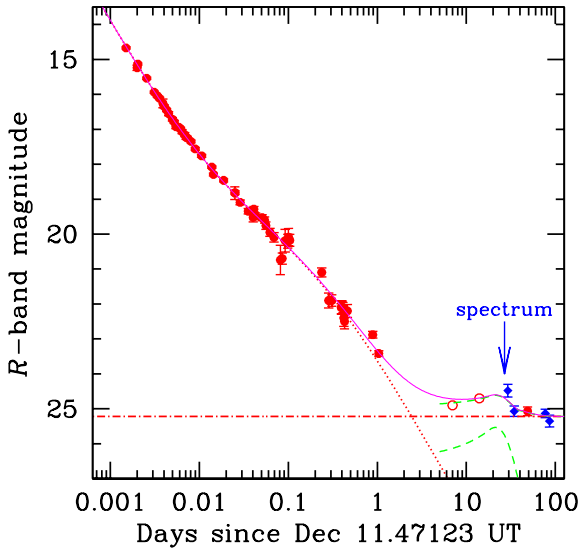

Figure 3.1: Light curve of the afterglow of GRB 021211. Filled circles represent data from Fox et al. (2003b), Li et al. (2003), Pandey et al. (2003a), Holland et al. (2004), and Nysewander et al. (2006). Open circles are converted from HST measurements (Fruchter et al. 2002). Filled diamonds indicate our data; the arrow shows the epoch of our spectrum. The dotted and dot-dashed lines represent the afterglow and host contribution respectively. The dashed line shows the light curve of SN 1994I reported at $z = 1.006$ and dereddened with $A_V = 2$ (from Lee et al. 1995). The solid line shows the sum of the three contributions.

Start UT	Exp time	Seeing	R magnitude
2003 Dec 27.09	70 min	$1.0''$	> 24.3
2003 Jan 9.7*	63 min	$1.1''$	24.48 ± 0.18
2003 Jan 15.33	15 min	$0.8''$	25.07 ± 0.15
2003 Feb 28.02	75 min	$0.8''$	25.13 ± 0.12
2003 Mar 9.01	50 min	$1.25''$	25.35 ± 0.17

Table 3.1: Summary of our photometric observations. Magnitudes are referred to the complex afterglow + host. Errors are 1-σ. *: average of two measurements obtained on Jan 9.3 and 10.2.

tures for the secondary calibrators were found very stable, and we decided to adopt for the target the innermost aperture magnitude, corrected for the aperture. The GRB host galaxy has been reported to be spatially resolved in HST images. However, its very compact size ($0\farcs15$) makes it effectively pointlike for ground-based observations.

Our results are listed in Table 3.1 and supersede our preliminary report (Testa et al. 2003). They have been complemented with a compilation of observations collected from literature and plotted in Fig. 3.1. A rebrightening is clearly seen, starting ~ 15 days after the burst (Fruchter et al. 2002) and reaching the maximum, $R \sim 24.5$, during the first week of January. The contribution of the host galaxy, estimated from our late-epoch images, is $R = 25.22 \pm 0.10$. Therefore, the intrinsic magnitude of the bump was $R = 25.24 \pm 0.38$.

The afterglow contribution is more uncertain. The early-time light curve presents several fluctuations, and cannot be easily extrapolated to later epochs. In particular, fitting all data up to 1 day after the GRB[1] with a (convex) broken powerlaw, as used by Li et al. (2003), yields an unacceptable $\chi^2/\mathrm{d.o.f.} = 115/45$. We suggest two possible alternatives. First, the shape of the lightcurve is consistent with the presence of two or three rebrightenings underlying a powerlaw component, similarly to what observed in GRB 021004 (Lazzati et al. 2002; Nakar et al. 2003) and several other afterglows at early times. Alternatively, a second break in the light curve could be present about 10 hours after the GRB. This may be the consequence of the passage of the synchrotron cooling frequency across the optical band, or to a jet break, or even to the cessation of energy from the central engine. A fit with a double broken powerlaw (i.e. with *two* breaks, see Fig. 3.1) yields $\chi^2/\mathrm{d.o.f.} = 55/43$; the improvement is highly significant (F-test chance probability less than 10^{-6}). We note that, whichever extrapolation is used, the contribution of the afterglow to the flux measured at the epoch at which our spectrum (the arrow in Fig. 3.1) was obtained, is negligible (less then 5% in the most conservative case). This fact strongly supports that the bump was powered by a different component other than the afterglow.

[1] We added in quadrature 0.03 mag to the errors of all points in order to account for the use of different telescopes and calibrations.

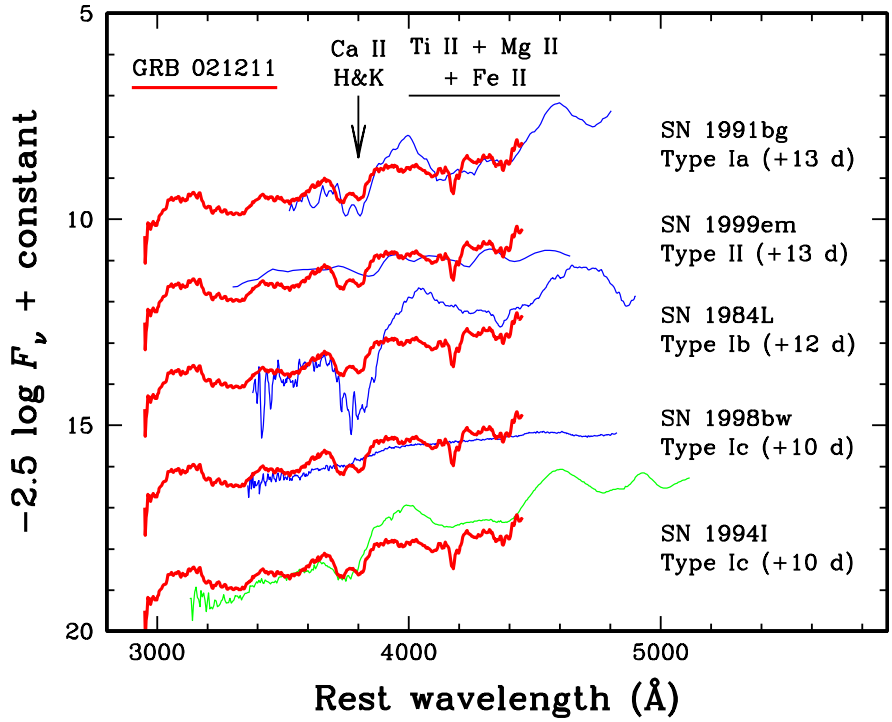

Figure 3.2: Rest-frame spectrum of the afterglow of GRB 021211 on 2003 Jan 8.27 UT, or 27 days after the GRB (thick lines), compared with that of several SNe (thin lines).

3.3 Spectral analysis.

We obtained a spectrum of the afterglow + host with FORS 2, on Jan 8.27 UT (27 days after the GRB), during the rebrightening phase shown in Fig. 3.1. The original spectrum covered the range of wavelengths (6000 – 11000) Å, although only the interval (6000 – 9000) Å afforded an acceptable S/N ($\gtrsim 3$). The resolution was about 19 Å, and the integration time was 4×1 h. The slit was rotated in such a way to include also the nearby galaxy reported by (Caldwell et al. 2002); this object was well detected and is clearly separated from our target (the seeing in the 4 exposures was 0.″6–1.″4). The extraction of the spectrum was performed within the MIDAS and IRAF environments, independently by three people. We clearly detected the emission line at 7472.9 Å already found by Vreeswijk et al. (2006). Interpreting this as [O II] 3727 Å in the rest frame of the host galaxy, this corresponds to

a redshift $z = 1.006$. Our spectrum, shown in the rest-frame of the GRB (thick lines in Fig. 3.2) was smoothed with a boxcar filter (55 Å width) and cleaned from the emission line [O II]. The spectrum is characterized by broad low-amplitude undulations blueward and redward of a broad absorption, the minimum of which is measured at ~ 3770 Å (in the rest frame of the GRB), whereas its blue wing extends up to ~ 3650 Å. We then compared our spectrum with those of several SNe arranged in different spectroscopic types and obtained at different epochs (Fig. 3.2, thin lines). The comparison includes the type-Ia SN 1991bg (Filippenko et al. 1992; Turatto et al. 1996), the type-II SN 1999em (Hamuy et al. 2001), the type-Ib SN 1984L (Harkness et al. 1987), the peculiar type-Ic SN 1998bw (Galama et al. 1998b; Patat et al. 2001), and the type-Ic SN 1994I (Filippenko et al. 1995). Both SN 1999em and SN 1998bw provide a poor match to the afterglow spectrum. Some similarity can be found with the type-Ia SN 1991bg and the type-Ib SN 1984L. A more convincing resemblance is found with the spectrum of the type-Ic SN 1994I, obtained 9 days after its B-band maximum (Filippenko et al. 1995). The comparison with SN 1994I (and to some extent also with SN 1991bg and SN 1984L) strongly supports the identification of the broad absorption with Ca II H+K; the blueshifts corresponding to the minimum of the absorption and to the edge of the blue wing imply velocities of $v \sim 14\,400$ km s^{-1} and $v \sim 23\,000$ km s^{-1}, respectively. In principle the Ca II from the host galaxy could contaminate our spectrum. However, since the typical FWHM of absorption (and emission) lines of galaxies is of the order of 10–15 Å (corresponding to less than 1 000 km s^{-1}), and the FWHM of the observed absorption is about 150 Å, one concludes that the Ca II of the host galaxy might affect the observed feature only marginally, if at all.

Based on the photometric and spectroscopic evidence presented above, the IAU has dubbed the SN associated with GRB 021211 as SN 2002lt (Della Valle et al. 2003b).

3.4 Time delay between the SN and the GRB.

Using SN 1994I as a template, our photometric and spectroscopic data allow us to estimate the time at which the SN exploded, and to compare it with the GRB onset time.

Spectroscopy. In order to further study the spectrum of the SN associated with the bump, we have used as a reference (see Fig. 3.3) the spectral

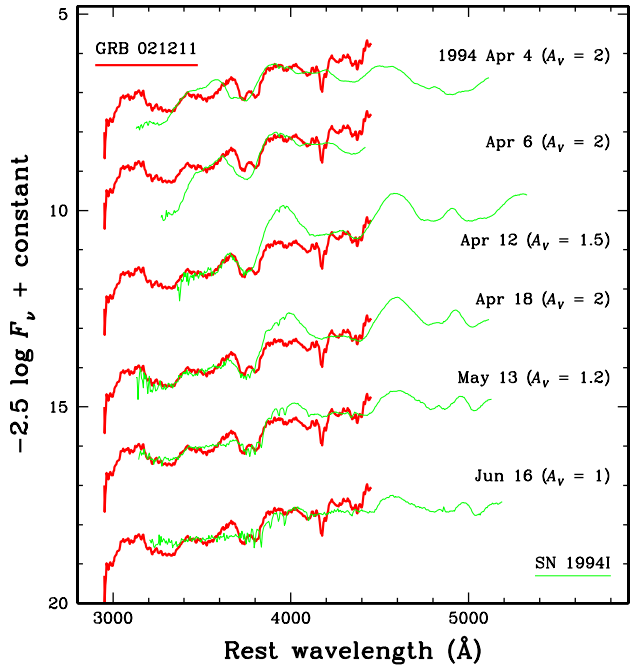

Figure 3.3: Comparison of the spectrum of the GRB bump to the ones of SN 1994I taken at different times. Each plot has a different A_V, in order to better match our spectrum (we adopted the extinction law by Cardelli et al. 1989. For reference, SN 1994I reached its B-band maximum on 1994 Apr 9.

evolution of SN 1994I (Filippenko et al. 1995). To find the best match, different reddenings in the range $A_V = 1.4 \pm 0.5$ (Richmond et al. 1996) were applied to each spectrum. The epochs before maximum light (April 9) seem to be excluded by the morphology of Ca feature, which is broader and located at shorter wavelengths than for GRB 021211 (the correctness of the wavelenght axis was checked by measuring the position of the NaD interstellar absorption in each spectrum). Spectra later than Jun 1 show a very weak Ca feature and exhibit a poor match with the afterglow spectrum in the (3200–3700) Å region. Therefore the match with the spectra is acceptable over the range $\sim$ Apr 9 to $\sim$ May 31 ($\sim$ 0 to 40 days after SN maximum light). However the fast decline which characterizes the luminosity evolution of type-Ic SNe after maximum (e.g. Hamuy 2003) makes epochs far from maximum light unlikely, because the SN should have become much fainter.

Since our spectrum was obtained on Jan 8, we estimate that the maximum

of the SN should have occurred between 2002 Oct 2 and 2003 Jan 8 (since the source was at $z = 1$). The exact epoch when the SN exploded depends crucially on the rise time (the time interval from the epoch of the explosion up to maximum light) of type-Ic SNe. The best documented cases are SN 1998bw and SN 1999ex. The latter (Stritzinger et al. 2002) reached B-band maximum ~ 18 days after the explosion, the former after ~ 16 days (Galama et al. 1998b) SN 1994I had a faster rise, reaching its maximum (in B) only 12 days after the explosion (Iwamoto et al. 1994). Adopting the latter value, we conclude that the SN exploded between $\sim$ Sep 11 and Dec 15, the later epochs being favored.

Photometry. In Fig. 3.1 we have superimposed to the light curve of the afterglow decay the light curve of SN 1994I (Lee et al. 1995), reported[2] at $z = 1.006$ and dereddened by $A_V = 2$ mag (Richmond et al. 1996). The K-correction has been computed from U-band data, considering that, at $z = 1.006$, the U-band roughly corresponds to the observed R band. The plot (solid line) shows that the luminosity at maximum of SN 1994I ($M_U = -18.9 \pm 0.3$ assuming $A_V = 2$; see Table 10 of Richmond et al. 1996) agrees very well with that of the bump ($M_U = -18.8 \pm 0.4$). We note that SN 1994I was significantly reddened, and its extinction was estimated to be $A_V = 1.4 \pm 0.5$ mag (Richmond et al. 1996). Note that we were forced to select the larger value of A_V to match the data, so that SN 2002lt was possibly somehow brighter than SN 1994I.

In the figure, a null time delay between the GRB and the SN explosion was used. Letting this delay free to vary did not significantly improve the fit (F-test chance probability of 36%); the best fit time delay is $t_{\rm GRB} - t_{\rm SN} = (-1.5 \pm 3)$ comoving days. Evidently the photometric observations provide a much tighter constraint on the SN-GRB delay. However the uncertainties above are only statistical, while systematics are more difficult to evaluate, especially in consideration of the paucity of observation of type-Ic SNe in their rising phase. Yet, the combination of our photometric and spectroscopic data provide evidence that the SN and the GRB explosions occurred within days from one another, at the most.

[2] At $z = 1.006$, the distance modulus is $\mu = 44.07$ mag.

3.5 Conclusions.

The detection of a broad (FWHM ~ 150 Å) absorption feature, in the spectrum of the 'bump', which we have identified with the Ca II H+K doublet (blueshifted by $\sim$ 15 000 km s^{-1}) suggests that the rebrightening of the GRB 021211 afterglow was powered by a SN. Assuming for this SN a spectroscopic and photometric behavior similar to that of SN 1994I, our data indicate that the SN and GRB explosion likely occurred almost simultaneuosly, or at most separated by a few days. The temporal coincidence between the SN and GRB 021211 holds for 'short' rise times, of the order of 10–12 days (as observed for SN 1994I; Iwamoto et al. 1994).

It is interesting to note that SN 1994I, the spectrum of which provides the best match to that observed in GRB 021211, is a typical type-Ic event rather than an hypernova, as the one proposed for association with GRB 980425, GRB 030329, GRB 031203 and GRB 060218 (Galama et al. 1998b; Stanek et al. 2003; Hjorth et al. 2003; Malesani et al. 2004; Pian et al. 2006). If SN 2002lt indeed shared the properties of SN 1994I, this would open the interesting possibility that GRBs may be associated with standard type-Ic SNe, and not only with the more powerful events. One caveat is that the recently studied SN 2002ap (Mazzali et al. 2002) shared some of the properties of hypernovae (e.g. a high expansion velocity), but was not significantly brighter than standard type-Ic SNe. Even if its pre-maximum spectra showed significantly broader lines than our case, this difference vanished after maximum, such that it may not be easy to distinguish between the two types of SNe. However, SN 2002ap had a broader light curve, and it was too faint in the U-band (Yoshii et al. 2003). It remains however not firmly estabilished whether GRB 021211 was associated with a standard type-Ic SN or with a "low-luminosity hypernova" similar to SN 2002ap. We last note that even if GRBs are indeed mainly associated with standard type-Ic SNe, the discovery of overluminous type-Ic events (like SN 1998bw) associated with GRBs is observationally favored, since the SN component can emerge and be observed at early times, when the transient is more frequently monitored. The case of SN 2002lt, however, outlines that variability may be present among GRB progenitors.

Chapter 4

Hypernova signatures in the late rebrightening of GRB 050525A

Albeit the four best-studied examples of SN/GRB connection (GRB 980425, GRB 030329, GRB 031203, and GRB 060218) clearly show that the associated SN were bright hypernovae, there is some evidence that the population of SNe associated with GRBs is more heterogeneous: several bumps have light curves which are well matched by SNe different from hypernovae (e.g. GRB 011121: Garnavich et al. 2003; Bloom et al. 2002b; GRB 021211: Della Valle et al. 2003a XRF 030723: Fynbo et al. 2004; GRB 020410: Levan et al. 2005; XRF 040701: Soderberg et al. 2005), rather than bright "hypernovae" such as SN 1998bw. Moreover, variations in the light curve shape has been observed in a few events. For example, the bump of GRB 041006 (Stanek et al. 2005) was found to have a significantly longer rise time than other events. On the contrary, SN 2006aj associated with GRB 060218 evolved much faster (Soderberg et al. 2006a; Pian et al. 2006; Modjaz et al. 2006; Sollerman et al. 2006; Mirabal et al. 2006; Cobb et al. 2006a; Ferrero et al. 2006). However, only spectroscopic observations can definitely assess the degree of diversity among GRB progenitors. Moreover, dust echos (e.g. Esin & Blandford 2000; Waxman & Draine 2000) can produce late-time rebrightenings resembling SN bumps, and spectroscopy is the most effective way to identify their nature. Despite the intense interest in detailing the diversity of GRB-SNe, only two *Swift* bursts with a clear SN association have been reported (namely, GRB 060218/SN 2006aj and GRB 050525A/SN 2005nc). This is very likely

due to the higher average redshift of *Swift* bursts ($\langle z \rangle = 2.8$; Jakobsson et al. 2006) compared with pre-*Swift* events. Actually, type-Ic SNe are deficient in flux at ultraviolet wavelength, due to heavy blancketting by metallic lines. Therefore, at $z \gtrsim 1$ (when the rest-frame UV enters the observed optical window) SNe becomes exceedingly faint to observe. Actually, only about 10% of the almost 100 *Swift* bursts have occured at redshift less than one. Thus, the discovery of low-redshift GRBs is a critical gateway for the study of GRB-SNe. In this chapter, I present observation of GRB 050525A at $z = 0.606$, showing the presence of a SN component at late epochs, as shown by Della Valle et al. (2006b). This SN was dubbed SN 2005nc (Della Valle et al. 2006c).

4.1 GRB 050525A

The long-duration GRB 050525A was discovered by the *Swift* satellite (Gehrels et al. 2004) on 2005 May 25.002 UT (Band et al. 2005). It was a bright event, with fluence $\mathcal{F} = (2.01 \pm 0.05) \times 10^{-5}$ erg cm^{-2} and duration $T_{90} = 8.8 \pm 0.5$ s. The burst was observed also by numerous other satellites (INTEGRAL: Götz et al. 2005; *Wind*: Golenetskii et al. 2005b), allowing for a detailed study of the high energy prompt emission spectrum. The optical afterglow was soon discovered by the ROTSE-III robotic telescope (Rykoff et al. 2005a), as a bright, fading source at $\alpha_{\rm J2000} = 18^{\rm h}32^{\rm m}32\overset{\rm s}{.}6$, $\delta_{\rm J2000} = +26^\circ 20' 23\overset{''}{.}5$ (Rykoff et al. 2005b). The optical and X-ray counterparts were also monitored in great detail by the X-Ray Telescope (XRT) and the Ultraviolet/Optical Telescope (UVOT) onboard *Swift* (Blustin et al. 2006). The brightness of the afterglow allowed an intense monitoring of this object, from optical (e.g. Klotz et al. 2005; Mirabal et al. 2005) to radio frequencies (Cameron & Frail 2005), including the first detection of a GRB at mid-infrared wavelengths (3.6 to 24 μm; Garnavich et al. 2005).

4.2 Observations and data analysis

A spectrum of the afterglow was obtained with the Gemini North telescope equipped with the GMOS instrument. The spectroscopic redshift was measured through both emission and absorption lines, yielding $z = 0.606$ (Foley et al. 2005; see also Fig. 4.1). This is at the low end of the GRB redshift

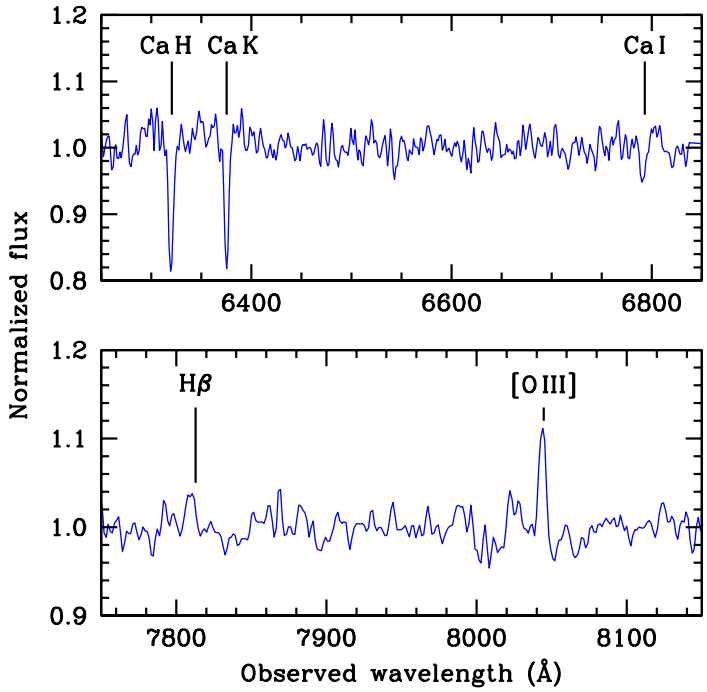

Figure 4.1: Normalized spectrum of the afterglow of GRB 050525A on 2005 May 25.4 UT, obtained on Gemini North with the GMOS instrument. Apart from clear absorption due to Ca H&K and Ca I, a few emission lines emerging from the host galaxy are also detectable.

distribution (Berger et al. 2005a; Bloom et al. 2003a; Jakobsson et al. 2006) and was the *Swift* long-duration GRB with the lowest redshift when it exploded (today, a handful of closeby events have been discovered). This event therefore offers a good opportunity for detailed analysis and modelling. We observed the optical afterglow of GRB 050525A with the VLT and TNG telescopes, during the period 2005 May – September (from a few hours up to > 100 d after the gamma-ray event, see Fig. 4.2). Data reduction was carried out following standard procedures. The photometric calibration was achieved by observing several standard star fields on different nights, yielding a zero-point accuracy of ≈ 0.02 mag. Photometric data (Fig. 4.2) show a flattening of the light curve at $R \sim 24$, starting about 5 d after the burst (observer rest frame) and lasting for about 20 d. The contribution of the host galaxy during this phase is $\lesssim 40\%$, as estimated from our late-epoch images which show the host magnitude is fainter than $R \sim 25$. The afterglow contribution,

as extrapolated from the earlier measurement, is negligible at these epochs ($< 3\%$ at 20 d after the GRB). This fact suggests that the flattening is powered by an additional source of energy. To further quantify this, we fitted the observed light curve including the contribution from the afterglow (a broken power law), the host galaxy, and a SN component:

$$F(t) = \frac{2F_{\rm b}}{[(t/t_{\rm b})^{\kappa\alpha_1} + (t/t_{\rm b})^{\kappa\alpha_2}]^{1/\kappa}} + F_{\rm h} + F_{\rm SN}[s(t-t_0)]. \qquad (4.1)$$

Here α_1, α_2 (the early- and late-time slopes) and $t_{\rm b}$ (the break time) characterize the afterglow decay (κ determines how sharp is the break). $F_{\rm h}$ and $F_{\rm SN}$ are the host galaxy and the SN flux, respectively. We allowed for a time offset t_0 between the SN and the GRB, for a temporal stretch s in the light curve, and for a magnitude difference. For the SN flux, we adopted the light curves of several type-Ic SNe (SN 1998bw: Galama et al. 1998b; SN 2002ap: Yoshii et al. 2003; Pandey et al. 2003b; Gal-Yam et al. 2002; Foley et al. 2003; SN 1994I: Richmond et al. 1996). Our approach is similar to that adopted by Zeh et al. (2004). The afterglow component is well fitted with $\alpha_1 = 1.1$, $\alpha_2 = 1.8$, and $t_{\rm b} = 0.3$ d. Interpreting the break as due to a jet effect, this value of $t_{\rm b}$ makes GRB 050525A consistent with the Ghirlanda relation (Ghirlanda et al. 2004; Nava et al. 2006). In Fig. 4.2, the solid line shows the best fit using SN 1998bw as a template, dimmed by 0.9 mag. The Galactic extinction towards GRB 050525A is $A_R = 0.25$ mag (Schlegel et al. 1998). The extinction inside the GRB host is uncertain. Blustin et al. (2006) suggest $E(B-V) \sim 0.1$ assuming an SMC extinction curve, so that the observed R band (roughly corresponding to the rest-frame B) suffers an additional $A'_R \sim 0.35$ mag. This implies that the SN associated with GRB 050525A may have a luminosity just about 0.3 mag fainter than SN 1998bw. However fits of comparable quality (both in terms of visual appearance and χ^2) can be obtained by assuming other SN templates. Figure 4.3 shows fits obtained with the hypernova SN 2002ap (brightened by 1.3 mag) and the standard type-Ic SN 1994I (brightened by 1.8 mag). Finally, we note that the best matches to the data points are obtained by allowing a time offset between a 1998bw-like SN and the GRB of ≈ 6 d (corresponding to ≈ 3.5 d in the GRB rest frame) or a time stretch factor $s = 0.7$. These fits reproduce the flat shape of the rebrightening. However, neither a simple stretch or a simple expansion provides a perfect description to the data. It looks that the bump associated with GRB 050525A raised fast to its maximum, and then evolved slowly, staying close to its maximum value. A more exotic scenario calls for

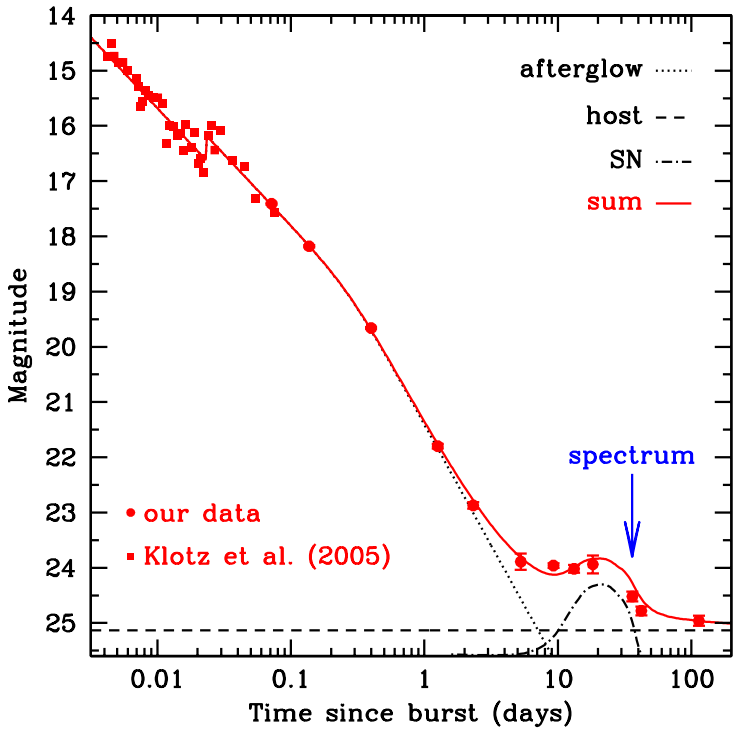

Figure 4.2: *R*-band light curve of the afterglow of GRB 050525A. Filled circles represent our observations (TNG, VLT). Squares are from Klotz et al. (2005), and were not included in the fit. The dotted, dashed and dot-dashed lines indicate the afterglow, the host galaxy, and the SN contributions, respectively.

the effect of a light echo. Indeed, sudden flattenings have been observed in the light curves of SNe due to the occurrence of light-echo components (e.g. Schmidt et al. 1994; Cappellaro et al. 2001) during the late SN decline. However in these cases the flattenings were characterized by much longer evolutionary time scales (∼700 d) than is observed for GRB afterglow bumps (∼ 10–20 d). In the SN 1991T echo-light, the spectrum at late stages was similar to that emitted by the SN at maximum light, although about 10 mag fainter. In our case, if the bump was due to an echo, we would expect to observe, in the spectrum obtained during the flattening, the signatures (at considerably fainter level of luminosity) of the very early optical afterglow. All of this indicates that a good set of photometric data *alone* may not constrain the SN type unambiguously. This task can be tackled only by means of spectroscopic observations (or, with reduced precision, studying colors).

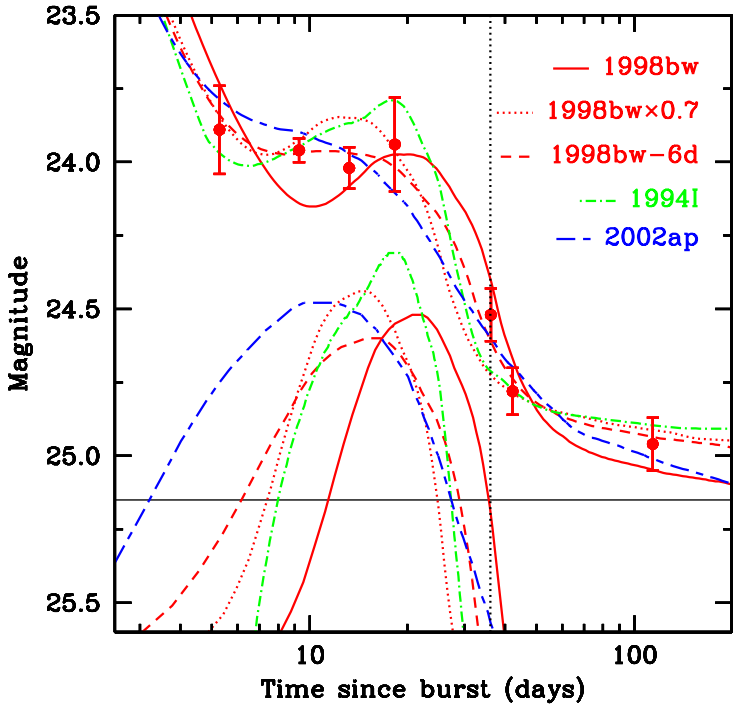

Figure 4.3: Fits to the data points by using different SN templates. The solid horizontal line shows the contribution of the host galaxy. The vertical dotted line represents the epoch of the spectrum.

4.3 Spectroscopy

A spectrum was obtained at the ESO VLT-UT1 with the FORS 2 instrument on 2005 Jun 28 (36 d after the burst, observer frame). The original spectrum (3×40 min integration) covered the range 5000–10000 Å with a resolution of ~ 20 Å. The extraction of the spectrum was performed inside the IRAF and MIDAS environments. This spectrum, shown in the rest-frame of the GRB as a grey line (Fig. 4.4), was smoothed with a 100 Å wide boxcar filter (blue line) and cleaned from the host galaxy emission features. As indicated by the light curve, this spectrum contains a significant contribution from the host galaxy. We thus subtracted from our spectrum a template of a blue star-forming galaxy (black line), normalized to the host brightness and $R-I$ color. The use of a template (average of 70 blue star-forming galaxies, from Cimatti et al. 2002), was necessary due to the faintness of the host galaxy. An unsuccessful attempt to get its spectrum with VLT was made

on 2005 Oct 1. This observation allowed us to set a robust upper limit to the magnitude of the host ($R = 25.2 \pm 0.1$). The use of a blue star-forming galaxy template is fully justified by several studies, which allow to conclude that GRB hosts belong to this type of systems (e.g. Djorgovski et al. 1998; Fruchter et al. 1999; Le Floc'h et al. 2003; Christensen et al. 2004). The prominent emission lines also confirm the starburst nature of the GRB 050525A host. The resulting spectrum (red line) is characterized by broad undulations resembling the spectra of SN 1998bw (Patat et al. 2001), obtained $\sim$ 5 d past maximum (green line). The best match is obtained by dimming SN 1998bw by $\Delta m \approx 0.9$ mag[1]. The bump at $\sim$ 5000 Å has some contribution from residuals of sky emissions that we were unable to remove. For comparison, we also show the spectrum of SN 1998bw $\sim$ 10 d past maximum (cyan line). Inspection of Fig. 4.4 reveals a poor match with the observed data, suggesting that SN 2005nc was not far from maximum when the spectrum was acquired. This result does not support the best fit to the photometric data, which suggested either a time lag between the SN and the GRB or a stretch factor < 1. Indeed, in these cases the spectrum would have been obtained about 10 d (rest frame) past maximum, which is excluded by spectroscopic observations (see Fig. 4.4). Spectra of SN 1994I (Filippenko et al. 1995) obtained close to maximum light also do not match the observed spectrum.

4.4 Discussion

Photometric and spectroscopic observations of the rebrightening associated with GRB 050525A support the idea that the bump was powered by an emerging SN (SN 2005nc). While photometric data alone are consistent (within the errors) with different SN morphologies (based on either SN 1998bw, SN 2002ap, or SN 1994I templates), the analysis of the spectrum obtained during the bump allowed us to select a SN akin to SN 1998bw as the best match, possibly dimmed by $\sim$ 0.3 mag. The flat shape of the bump light curve implies that SN 2005nc brightened relatively quickly after the GRB, with a rise time $\tau \sim$ 10–12 d in the B band (for SN 1998bw, $\tau_B \sim 14$ d). This can be explained either by introducing a significant stretch factor (< 1) or a time lag between the SN and the GRB. Both possibilities would imply

[1] The use of a template slightly brighter or fainter than $R = 25.2$ shifts the date of the best match with SN 1998bw by about 2 d later and earlier, respectively.

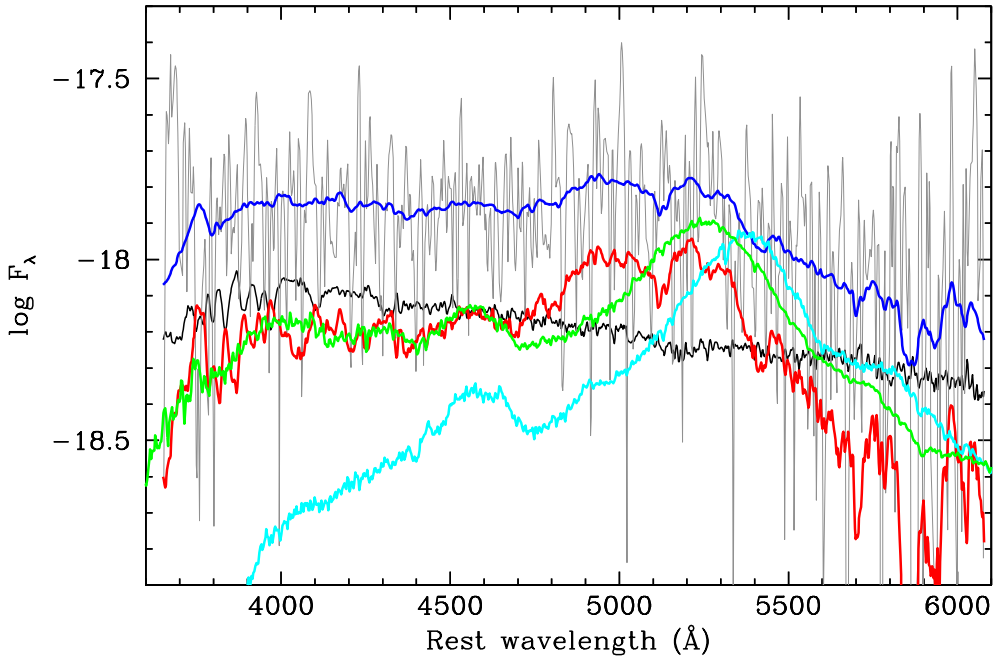

Figure 4.4: Grey line: observed spectrum of GRB 050525A, obtained during the bump. Blue line: rebinned spectrum. Black line: template spectrum for a blue starforming galaxy. Red line: subtracted spectrum (blue−black). Green line: spectrum of SN 1998bw 5d past maximum. Cyan line: spectrum of SN 1998bw 10 d past maximum.

that at the epoch of our spectrum (36 d after the GRB) the SN provided a very small contribution to the observed light. This is inconsistent with our spectroscopic observations, which suggest that the SN and the host galaxy had comparable brightness ($R \sim 25.2$) at that epoch. We thus conclude that SN 2005nc had a different light curve from the templates we adopted. Differences among GRB-SNe were noticed before the present study (e.g. Cobb et al. 2004). We find that the SN associated with 050525A had a faster rise than SN 1998bw, but that it was characterized by a broader, long-lasting maximum. On the other hand Maeda et al. (2006) showed that asymmetric SNe peak earlier if observed close to their polar axis. GRB 050525A was a bright event, likely observed on-axis. On the contrary, SN 1998bw may have been observed off-axis (Yamazaki et al. 2003), so that an earlier peak for SN 2005nc could be expected in this scenario. In spite of the putative existence of a broad range in the magnitudes at maximum of SNe associated

with GRBs, all GRB-associated SNe with clear spectroscopic confirmation (see Della Valle 2006a and Woosley & Bloom 2006 for reviews) appear to belong to the bright tail of the type-Ib/c SN population ($M_B \sim -19$). Whether this is the effect of an observational bias (which favors the spectroscopic observations of bright SNe) operating on a small number of objects, or whether it has a deeper physical meaning is not yet clear. GRB 050525A presents another case of association between a GRB and a bright hypernova, based on both robust photometric grounds and spectroscopic evidence.

Mean time (UT)	$t - t_0$ (d)	Telescope	Exp. time (s)	Seeing ($''$)	Magnitude (R band)
May 25.073	0.072	TNG+LRS	2×120	1.2	17.41±0.02
May 25.139	0.137	TNG+LRS	2×120	1.2	18.18±0.02
May 25.402	0.400	VLT+FORS2	6×120	1.1	19.66±0.02
May 26.262	1.260	VLT+FORS2	20×90	0.6	21.80±0.04
May 27.326	2.324	VLT+FORS2	20×90	0.4	22.87±0.06
May 30.280	5.278	VLT+FORS1	12×180	1.0	23.89±0.15
Jun 03.279	9.277	VLT+FORS2	10×180	0.4	23.96±0.04
Jun 07.242	13.240	VLT+FORS1	10×180	0.9	24.02±0.07
Jun 12.302	18.300	VLT+FORS2	10×180	0.6	23.94±0.16
Jun 30.155	36.153	VLT+FORS2	20×90	0.4	24.52±0.09
Jul 06.190	42.188	VLT+FORS2	10×180	0.4	24.78±0.08
Sep 07.121	105.119	VLT+FORS2	8×240	0.5	24.96±0.09

Table 4.1: Log of our R-band photometry.

Chapter 5

Messing up matters: no hypernova for GRB 060614

In the previous chapters evidence has been reported leading to an association between long-duration GRBs and core-collapse SNe. The best-studied cases have indicated that many GRBs are associated with hypernovae. These are defined as type-Ic (or -Ib) SNe with a large kinetic energy ($> 10^{52}$ erg) in the ejecta. This is usually revealed in the peculiar spectra of these objects: the large expansion velocities (up to 30 000 km s^{-1}) imply very wide absorption features. GRB-associated hypernovae are usually bright ($M_V \sim -19$), even if brightness alone is not the defining characteristic of a hypernova (see e.g. Mazzali et al. 2002). All the bumps in the sample of Zeh et al. (2004) could be fitted by a SN template with peak brightness within a factor of 2 from that of SN 1998bw. Hypernoave are associated with both bright, cosmological GRBS (such as GRB 030329 and GRB 050525A) and the faint ones like GRB 980425 and GRB 031203.

However, a few, puzzling cases looked different. Price et al. (2003) put limits for any SN associated with GRB 010921 to be fainter by 1.3 mag than SN 1998bw. More recently, using HST data, Soderberg et al. (2005) put a very strong limit for the X-ray flash XRF 040701 at $z = 0.2146$ (albeit the ligth curve was only sampled sparsely). Taking account possible extinction, a SN fainter than SN 1998bw by 3.3 mag was required. Howewer, no bright optical counterpart was discovered for this burst, leaving the identification somehow less certain. Furthermore, the lack of any optical emission leaves open the possibility of significant dust obscuration, which would hide both the afterglow and the SN (e.g. Mannucci et al. 2003). Recently, Fynbo et

al. (2006) reported limits for GRB 060505 at $z = 0.089$, corresponding to a SN fainter than SN 1998bw by at least 6 mag. The above evidence cases has opened the interesting possibility that also faint SNe can accompany GRBs.

In this chapter, I will present a strong case of long-duration GRB with deep limits on the associated SN. In particular, thanks to the optical and X-ray observations, the local extinction can be constrained to be very small. This material has been presented by Della Valle et al. (2006d, see also Fynbo et al. 2006; Gal-Yam et al. 2006).

5.1 GRB 060614

GRB 060614 was a long-duration GRB detected by the *Swift* satellite. Its X-ray and optical afterglows were promptly discovered by the XRT and UVOT telescopes (Parsons et al. 2006; Mangano et al. 2006) onboard *Swift*. Emission lines in the optical spectrum allowed to measure its relatively low redshift $z = 0.125$ (Price et al. 2006b). This fact makes GRB 060614 one of the closest GRBs ever discovered and, therefore, particularly suitable for studying the associated SN. Also, its host galaxy is very faint, so that any SN component should easily emerge. We obtained spectra of the host galaxy with the European Sourhern Observatory (ESO) 8.2m Very Large Telescope (VLT). Nebular emission lines are apparent (Fig. 5.1), indicating that star formation is currently ongoing. From the Hα flux (3.9×10^{17} erg cm^{-2} s^{-1}) we infer a low value for the star formation rate (1.3×10^{-2} $M_\odot$ yr^{-1}), after adopting the conversion factor of Kennicutt (1998). The flux was computed by normalizing the spectrum to the R-band photometry. Given the faintness of the galaxy ($M_B \approx -15.55$), however, the specific star formation rate ($2\,L/L^*\,M_\odot$ yr^{-1}, assuming $M_B^* = -21$) is non negligible, and implies that young, massive stars were present in the galaxy. This value is at the faint end of the distribution found for long-duration GRB hosts (Christensen et al. 2004). From the detected emission lines, we measure a redshift $z = 0.1255 \pm 0.0005$, confirming the value suggested by Price et al. (2006b). From the limits on [N II] and the observed flux of [O III] we infer a metallicity larger than $\sim 1/20$ solar.

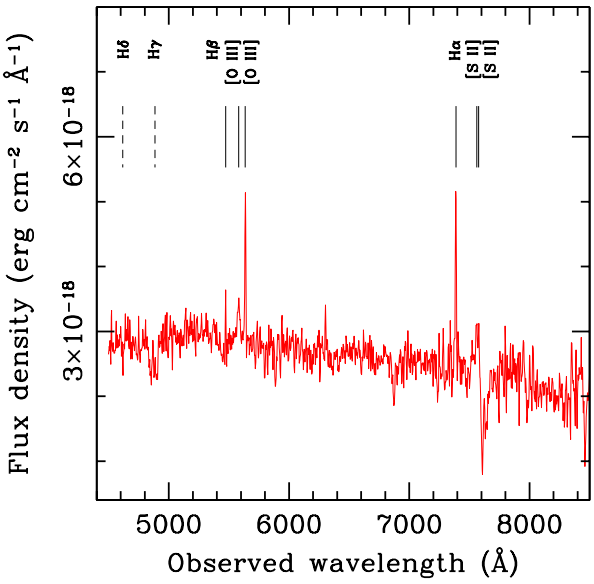

Figure 5.1: Spectrum of the host galaxy of GRB 060614. This is the average of several spectra taken during the period 2006 June 20 – Jul 30 with VLT equipped with FORS2 (see the observation log in Table 5.2. A few lines used to measure the redshift are indicated (solid vertical bars). The Hγ and Hδ lines are seen in absorption (dashed vertical bars).

5.2 Light curve monitoring

Starting from 15 hr after the burst, we monitored the light curve of the GRB optical transient with VLT + FORS 1. Adopting the same instrument allowed to obtain an accurate relative photometry (particularly important in case of galaxies with emission lines). Large apertures were adopted in order to include all the flux from the host galaxy even with variable seeing. Flux calibration was achieved by observing several Landolt standard fields.

Surprisingly enough, deep observations obtained in the R band (corresponding to the V band in the GRB rest frame) up to 48 days after the burst did not reveal the emergence of a SN component (Fig. 5.2), as observed in a number of nearby and cosmological GRBs (Zeh et al. 2004). Our data are consistent with no SN contribution at all (blue line). The best fit (χ^2/dof = 15.3/19) is given by the sum of an afterglow component plus the host galaxy, with the afterglow being described by a broken power law (a

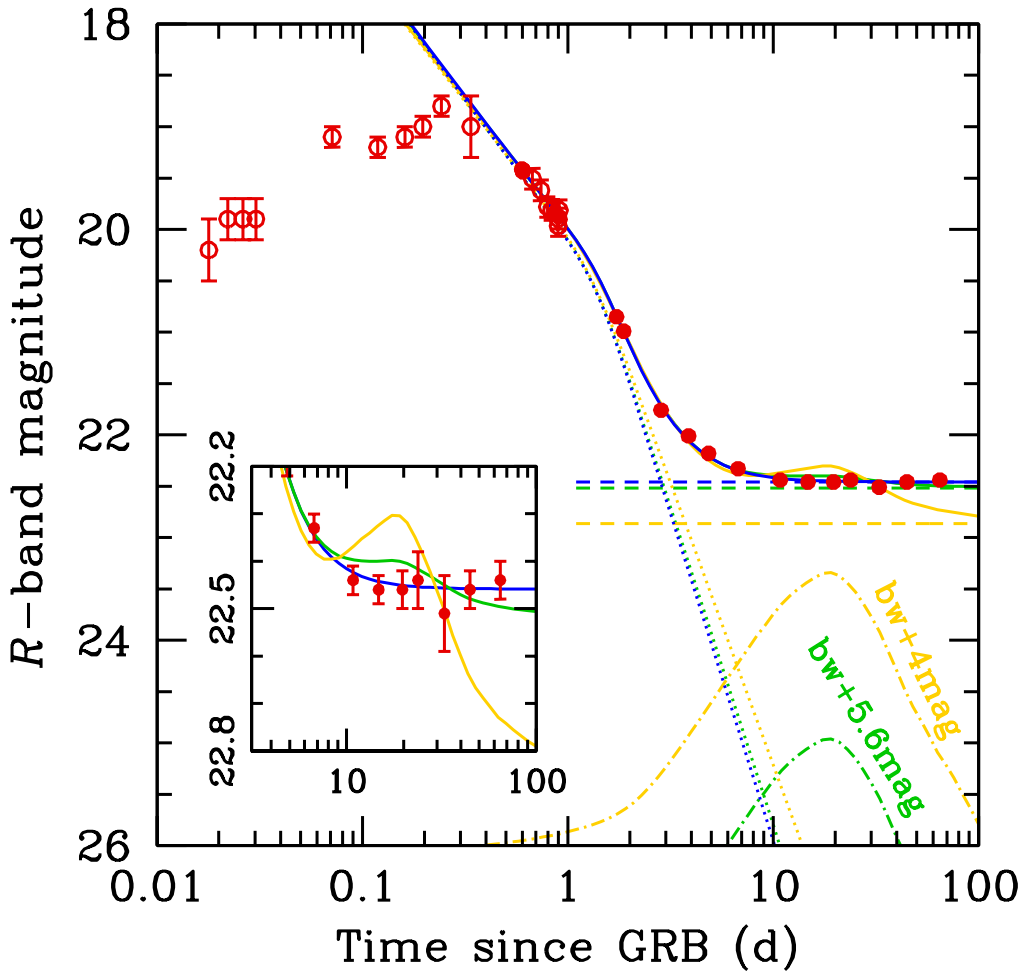

Figure 5.2: R-band light curve of the GRB 060614 afterglow. Empty circles show data from the literature (not used in the fits; Schmidt et al. 2006; French et al. 2006; Thöne et al. 2006; Fynbo et al. 2006) while filled points represent our VLT data (Table 5.1). Different linestyles represent the various components: the afterglow (dotted lines), the host (dashed lines) and a SN akin to SN1998bw but rescaled in flux (dot-dashed lines). Solid lines show their sums. The different colors correspond to different contributions from the SN: no contribution (blue), a SN fainter by 5.3 mag (green), and a SN fainter by 4 mag (yellow). The green model corresponds to the brightest SN allowed by our data, $M_V > -13.7$, at the 3-σ level. The yellow model is clearly inadequate and is put only for visualization purposes. The inset shows a zoomed version of the epochs around the putative SN maximum.

single power law provides an unacceptable fit with $\chi^2/\mathrm{dof} = 565/21$). The best fit yields decay slopes $\alpha_1 = 1.08 \pm 0.03$ and $\alpha_2 = 2.48 \pm 0.07$, respectively before and after the break time $t_{\mathrm{break}} = 1.38 \pm 0.04$ days.

Addition of a SN component did not improve the fit. Adopting as a template the light curve of SN 1998bw (Galama et al. 1998b; McKenzie & Schaefer 2000), we constrain the brightness of a SN associated with GRB 060614 to be at least 5.3 mag fainter than the template (3-σ limit; green lines in Fig. 5.2). This corresponds to a peak absolute magnitude $M_V > -13.7$ ($M_V > -13.1$ at the 2-σ level). Similar limiting magnitudes are obtained adopting different SN light curve templates, such as SN 2006aj (Soderberg et al. 2006a; Pian et al. 2006; Modjaz et al. 2006; Sollerman et al. 2006; Mirabal et al. 2006; Cobb et al. 2006a; Ferrero et al. 2006). A brighter SN (yellow lines in Fig. 5.2) would provide a totally inadequate fit. The faintness of a possible SN at optical wavelengths was further confirmed by a series of ~ 10 spectra obtained at the VLT in the range 4000–8000 Å between 2006 June 15 and July 30. None of them shows the broad undulations typical of SNe.

Such faintness cannot be due to dust extinction. First, the afterglow optical spectra are not particularly red. The afterglow is also bright in the ultraviolet (Mangano et al. 2006; Brown et al. 2006), where extinction would be more severe. X-ray spectra show also little absorbing material along the line of sight (yielding a rest-frame $N_{\mathrm{H}} < 2 \times 10^{20}$ cm^{-2} at 90% confidence level). Fig. 5.3 shows the optical/X-ray spectral energy distribution. Optical data were reported at the common epoch $t = 1.73$ days after the burst (the time around which our measurements cluster) using the best-fit light curve. After correcting for the Galactic extinction ($A_V = 0.07$ mag), the optical spectrum is well fit by a power-law ($F_\nu \propto \nu^{-\beta}$) with index $\beta = 0.94 \pm 0.08$ (dashed line). At the same time, the X-ray spectrum is described by a power law with index $\beta = 0.77 \pm 0.11$ (Mangano et al. 2006). Visual inspection shows that the optical and X-ray data belong to the same power-law segment. Assuming an SMC-like extinction curve, to make the optical data match the X-ray flux an amount of extinction $A_V = 0.07$ mag is required. Since the rest-frame V band corresponds to the observed R band, this is also the amount of extinction suffered by our measurements. Assuming different extinction curves, the absorption corresponding to the observed R band does not change significantly and is always less than $A_R < 0.1$ mag. The total extinction is thus constrained to be $\lesssim 0.2$ mag. Allowing for such amount of extinction, we thus refine our limit for the SN peak magnitude $M_V > -13.9$ (3-σ).

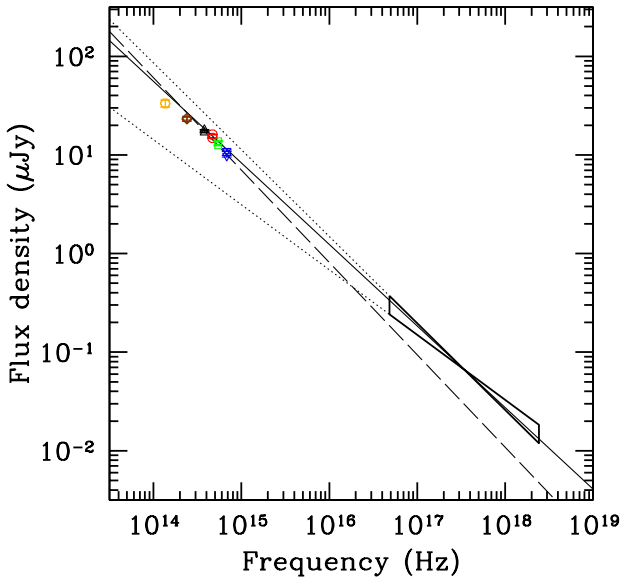

Figure 5.3: Broad-band spectral energy distribution of the afterglow of GRB 060614 at $t = 1.7$ days after the burst. The dashed line shows the extrapolation of to optical data to the X-ray band, assuming no extinction in the host. Adding small dust in the GRB frame ($A_V = 0.07$ mag) the extrapolation of optical data matches perfectly the X-ray slope and normalization.

5.3 Discussion

The inferred value for the SN peak brightness is very faint, more than an order of magnitude fainter than observed in SN 2002ap (Mazzali et al. 2002), one of the weakest hypernovae ever recorded ($M_V \sim -17$). Moreover, had the progenitor been a hypernova, its expected colour at maximum light would have been $\langle B - V \rangle \sim 0.5 \pm 0.1$, as measured in well-observed events such as SN 2006aj (Ferrero et al. 2006), SN 2002ap (Foley et al. 2003) and SN 1998bw (Galama et al. 1998b), as well as several type-Ib/c SNe. From the tables provided by Romaniello et al. (2002), we find that such color corresponds to an effective temperature $T_{\rm max} \sim 6\,500$ K, which, combined with the lower limit to the absolute magnitude, provides a strict upper limit to the bolometric luminosity, at maximum light, $L < 1.2 \times 10^{41}$ erg s^{-1}. Therefore the radius of the emitting region is bound to be $R \sim \sqrt{L/(4\pi\sigma_{\rm T}T^4)} < 3 \times 10^{14}$ cm (where $\sigma_{\rm T}$ is the Stefan-Boltzmann constant). Since the rising times to max-

imum light of type-Ib/c SNe range between 10 and 20 days (Hamuy 2003; Panagia 2003) in the V band, the upper limit to the radius implies an upper limit to the expansion velocity in the range 1 700–3 500 km s^{-1}. This value is an order of magnitude smaller than observed in SNe associated with GRBs, and definitely excludes the possibility that a hypernova was associated with GRB 060614. One caveat about this interpretation concern, of course, the temperature of the ejecta. If little ^{56}Ni was produced for this event (as suggested by the low luminosity), little heating was provided to the ejecta. In this case, the radius might have been larger, allowing a high expansion velocity. Lacking direct information on the SN colors, this possibility cannot be excluded.

In any case, our data do not allow us to rule out a different kind of core-collapse SN progenitor for GRB 060614, although so far only type-Ib/c events have been clearly associated with GRBs. The low expansion velocity and the faint luminosity implied for a possible SN progenitor are reminiscent of a class of very faint core-collapse SNe recently discovered in the local Universe (Pastorello et al. 2004). They are of type II, have absolute magnitudes at maximum in the range $-13 > M_V > -15$, and show very small expansion velocities ($\sim$ 1000 km s^{-1}). The properties of such objects may well be consistent with the available data on GRB 060614. Actually, if the progenitor was a type-II SN, adopting their typical color at maximum light $B-V \sim 0$ (corresponding to $T \sim 10\,000$ K), we would derive an even smaller upper limit to the expansion velocity, in the range 750–1500 km s^{-1}. This is indeed similar to what has been observed for these faint core-collapse events (Pastorello et al. 2004).

Faint type-II SNe have been interpreted in terms of collapse of massive stars with an explosion energy so small that most of ^{56}Ni falls back onto the compact stellar remnant (Nomoto et al. 2004; so-called fallback SNe). Such SNe share properties with the present case, both for the observational characteristics and for originating from a black hole (which is believed to be necessary for the production of a GRB). However, the possibility that such SN progenitors are able to power GRBs has still to be explored by the theoretical modelling. In particular, the hydrogen stellar envelope would need to be absent for the relativistic jets to emerge out of the star surface. This might thus be an example of a type-Ib/c fallback SN. More exotic scenarios, in which long-duration GRBs are not directly produced by a SN explosion cannot be excluded by our data (though they are not required). For example, scenarios in which the SN precedes the GRB event (Vietri & Stella 1998) are

compatible with our data. Also a binary merger mechanism (Belczyński et al. 2002), similar to that proposed to power short GRBs, or some type of collapsars model (Woosley et al. 2003), are not expected to produce a SN.

The gamma-ray energy of GRB 060614 ($E_{\rm iso} \sim 10^{51}$ erg) is within the distribution observed for other GRBs, albeit towards its faint end. So it is possible that a significant fraction of GRBs also observed at high redshift are associated with faint, low-velocity SNe. The properties of the relativstic ejecta of GRB 060614 look overall similar to those of classical GRBs rather than to short nearby events akin to GRB 980425, even if this may be a "bridging" event.

The available data clearly indicate that, if a SN was associated with GRB 060614, it was, at optical wavelengths, at least 100 times fainter than SNe found so far connected with GRBs. The corresponding maximum bolometric luminosity is an order of magnitude fainter than observed in the dimmest hypernovae ever recorded. The expansion velocity would be lower than 3 500 km s^{-1}. All together these results challenge the commonly accepted scenario, in which GRBs are produced by SN explosions characterized by very high expansion velocities of the ejecta ($\sim$ 30 000 km s^{-1}), and exceptionally high luminosities at maximum light. Not all long-duration GRBs are produced in such a way.

5.3.1 A chance coincidence?

The peculiar properties of GRB 060614, namely the lack of a bright hypernova, have led some authors to investigate whether GRB 060614 was really at redshift $z = 0.1255$. In fact, no absorption lines are present in the burst spectrum, and the redshift could be computed only for the host galaxy. It is possible, in principle, that the galaxy at $z = 0.1255$ is a foreground object, by chance aligned with the GRB. Schaefer & Xiao (2006) have computed the pseudo-redshift of GRB 060614 using several indicators based on gamma-ray properties alone, finding $1.44 < z < 2.8$ (1-σ confidence level), a value larger than inferred from the galaxy emission lines. The actual redshift is constrained to be lower ($z < 1.1$), since the aterglow has been detected by *Swift*/UVOT in the ultraviolet UVW2 filter (centered at 1930 Å). At such a redshift, the lack of a SN would be less surprising. They also computed the probability of a chance association between the GRB and a foreground galaxy, also taking in mind the other case of "SN-less GRB" (GRB 060505; Fynbo et al. 2006), finding a probability $P = 0.8\%$. A similar estimate

was achieved by Cobb et al. (2006b), who found $P \approx 1\%$ by computing the fraction of the sky covered by galaxies as bright as the one associated with GRB 060614. Although such probabilities are small, the *Swift* sample, which is now composed by more than 100 events, may suffer from this problem.

Although the issue of a chance association between GRBs and foreground objects is surely relevant for the *Swift* sample, it is of course hard to provide a conclusive statement for individual cases. There are, however, arguments against a chance association for the specific case of GRB 060614. First, the probability computed by Schaefer & Xiao (2006) assumed a maximum offset between the GRB and the host galaxy as large as $4\farcs3$. This is the separation between the optical afterglow of GRB 060605 and the center of its host galaxy[1] (Fynbo et al. 2006). This offset is much larger than in the case of GRB 060614, where the separation is less than $1''$. The corresponding probability is thus significantly reduced for this event. Furthermore, Gal-Yam et al. (2006) performed a similar analysis to that carried out by Cobb et al. (2006b) using HST photometry. In these space-born images, the fraction of the sky occupied by galaxies is reduced due to the lack of the blurring effect of the atmosphere, again leading to a smaller chance association probability.

The most important piece of information arguing against a chance association is the lack of a host galaxy in deep HST images at the position of the optical afterglow (apart from the galaxy at $z = 0.1255$). This would be quite exceptional for a GRB host galaxy at $z < 1$ (as imposed by the UVOT detection). Gal-Yam et al. (2006) have performed simulations, showing that only one out 30 GRB host galaxies detected by HST would have been missed in the GRB 060614 images if put at $z = 1$. Indeed, there are a few cases where a foreground galaxy has been observed close to the GRB afterglow, but in all these cases also the GRB host galaxy has been detected (see e.g. Fig. 5.4).

Last, the gamma-ray properties of this event are also puzzling. The burst was composed by an initial hard spike lasting ~ 5 s, followed by a softer, long-lasting emission which comprises $\sim 80\%$ of the burst fluence. A striking feature is the very small spectral lag measured for this event (Gehrels et al. 2006). Such small lags have been never observed in long-duration GRBs, and are typical of short events. Therefore, albeit this burst is for sure a long-

[1]It should be noted, however, that the afterglow of GRB 060605 was lying right in the middle of a star-forming region at the same redshift of the main part of the galaxy, so that the chance association probability is somehow reduced.

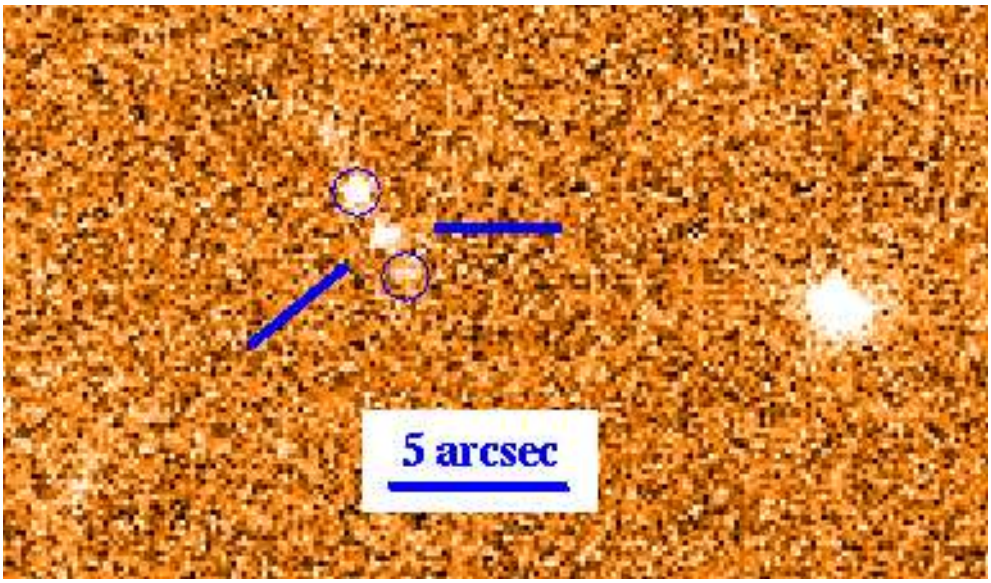

Figure 5.4: The field of the long-duration GRB 060418 as imaged by VLT in the J band. The host galaxy is marked by the solid lines, and closeby objects are indicated by circles. Such objects are very likely the foreground sources responsible for the intermediate-redshift strong absorption systems seen in the afterglow spectra (Ellison et al. 2006). These objects are perfect examples of chance association between the afterglow and foreground objects. However, the GRB host galaxy is clearly visible and distinguishable from the other ones, allowing to single out the correct association.

duration event, it has also peculiar properties. Therefore, it is not surprising that also the associated SN is peculiar.

Mean date (UT)	$t - t_0$ (days)	Filter	Exposure (s)	Seeing ($''$)	Instrument	Magnitude
2006 Jun 16.27492	1.74450	B	4×90	0.60	VLT+FORS1	21.72±0.02
2006 Sep 02.05099	79.52057	B	10×120	1.30	VLT+FORS1	23.62±0.15
2006 Jun 16.25076	1.72034	V	2×120	0.55	VLT+FORS1	21.20±0.01
2006 Jun 17.36557	2.83515	V	4×90	0.50	VLT+FORS1	22.16±0.02
2006 Jun 18.39119	3.86077	V	6×180	0.80	VLT+FORS1	22.47±0.02
2006 Jul 08.33006	23.79964	V	2×120	1.20	VLT+FORS1	22.75±0.07
2006 Jul 17.31686	32.78644	V	5×120	1.10	VLT+FORS1	22.74±0.09
2006 Jun 15.12757	0.59715	R	1×20	2.44	VLT+FORS2	19.41±0.03
2006 Jun 15.12927	0.59885	R	1×60	2.41	VLT+FORS2	19.42±0.02
2006 Jun 15.13031	0.59989	R	1×60	2.39	VLT+FORS2	19.41±0.02
2006 Jun 15.13136	0.60094	R	1×60	2.37	VLT+FORS2	19.43±0.02
2006 Jun 15.13242	0.60200	R	1×60	2.35	VLT+FORS2	19.43±0.02
2006 Jun 15.13355	0.60313	R	1×60	2.33	VLT+FORS2	19.42±0.02
2006 Jun 15.13460	0.60418	R	1×60	2.31	VLT+FORS2	19.44±0.02
2006 Jun 15.13566	0.60524	R	1×60	2.29	VLT+FORS2	19.43±0.02
2006 Jun 15.13672	0.60630	R	1×60	2.27	VLT+FORS2	19.43±0.02
2006 Jun 15.40052	0.87010	R	1×10	1.16	VLT+FORS2	19.83±0.03
2006 Jun 15.43038	0.89996	R	1×60	1.22	VLT+FORS2	19.87±0.02
2006 Jun 16.25625	1.72583	R	2×120	1.22	VLT+FORS1	20.85±0.01
2006 Jun 16.40016	1.86974	R	2×120	0.45	VLT+FORS1	20.99±0.01
2006 Jun 17.37241	2.84199	R	2×120	0.50	VLT+FORS1	21.76±0.02
2006 Jun 18.39941	3.86899	R	6×180	0.65	VLT+FORS1	22.01±0.02
2006 Jun 19.37407	4.84365	R	2×180	0.50	VLT+FORS1	22.18±0.04
2006 Jun 21.27125	6.74083	R	3×180	0.60	VLT+FORS1	22.33±0.03
2006 Jun 25.34483	10.81441	R	2×300	0.90	VLT+FORS1	22.44±0.03
2006 Jun 29.30301	14.77259	R	11×180	0.50	VLT+FORS1	22.46±0.03
2006 Jul 04.20860	19.67818	R	6×240	0.60	VLT+FORS1	22.46±0.04
2006 Jul 08.33536	23.80494	R	2×120	1.40	VLT+FORS1	22.44±0.06
2006 Jul 17.32709	32.79667	R	3×180	1.10	VLT+FORS1	22.51±0.08
2006 Jul 29.26643	44.73601	R	5×240	0.90	VLT+FORS1	22.46±0.04
2006 Aug 18.23409	64.70367	R	12×300	0.60	VLT+FORS1	22.44±0.04
2006 Jun 16.26278	1.73236	I	3×120	0.55	VLT+FORS1	20.49±0.01
2006 Jun 17.37868	2.84826	I	3×120	0.43	VLT+FORS1	21.25±0.02
2006 Jun 18.38882	3.85840	I	4×300	0.75	VLT+FORS1	21.50±0.02
2006 Jul 08.34050	23.81008	I	2×120	1.10	VLT+FORS1	21.70±0.06
2006 Jul 17.33614	32.80572	I	3×180	0.95	VLT+FORS1	21.76±0.07
2006 Jun 15.30022	0.76980	J	15×60	1.20	NTT+SofI	18.51±0.02
2006 Jun 15.28454	0.75411	K	8×60	1.15	NTT+SofI	17.23±0.07
2006 Jun 15.29074	0.76032	K	7×60	1.15	NTT+SofI	17.26±0.08
2006 Jun 16.20839	1.67797	K	10×60	1.10	NTT+SofI	18.18±0.09

Table 5.1: Observation log of our VLT observations. t_0 is the GRB trigger time (2006 Jun 14.53042 UT).

Date (UT)	$t - t_0$ (days)	Grism	Exp. time (s)	Instrument
2006 Jun 15.4161	15.42	300V	5×360	VLT+FORS2
2006 Jun 16.3132	16.31	300V	5×600	VLT+FORS1
2006 Jun 21.3645	21.36	300V	2×1500	VLT+FORS2
2006 Jun 23.4210	23.42	300V	1×1500	VLT+FORS2
2006 Jun 30.2940	30.29	300V	3×2400	VLT+FORS2
2006 Jul 23.1921	38.19	300V	5×2700	VLT+FORS2
2006 Jun 30.2234	45.22	300V	2×2700	VLT+FORS2
2006 Jun 31.2046	46.20	300V	2×2700	VLT+FORS2

Table 5.2: Observation log of our VLT spectroscopic observations. t_0 is the GRB trigger time (2006 Jun 14.53042 UT). All spectra taken after Jun 20 were used to create the average shown in Fig. 5.1, when the afterglow contribution was $< 10\%$.

Chapter 6

The short/hard GRB 050709 in a star-forming galaxy

The great progress in the understanding of long-duration GRBs has been largely due to the discovery of their broad-band afterglows. First, optical spectra have allowed to measure their redshifts, and hence to infer the distance scale and energetics. Second, the precise localizations had pinpointed the GRB host galaxies, thus allowing the study of the enviroments inside which GRB progenitors were born. The final clue to the origin of long-duration bursts has arrived with the discovery of the "smoking guns", the distinct SN signatures observed in afterglow light curves and spectra.

Until recently, however, no comparable advance could be achieved for short GRBs. In fact, until 2005, these events have remained undetected at wavelengths other than gamma-rays. The *Beppo*SAX Wide-Field Camera could never localize a short burst, likely bacause of its small field-of-view and the spectral hardness of the events. No real-time trigger could thus be provided. The Interplanetary Network could provide only delayed, poorly-constrained positions. The HETE-II satellite, in principle capable to detect short bursts, provided very few triggers (e.g. Lamb et al. 2003), leading to no convincing afterglow discovery (Klotz et al. 2003; Hurley et al. 2002; Castro-Tirado et al. 2002). The only evidence for long-lasting emission was provided by Lazzati et al. (2001), which coadded the light curves of a large number of BATSE GRBs, and found excess soft emission in the first ~ 100 s. This was also confirmed by performing a similar procedure on the short burst detected by the *Beppo*SAX Gamma-Ray Burst Monitor (Montanari et al. 2005).

The breakthrough, similar to what happened for long-duration GRBs, ar-

rived in 2005, with the discovery of short GRB afterglows at X-ray, optical, and radio wavelengths. This was indeed one of the main goals of *Swift*, which was spectacularly achieved. With a bit of irony, HETE-II also started providing good triggers. The first short burst detected by *Swift* (GRB 050202; Tueller et al. 2005) was unluckily too close to the Sun to be observed, but the following one was not missed. A very weak X-ray afterglow for GRB 050509B was discovered by *Swift*-XRT. Albeit just few photons were collected, this was enough to pinpoint with a decent accuration the source position (Gehrels et al. 2005). Remarkably, a bright, elliptical galaxy at $z = 0.2248$ was lying $\sim 11''$ away (40 kpc at that redshift; Bloom et al. 2006a; Hjorth et al. 2005b; Castro-Tirado et al. 2005). The chance association probability, albeit computed a posteriori, is low enough to suggest a physical relation between the two objects. However, despite intense efforts, no optical emission was discovered for this faint event. However, there was no need to wait much. A few months later, two bursts displayed, for the first time, an optical (GRB 050709: Villasenor et al. 2005; Fox et al. 2005b; Hjorth et al. 2005a; Covino et al. 2006) and radio (GRB 050724: Barthelmy et al. 2005a; Berger et al. 2005b) afterglow. Here I report observations of the optical afterglow and host galaxy of GRB 050709, the first short GRB presenting detected optical emission and the first case with an unquestionable associated host galaxy. This material has been presented in Covino et al. (2006)

6.1 GRB 050709

GRB 050709 was discovered by HETE-II on 2005 Jul 9.94209 UT (Villasenor et al. 2005). Its prompt emission consisted of a single pulse lasting 70 ms in the 3–400 keV energy band, followed by a weaker, soft bump ~ 100 s long. This second episode may be due to the afterglow onset (Villasenor et al. 2005), or to flaring activity (Barthelmy et al. 2005a; King et al. 2005; Perna et al. 2006). Indeed, such soft, delayed emission seems common among short GRBs (Lazzati et al. 2001; Barthelmy et al. 2005a,b). In any case, the prompt emission properties are consistent with those of a short/hard GRB (see also Donaghy et al. 2006a).

Follow-up observations with the *Chandra* X-ray observatory revealed a faint, uncatalogued X-ray source inside the HETE-II error circle (Fox et al. 2005a). At the coordinates $\alpha_{J2000} = 23^{h}01^{m}26\overset{s}{.}9$, $\delta_{J2000} = -38°58'39\overset{''}{.}5$ ($0\overset{''}{.}4$ error), it was coincident with a pointlike object embedded in a bright galaxy

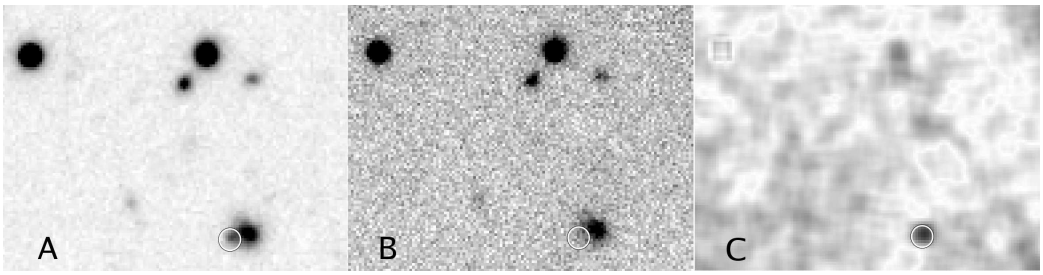

Figure 6.1: R-band image of the field of GRB 050709, on 2005 Jul 12.41 (A) and 20.42 (B). Panel C shows the result of the subtraction, evidencing a fading source coincident with the *Chandra* counterpart (circle). The boxes cover a region $30'' \times 20''$ wide.

(Jensen et al. 2005) at $z = 0.16$ (Price et al. 2005a). The variability of this source led Price et al. (2005b) to propose it as the optical counterpart of GRB 050709.

6.2 Observations and data analysis

We observed the field of GRB 050709 with the ESO Very Large Telescope (VLT), using the FORS 1 and FORS 2 instruments. In our first images, taken on 2005 Jul 12, the pointlike object reported by Jensen et al. (2005) was clearly visible in the V and R bands (Fig. 6.1). Its coordinates are $\alpha_{\rm J2000} = 23^{\rm h}01^{\rm m}26\overset{\rm s}{.}96$, $\delta_{\rm J2000} = -38^\circ 58' 39\overset{''}{.}3$ ($0\overset{''}{.}25$ error), fully consistent with the *Chandra* position. The object lies inside a bright galaxy ($\approx 1\overset{''}{.}2$ away from its nucleus), whose magnitudes are $V = 21.35 \pm 0.07$, $R = 21.08 \pm 0.07$, and $I = 20.63 \pm 0.08$. To search for brightness variations, we monitored the field at several epochs. Data analysis was performed by adopting a subtraction technique (Alard & Lupton 1998), well suited to identify variable objects even when blended with nearby sources. The pointlike object was found to be variable (at the $\sim 10\sigma$ level), being undetectable from Jul 14 onwards. This confirms the independent finding of Hjorth et al. (2005a). Magnitudes of the variable source were computed assuming a negligible flux in the reference epoch (see Table 6.1). Photometry of the transient was performed by inserting artificial stars of known brightness and calibrated by observing Landolt standard fields.

On Jul 30 we took medium-resolution spectra of the host galaxy. Obser-

Date (UT)	**Instrument**	**Exp.** (min)	**Filter**	**Magnitude**
2005/07/12 09:44	FORS 2	6	V	24.38 ± 0.10
2005/07/14 07:21	FORS 1	6	V	> 25.00
2005/07/20 10:16	FORS 1	6	V	(reference)
2005/07/30 02:37	FORS 2	9	V	> 25.20
2005/07/12 09:57	FORS 2	5	R	23.83 ± 0.07
2005/07/20 10:07	FORS 1	6	R	(reference)
2005/07/30 02:54	FORS 2	50	R	> 25.00
2005/07/12 09:32	FORS 2	10	I	> 23.25
2005/07/14 07:32	FORS 1	5	I	> 24.10
2005/07/18 06:38	FORS 1	20	I	(reference)
2005/07/30 04:10	FORS 2	9	I	> 23.50

Table 6.1: Observation log and photometry of the transient source. Errors are at the 1σ confidence level, while upper limits are at 3σ. Data were not corrected for Galactic extinction. Only upper limits could be derived in the I band due to the poorer image quality. The epoch indicated as reference was assumed to contribute negligible flux from the object.

vations were carried out with the FORS 2 instrument at the VLT-UT1, with the 300V grism, covering the wavelength range 6000–9200 Å (6 Å FWHM). From the detection of several emission lines, among them Hα, Hβ, and [O II], we derived a redshift $z = 0.1606 \pm 0.0002$. This is consistent with the results of Fox et al. (2005b). Therefore, the rest-frame B-band luminosity of the host is $L_B \sim 3.5 \times 10^{42}$ erg s^{-1} ($\sim 0.10 L_*$, assuming $M_B^* = -20.13$ as determined from the SDSS survey; Blanton et al. 2003) and the candidate afterglow lies at a projected distance of ≈ 3.3 kpc from the galaxy core.

6.3 Discussion

The chance probability of finding a galaxy brighter than $R = 21.08$ within $1\farcs2$ of the X-ray and optical afterglow candidate is small ($P \sim 4 \times 10^{-4}$; McCracken et al. 2003), thus indicating a physical association between the two objects. On the other hand, the probability of detecting a serendipitous X-ray source inside the SXC error circle with a flux larger than the *Chandra* source is non-negligible ($P \sim 0.10$; Moretti et al. 2003). However, due to

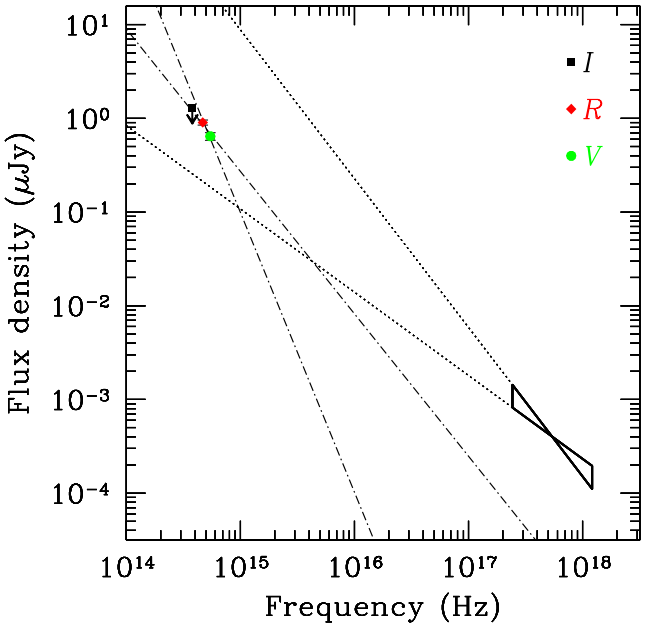

Figure 6.2: Spectral energy distribution of the afterglow of GRB 050709 on Jul 12.4 UT. The bow-tie shaped region represent the simultaneous X-ray spectrum taken from *Chandra* (Fox et al. 2005b). The dot-dashed and dotted lines indicate the extrapolation of the optical and X-ray spectra, respectively.

its significant offset from the centre of the galaxy, the X-ray source cannot be associated with an active nucleus. It could be a background AGN, but in this case the probability of finding an X-ray selected source with an X-ray-to-optical ratio larger than ~ 25 is also small ($P \sim 0.10$; Fiore et al. 2003), further reducing the chance coincidence probability. At $z = 0.16$, the corresponding X-ray luminosity (2×10^{42} erg s^{-1}) would be a factor $\gtrsim 10$ larger than the brightest ultra-luminous X-ray source ever detected (Humphrey et al. 2003). X-ray emission from starburst activity is expected to have an intensity $\sim 10^4$ times lower than that observed, given the star formation rate inferred for this galaxy (see below; Grimm et al. 2003). By a process of elimination, we therefore conclude that the optical variability, the X-ray emission and the association with the galaxy firmly establish this object as the optical counterpart to GRB 050709.

Assuming a power-law flux decay ($F(t) \propto t^{-\alpha}$), our observations constrain

α to be greater than 1.0 in the V band (3σ upper limit). This limit is consistent with the optical decay found by Fox et al. (2005b) using HST data between 5 and 10 d after the GRB (see also Hjorth et al. 2005a; Watson et al. 2006c). A similar limit was also put to the X-ray afterglow decay. Flaring activity was reported in the X-ray light curve (Fox et al. 2005b). Given the limited available data, it is difficult to say whether a similar behaviour was present also in the optical band. Our measurements on Jul 12 are nearly simultaneous with the first *Chandra* observation, so we can construct the broad-band spectral energy distribution (Fig. 6.2). The X-ray spectral index is similar to that of long GRB afterglows (De Pasquale et al. 2003; Nousek et al. 2006). The extrapolation of the X-ray spectrum matches the optical flux (that is, the optical-to-X-ray slope $\beta_{\rm OX} = 1.1$ is consistent with the X-ray slope $\beta_{\rm X} = 1.24 \pm 0.35$). The spectrum corresponding to the optical colours is quite red ($\beta_{\rm opt} = 2.3 \pm 0.7$), but given its large uncertainty it is consistent with $\beta_{\rm OX}$ at the 1.7σ level. Small dust extinction ($A_V \approx 0.2$ mag; Fox et al. 2005b) would make the intrinsic color bluer and fully consistent with the X-ray slope, so that the optical and X-ray emission may constitute a single component. However, the sparseness of the data prevents us from drawing any robust conclusion.

The properties of the host galaxy are intriguing. Its colours are consistent with those of an irregular galaxy at $z \approx 0.2$ (Fukugita et al. 1995), and are much bluer than those of ellipticals (like those associated with other short GRBs). Moreover, hints of morphological structure are seen in our best-seeing images. A close inspection of the spectrum shows that both the Hα and Hβ lines have a narrow emission component (FWHM < 6 Å) partially filling a wider (~ 12 Å FWHM) absorption feature (Fig. 6.3). This classical signature (Dressler & Gunn 1983) identifies a dominant stellar population ~ 1 Gyr old (mostly A-dwarf stars), together with a younger, hotter component. As indicated from the prominent nebular emission lines, star formation is still present. From the Hα and [O II] emission lines (having luminosities 2.62×10^{40} and 2.45×10^{40} erg s^{-1}, respectively), we infer a star formation rate of 0.21 and 0.34 $M_\odot$ yr^{-1} (Kennicutt 1998), which corresponds to $\sim$ 2–3.5 $M_\odot$ yr^{-1} once normalised to L_*. This is significantly less than that typically observed in long GRB host galaxies at high (Christensen et al. 2004) and low (Sollerman et al. 2006; Modjaz et al. 2006) redshift[1], but much larger than that in the

[1] Note that this value is however only the half of that of the host galaxy of GRB 980425, as reported by Sollerman et al. (2006).

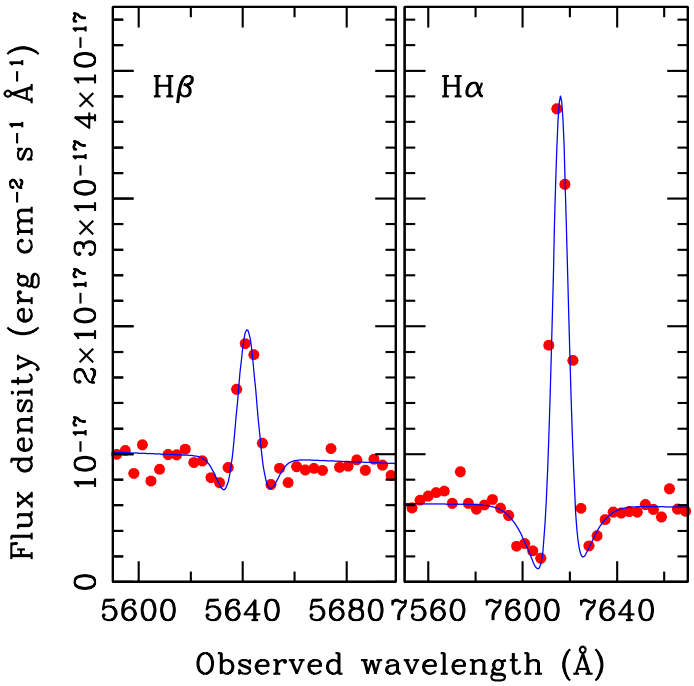

Figure 6.3: Details of the GRB 050709 host galaxy spectrum close to the Hα and Hβ lines, showing that the narrow emission emissions are superimposed on wider absorption features.

hosts of GRB 050509B (Bloom et al. 2006a) and GRB 050724 (Berger et al. 2005b), by factors of > 50 and > 150, respectively.

6.4 Which origin for short GRBs?

The quest for the progenitors of short GRBs has just started, with the discovery of a few afterglows. Table 6.2 shows the properties of short GRBs discovered from the beginning of 2005 until now (2006 August), and localized at least with arcmin accuracy. The choice of this period, although subjective, ensures the presence of the very efficient follow-up system which has been available in the *Swift* era. As it can be seen, most short GRBs have an X-ray afterglow, albeit in some cases it is very faint, and fades quickly after the burst. For these events, the X-ray radiation may be possibly high-latitude

GRB	Inst.	X-ray	Opt.	Host	z	Notes
050202	*Swift*	N/A	N/A	N/A	N/A	Close to the Sun
050509B	*Swift*	yes	no	likely	0.2249	Outside an elliptical
050709	HETE-II	yes	yes	yes	0.16	Star forming galaxy
050724	*Swift*	yes	yes	yes	0.257	Elliptical
050813	*Swift*	yes	no	maybe	0.7–1.8	Cluster
050906	*Swift*	no	no	IC328?	0.0308?	Tentative association
050911?	*Swift*	no	no	N/A	N/A	Perhaps long GRB?
050925	*Swift*	no	no	N/A	N/A	Galactic SGR?
051103	IPN	N/A	no	M81?	N/A	Dubious association
051105A	*Swift*	no	no	N/A	N/A	
051114	*Swift*	no	no	N/A	N/A	Late XRT follow-up
051210	*Swift*	yes	no	likely	N/A	
051221A	*Swift*	yes	yes	yes	0.5465	Star forming galaxy
051227	*Swift*	yes	yes	yes	N/A	Blue galaxy
060121	HETE-II	yes	yes	maybe	N/A	Faint, closeby galaxy
060313	*Swift*	yes	yes	N/A	N/A	
060502B	*Swift*	yes	no	likely	0.287	Outside an elliptical
060801	*Swift*	yes	no	maybe	N/A	

Table 6.2: Properties of short GRBs discovered since 2005. "N/A" indicates that there have been no observations to constrain the property. The words "likely" and "maybe" represent a subjective way to quantify how sure is the assocation with a host galaxy.

emission from the prompt burst rather than a true afterglow (La Parola et al. 2006). Nonetheless, bright X-ray afterglows have been indeed detected (Campana et al. 2006; Burrows et al. 2006). At optical wavelengths, the search has been less successful. Among the best-studied cases (excluding GRB 050202, GRB 051103 and GRB 051114), six events out of fifteen have have been detected at optical/NIR wavelengths.

Short GRB afterglow light curves are, overall, quite similar to those of long-duration GRBs. The most important difference is that they are, on the average, fainter. It has been suggested that short GRBs have weak afterglows due to a low-density environment inside which they explode (Panaitescu et al. 2001b). However, it is now apparent that the dominant factor is the much lower energy budget with respect to long bursts. With the few measured redshifts, the energies of short GRBs range from 10^{48} to 10^{51} erg (isotropic equivalent; Gehrels et al. 2005; Soderberg et al. 2006b), which is 2–3 orders of

magnitude lower than for long GRBs. Similarly, the fireball kinetic energies have been constrained through afterglow modeling, and are comparably lower (Berger et al. 2005b; Panaitescu et al. 2006a; Soderberg et al. 2006b). The density effect, however, has anyway some role. Circumburst densities of the order of 0.1 cm^{-3} or less have been determined. Furthermore, it is remarkable that when the X-ray counterpart is located outside the putative host galaxy (namely, in GRB 050509B and GRB 060502B; Bloom et al. 2006a,b), no optical afterglow has been detected (in such low-density environment, little emission is expected).

Similar to long bursts, short GRBs have shown some evidence for collimation. Fox et al. (2005b) have claimed the detection of a jet break in the optical afterglow of GRB 050709, but this has been questioned by (Watson et al. 2006c), based on a larger dataset. Only for GRB 051221A such a break has been clearly identified (Burrows et al. 2006), corresponding to an opening angle $\vartheta_{\rm jet}$ =4–8°. The data are however still sparse, and other events may be less collimated.

Last, short GRB afterglows exhibit other features typical of long GRBs, among which one or more X-ray flares superimposed to the decay trend (Fox et al. 2005b; Barthelmy et al. 2005a), and slowly-decaying segments (Burrows et al. 2006; Roming et al. 2006).

Short GRB galaxies have been found to be diverse. Firm associations have been discovered with both early- and late-type systems. The star formation rate varies by more than two orders of magnitude between these objects, but is never as large as in long-duration events. The association with early-type objects rules out the possibility that short GRBs are associated uniquely with dying massive stars. The host luminosities are varied as well. For example, the elliptical host of GRB 050509B and GRB 050724 had a luminosity larger than L_*, while GRB 050709 has $L \sim 0.1 L_*$. There seems to be no difference between GRB afterglows lying in early- and late-type galaxies, albeit the small number of events does not allow to draw any solid conclusion. Stellar ages of short GRB hosts (0.1–1 Gyr; Gorosabel et al. 2006) are significantly older than for long GRBs (< 100 Myr; Christensen et al. 2004). Last, it is remarkable that a few afterglows presented a large offset (several tens kpc) with respect to their putative host galaxy, while others are well inside them.

The most popular model for short/hard GRBs is the merger of a binary compact object system (e.g. Eichler et al. 1989). Such events can occur either in early- and late-type galaxies (Belczyński & Kalogera 2001), and give rise to short GRBs (Perna & Belczyński 2002). The critical parameter is

the time delay between the stellar formation and the merging episode. This value is strongly dependent upon the initial separation of the binary. Thus, a wide range of delays is in principle possible. This can explain the different evolutionary status of the hosting systems. Long-delay mergers would preferentially explode in elliptical galaxies, while short-delay events will explode while the star formation burst is still ongoing. Delay times as short as 10 Myr are possible. Binary mergers also allow, in principle, to explain large offsets between the host galaxies and the explosion sites, thanks to the kick velocity imparted to the system at the moment of the SN explosion. The explosion delay, the initial velocity, and the strength of the gravitatioonal potential well of the host galaxy determine the final separation. In particular, it looks strange that the two GRBs with the largest separation are associated to massive galaxies (Bloom et al. 2006a,b). However, these systems also have old stellar population, suggesting a large time delay between the SN and GRB explosion.

For merging timescales of the order of 10 Myr, small offsets between the explosion site and the galaxy core are possible. Therefore, GRB 050709 might have been produced in a tightly bound system, with a short merging time. However, we also note that according to the standard Faber-Jackson relation, the escape velocity from the GRB 050709 host is quite large (about 300 km s^{-1}), so that only a fraction of binary systems may be able to escape its potential well. In this case, a larger delay ($\sim$ 1 Gyr) would be consistent both with the observed offset and with the age of the older stellar population. A large instantaneous star formation rate would not be expected in this case, even if this does not pose any problem for the merger model.

The presence of pronounced star formation activity in the host galaxies of GRB 050709 and GRB 051221A, however, prompts us to investigate whether these events could be directly related to young stars. Recently, it was proposed that short GRBs may be produced by giant flares from soft gamma-ray repeaters (e.g. Hurley et al. 2005). However, the luminosity of GRB 050709 would be a factor $\sim 10^3$ larger than that of the giant flare from SGR 1806-20. The prompt emission properties also make this hypothesis unlikely (Villasenor et al. 2005), since giant flare spectra have usually a thermal shape. Furthermore, our photometry can put strong constraints on the presence of an unextinguished supernova (SN) exploded simultaneously with the GRB (see Fig. 6.4). Our limits impose a SN $\gtrsim$ 100 times fainter than a typical type-Ia SN or a bright hypernova like SN 1998bw. Also fainter events like SN 1994I and even SN 1987A are incompatible with our data. An

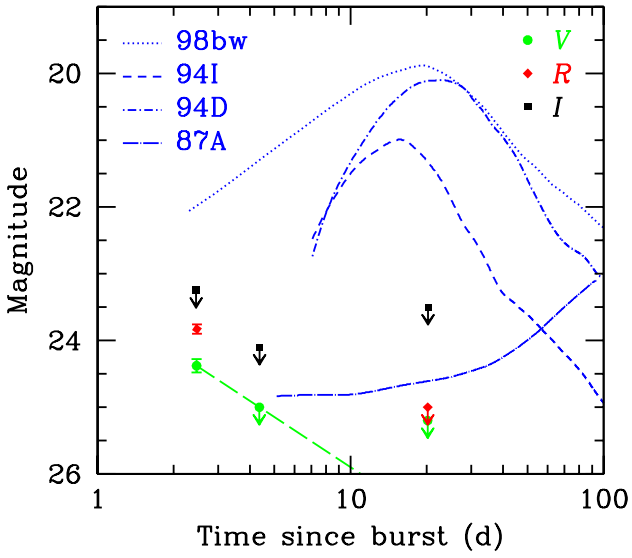

Figure 6.4: Light curve of the GRB 050709 afterglow (points), compared to those of several SNe (R band). Zero extinction is assumed at the GRB site.

association with a SN seems therefore ruled out for GRB 050709 (see also Hjorth et al. 2005b,a; Fox et al. 2005b). The properties of the GRB 050709 host are however consistent with the models proposed by MacFadyen et al. (2005) and Dermer & Atoyan (2006), which advocate a collapsing neutron star accreting from a close non-compact companion. Such model would also naturally explain the flares observed in the X-ray light curve.

It should be said that the merging model overall "performs" well with the available data. The current sample, however, needs to be significantly expanded, in order to build statistical distributions for the observable properties, and try to match them with models predictions (e.g. Belczyński et al. 2006). Up to now, this has already been attempted, providing encouraging, but not conclusive, results (e.g. Guetta & Piran 2005, 2006; Nakar et al. 2006a). For example, the predicted redshift distribution has a median redshift larger than observed. With so few available redshifts, however, any conclusion cannot be considered definitive. Also, the flaring activity observed in several X-ray afterglows is not trivial to explain for a merging model. The real "smoking gun" unveiling a merger origin for short GRBs may be the detection of gravitational radiation.

To summarize, the present observational status presents a rich variety of

properties for short GRBs. GRB 050709 has been the first case to show this complexity, providing the first evidence for a star forming host galaxy. The merger model, thanks to the degree of freedom provided by the variable time delay, is in pricinple able to explain a wide variety of possibilities. On the other hand, the hypothesis that different groups of progenitors contribute to the observed population cannot be discarded. For example, Tanvir et al. (2005) have analyzed BATSE data and found a correlation for a fraction ($\sim 1/4$) of them with nearby galaxies ($z < 0.025$). This, compared to the known redshift distribution ($\langle z \rangle \approx 0.2$), may imply a two-population sample. Also, a contribution from SGR giant flares cannot be excluded, even if current observational constraints limit the fraction of such events to be quite low (Lazzati et al. 2005; Nakar et al. 2006b).

Chapter 7

The dark GRB 050326: a high-redshift candidate?

Since the *Beppo*SAX era, almost all long-duration GRBs have shown an afterglow at X-ray wavelengths (e.g. De Pasquale et al. 2005). On the contrary, the fraction of bursts without optical afterglow has been significant. In the early years of the afterglow era, more than 50% of burst were optically dark (Lazzati et al. 2002). This could not be entirely due to too slow or too shallow follow-up, since limits were significantly deeper than for optically bright GRBs. Of course, the existence of faint events is not surprising. They could be simply have a lower energy or be more distant. In fact, as the follow-up mechanism improved in efficiency, faint afterglows were discovered (e.g. Fynbo et al. 2001; Berger et al. 2002; Li et al. 2003; Fox et al. 2003b). Moreover, an analysis of *Beppo*SAX data (De Pasquale et al. 2003) showed that X-ray afterlows of dark GRBs were, on the average, dimmer than those corresponding to optically-bright events. It would be more interesting to single out dark bursts with (relatively) bright X-ray afterglows.

In the standard model of afterglows, the spectrum between the optical and X-ray frequencies bands should be in the form of a single or power law, depending on the location of the so-called cooling frequency. This is based on standard synchrotron theory, and is quite a robust prediction. It is also well supported by available observations. For synchrotron radiation emitted by a population of relativistic electrons with power-law energy distribution ($\mathrm{d}N/\mathrm{d}\gamma \propto \gamma^{-p}$), the spectrum has a power law shape $F_\nu \propto \nu^{-\beta}$, with $\beta = (p-1)/2$ or $\beta = p/2$, below and above the cooling frequency, respectively. Even if not firmly estabilished from first principles, it is believed that the

electron index p should be larger than 2. This seems to be confirmed by the data. For example, by analysing the SED of 22 *Swift* afterglows, Tagliaferri et al. (2006) have found $p > 2$ in almost all cases. By assuming $p \geq 2$, the hard limit for the optical-to-X-ray spectral slope $\beta_{\rm OX} \geq 0.5$ slope is implied. It is thus meaningful to define a "dark" burst every afterglow which violates this condition (Jakobsson et al. 2004).

There may several explanations for a burst to be dark. First, the simplest synchrotron model may not work. For example, if the X-ray emission is dominated by some other emission mechanism (e.g., Compton emission), the optical/X-ray ratio may be lower. Second, optical light is strongly affected by dust. Keeping in mind the association between long GRBs and star formation, the existence of a population of obscured events would not be surprising. Last, high-redshift bursts ($z \gtrsim 6$) are also expected to be optically dark, due to the redshifting of the Lyα dropout inside the optical band. All three these interpretations are potentially very interesting.

Pinpointing dark GRBs has not been easy, however. The limit $\beta_{\rm OX} > 0.5$ requires very deep imaging at optical frequencies, given the typical X-ray fluxes (a source with $F_{\rm X} = 10^{-13}$ erg cm^{-2} s^{-1} needs $R > 23.5$ to be classified as dark). For example, only a handful of dark GRBs were identified using the (conservative) criteria of Jakobsson et al. (2004) and Rol et al. (2005). The advent of *Swift* has enabled deep and early searches, when the X-ray fluxes are very bright. Surprisingly, the fraction of optically-dark bursts has actually increased (Roming et al. 2005b). This is likely due to larger average redshift of *Swift* bursts (Jakobsson et al. 2006). In this Chapter, I will present X-ray and optical observations of GRB 050326, showing that this is definitely a dark burst, and possibly lies at high redshift. This material has been published by Moretti et al. (2006b).

Swift carries on bard two narrow-field instruments, the X-Ray Telescope (XRT; Burrows et al. 2005a) and the Ultraviolet/Optical Telescope (UVOT; Roming et al. 2005a). During the first year of operation, *Swift* has observed some 75 GRB afterglows, already doubling the pre-*Swift* sample. This rich dataset has allowed to study in detail the X-ray light curves, both at early and late times, leading to the discovery of a complex behaviour (e.g Tagliaferri et al. 2005a; Nousek et al. 2006; Chincarini et al. 2005; Cusumano et al. 2006a). The study of high-redshift GRBs has also started, with the discovery of the first burst at $z > 6$ (Watson et al. 2006b; Cusumano et al. 2006b; Haislip et al. 2006; Price et al. 2006a; Tagliaferri et al. 2005b; Kawai et al. 2006).

7.1 GRB 050326

The bright GRB 050326 was discovered by BAT on 2005 Mar 26 at 9:53:55 UT (Markwardt et al. 2005). Its coordinates were $\alpha_{\rm J2000} = 00^{\rm h}27^{\rm m}34^{\rm s}$, $\delta_{\rm J2000} = -71^\circ 22' 34''$, with an uncertainty radius of $3'$ (95% containment; Cummings et al. 2005). This burst was also detected by the *Wind*-Konus experiment (Golenteskii et al. 2005a), leading to the characterization of its broad-band gamma-ray spectrum.

The *Swift* narrow field instruments could begin observing only 54 min after the BAT trigger due to visibility constraints. A bright, uncatalogued X-ray source was detected by XRT inside the BAT error circle, and was proposed to be the X-ray afterglow (Moretti et al. 2005a). However, no source was detected by UVOT at this location (Holland et al. 2005). XRT collected data up to 6.15 d after the burst. Subsequently, the decay of the light curve prevented any further detection of the afterglow. This object was also observed for 45.8 ks by XMM-*Newton* (Ehle & Perez Martinez 2005; De Luca et al. 2005a), starting 8.5 hr after the trigger.

Only limited ground-based follow-up was reported for this burst. This was likely due to its unfavorable location in the sky (very few telescopes can point at such low declination), as well as to the brightness of the Moon (which was 99% full at the time of the GRB explosion). No counterpart at wavelengths other than the X rays was reported. Deep searches of the host galaxy were performed with the VLT in the K band, leading to the discovery of two faint objects ($K \sim 21$) consistent with the XRT position (Pellizza et al. 2006), but not with the refined XMM position.

In this Chapter, all errors will be quoted at 90% confidence level for one parameter of interest, unless otherwise specified. The reduced χ^2 will be denoted as χ^2_ν, and the number of degrees of freedom with the abbreviation "d.o.f.". We follow the convention $F_\nu(\nu, t) \propto t^{-\alpha}\nu^{-\beta}$, where α and β are the temporal decay slope and the spectral index, respectively. As time origin, we will adopt the BAT trigger (Markwardt et al. 2005). The photon index is $\Gamma = 1 + \beta$.

7.2 Prompt emission

We reduced the BAT data using the latest available release of the HEADAS software (version 1.4). The light curve in the BAT energy band (20–150 keV)

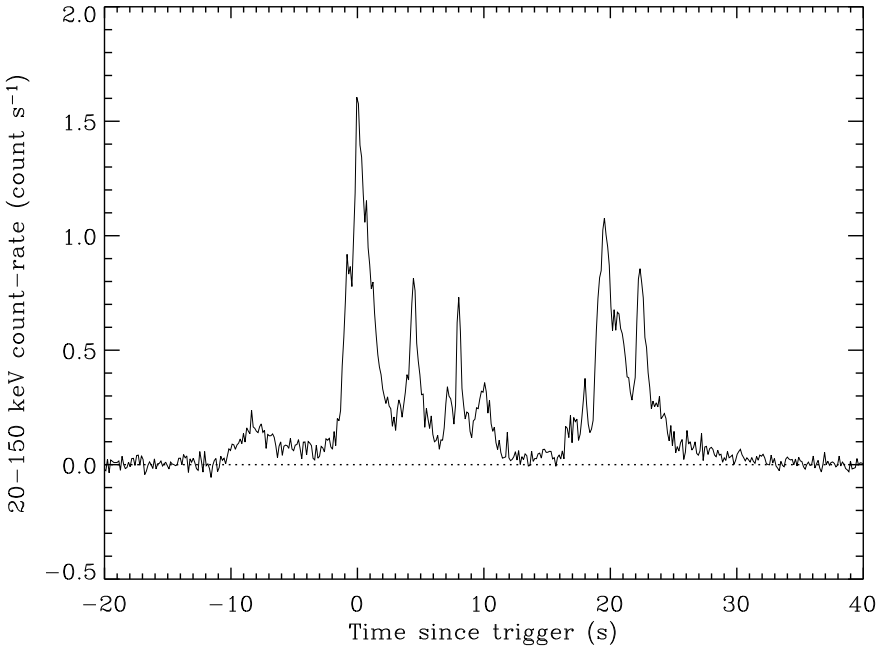

Figure 7.1: The background-subtracted BAT light curve in the 20–150 keV energy band. The origin of the time axis was set to the instrument trigger, but a weak peak is apparent ≈ 9 s before.

presents an initial, weak peak, 9 s before the trigger, followed by several bright distinct peaks (Fig. 7.1). The T_{90} and T_{50} durations of the burst were 29.5 and 19.3 s, in the 20–150 keV band, respectively. We first modeled the BAT spectrum as a single power law with photon index Γ. This provided a good fit ($\chi^2_\nu = 1.06$ for 53 d.o.f.), yielding $\Gamma = 1.25 \pm 0.03$ in the 20–150 keV energy range. The fluence in the same band was $(7.7 \pm 0.9) \times 10^{-6}$ erg cm^{-2}.

GRB 050326 also triggered the *Wind*-Konus detector (Golenteskii et al. 2005a): in the 20 keV–3 MeV energy range it lasted 38 s, and had a fluence of $(3.22 \pm 0.05) \times 10^{-5}$ erg cm^{-2}. Golenteskii et al. (2005a) fitted the time-integrated spectrum of the burst as measured by the *Wind*-Konus detector with a Band model (Band et al. 1993), that is a smoothly joined broken power law with low- and high-energy photon indices Γ_1 and Γ_2, respectively, and break energy E_0. The best fit provided $\Gamma_1 = 0.74 \pm 0.09$, $\Gamma_2 = 2.49 \pm 0.16$, and $E_0 = 160 \pm 22$ keV. The corresponding observed peak energy (that

is, the energy at which the maximum of the emission is reached) is $E_{\rm p,obs} = (2-\Gamma_1)E_0 = 200 \pm 30$ keV. Motivated by their results, we also performed a fit to the BAT data using the Band function. Since the break energy E_0 lies close to the upper boundary of the BAT energy range (150 keV), we were forced to freeze E_0 and Γ_2 to the values determined by *Wind*-Konus. The fit was again good ($\chi^2_\nu = 1.14$ for 53 d.o.f.), and provided $\Gamma_1 = 0.87 \pm 0.03$, in fair agreement with the value found by Golenteskii et al. (2005a). It is not surprising that both functional forms provide a good fit to the data, since they do not differ significantly inside the BAT energy range. Nevertheless, thanks to the very broad band covered by the *Wind*-Konus instrument, for this burst the break energy could be clearly constrained. In the following, we will consider the Band model as the best description of the GRB 050326 spectrum. With this fit, the fluence in the 20–150 keV band was $(7.6 \pm 0.8) \times 10^{-6}$ erg cm^{-2}. Integrating the burst spectrum from 1 to 10 000 keV, we could evaluate the bolometric fluence $\mathcal{F}$ of the burst, finding $\mathcal{F} = 2.4 \times 10^{-5}$ erg cm^{-2}.

No spectral evolution could be detected in the BAT data. We splitted the observation in three time intervals, covering the ranges $[-9, -1]$, $[-1, 13]$, and $[13, 29]$ s (relative to the BAT trigger). By fitting the data with either a simple power law or with the Band model, the resulting parameters were always consistent with those derived by fitting the whole spectrum.

7.3 XRT data analysis and results

7.3.1 Data reduction

For a technical description of XRT and its operations, we refer, e.g., to Burrows et al. (2005a) and Hill et al. (2004). XRT started observing the field of GRB 050326 on 2005 Mar 26 at 10:48:27 UT, that is, 3307 s after the BAT trigger. The last observation ended on 2005 Apr 1 at 13:30:53, i.e. 6.15 d after the burst. Occasionally, some reflected light from the Earth limb made the very low energy (< 0.2 keV) background increase abnormously, so that XRT incorrectly switched from the photon counting (PC) to the windowed timing (WT) mode, even if the target count rate was well below 1 count s^{-1}. The effective exposure time was 59.6 ks in PC mode and 20.7 ks in WT mode, leading to the collection of 614 and 580 photons, respectively (0.3–10 keV energy band). As the satellite settled on the target, XRT recorded a source count rate of 1.3 count s^{-1}, which dropped to 3×10^{-4} count s^{-1} at the

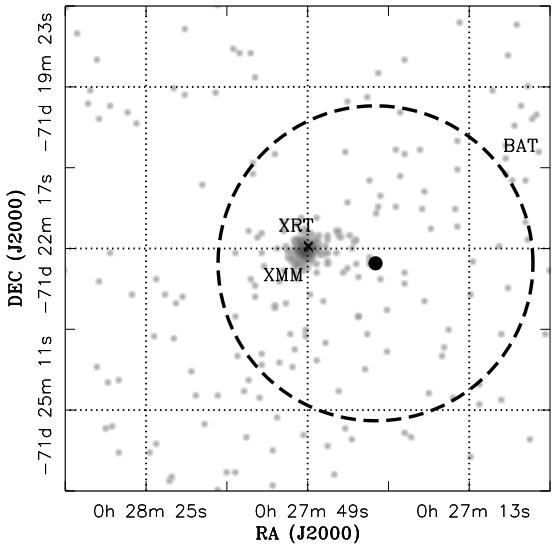

Figure 7.2: XRT image of the field of GRB 050326, smoothed with a Gaussian kernel (4.″7 full width half maximum). Events were accumulated from the first segment of the observation (589 s exposure time). The BAT refined position (black dot) is also shown together with its 95% containment error circle (3′ radius, dashed line). The XRT and XMM-*Newton* positions (1.″7 apart) are also plotted (crosses), and are almost indistinguishable. The X-ray error circles (3.″6 and 1.″5 radius, respectively) are too small to be seen with this scale.

end of the observing campaign (2005 Apr 1). From the third orbit after the start of the observation onwards, the source count rate was < 0.1 count s^{-1}, while the background level was typically > 3 count s^{-1} over the whole field of view. Since WT data have only one dimensional spatial information, their S/N ratio was much lower than that of PC mode data. We therefore decided to consider WT data only for the first two orbits, when the source S/N was higher. Data were reduced using the `xrtpipeline` task of the latest available release of the HEADAS software (version 1.4). Accumulating the PC data from all observations, we found that the centroid position of the afterglow had coordinates $\alpha_{\rm J2000} = 00^{\rm h}27^{\rm m}49\overset{\rm s}{.}16$, $\delta_{\rm J2000} = -71^\circ 22' 14\overset{''}{.}6$, with a 3.″6 uncertainty radius (95% containment, Fig. 7.2). This position takes into account the correction for the misalignment between the telescope and the satellite optical axis (Moretti et al. 2006a). This position is 1.′3 away from the refined BAT position (Cummings et al. 2005), and 3.″4 away from

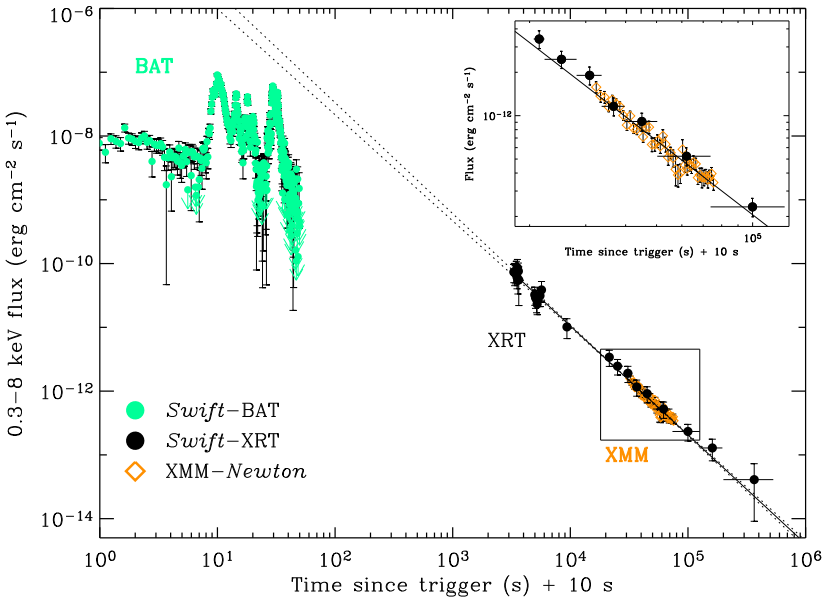

Figure 7.3: The light curve of GRB 050326 and of its afterglow in the 0.3–8 keV energy band (see text for the computation of the flux conversion factors). XRT (black circles) and XMM-*Newton* data (empty diamonds) show a very good agreement (see also the inset). The solid line shows the fit to the combined XRT/XMM afterglow light curve. The dotted lines indicate the 90% errors of the extrapolated X-ray light curve. Light filled circles indicate the extrapolation of the BAT data to the 0.3–8 keV energy range, assuming the Band model as the best-fit spectrum. In this figure, the time origin was set 10 s before the nominal trigger time, to show the weak, untriggered precursor. This has no effect on the determination of the afterglow decay slope, due to the late beginning of the XRT observation.

the preliminary XRT position (Moretti et al. 2005a), calculated using only the data from the first orbit and without the misalignment correction.

7.3.2 Temporal analysis

In order to extract the light curve, we considered all PC data, but discarded the WT data taken after the second orbit of the XRT observation ($t >$ 20 ks). PC events were selected having grades 0–12 from a circle with 20 pixel radius (47″), corresponding to 92% of the encircled energy fraction (EEF) at 1.5 keV (Moretti et al. 2005b). Only the data in the 0.3–10 keV

band energy range were considered (even if there are no events above 7 keV). To take into account the pile-up effect, during the initial part of the first orbit ($t \lesssim 4\,000$ s) an annular extraction region with inner radius of 3 pixels ($7''$) was adopted for PC data. This area includes 40% of the EEF, and the deriving PSF losses were consequently taken into account. The accuracy of the PSF model in its central part is $\sim 5\%$ (Moretti et al. 2005b). This error was properly propagated when evaluating the final uncertainty of the PSF-corrected points in the light curve. The background in PC mode was evaluated by integrating the signal from an annulus with inner and outer radii of 50 and 90 pixels, respectively, centered at the afterglow position. Inside this region, the contamination from the afterglow is expected to be negligible. In WT mode, events were selected having grades 0–2 from a 20 pixel ($47''$) wide rectangular region, centered on the detector X coordinate of the afterglow. To estimate the background in WT mode, we considered a region of the same size centered 40 pixels ($94''$) away from the center of the afterglow.

The XRT observation was split in different time segments because of the Earth occultation constraints. Each satellite orbit lasts $\approx 5\,800$ s, while the target could be typically observed for approximately 1 000 s per orbit. To extract the light curve, the source events were binned in 10 s intervals, and these bins were further grouped to ensure a minimum of 50 counts per bin. When the counts in the last bin of each orbit were less than half of the required minimum (25 counts), the bin was merged with the previous one. From the fifth orbit onwards, XRT did not collect enough photons within a single orbit, so data from different orbits were merged. We eventually obtained a background-subtracted light curve composed by 25 points, with a minimum of 10 and a maximum of 57 counts per bin.

The resulting light curve is shown in Fig. 7.3, and displays a uniform decay rate, with no indications of breaks or flares. A single power law fit provides a good description to the data, yielding a decay slope $\alpha = 1.64 \pm 0.07$. In order to look for spectral variations across the observation, we computed the afterglow hardness ratio as a function of time. To this end, we selected the events with energy below and above several pivotal energies, and computed their number ratio. No significant variation was found during the whole observation, after setting the pivotal energy to 1, 1.5 and 2 keV.

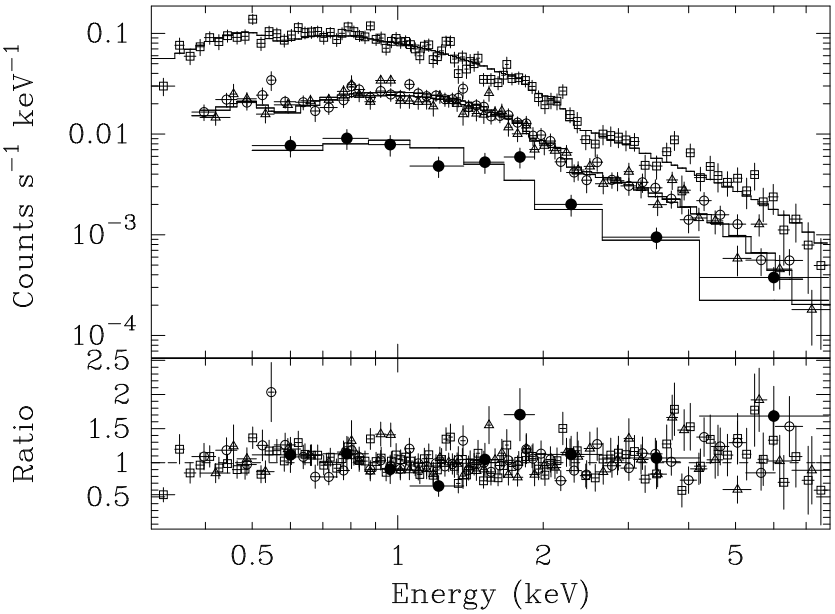

Figure 7.4: The spectra of the GRB 050326 afterglow as observed by XMM-*Newton* (PN: squares; MOS1: open circles; MOS2: triangles) and by *Swift*-XRT (filled circles). The solid lines represent the best-fit absorbed power-law model convolved with the instrumental responses (see Table 7.2 for the best-fit parameters). XRT data were selected from the time interval covered by the XMM-*Newton* observation.

7.3.3 Spectral analysis

To extract the spectrum of the source in WT mode, we used the same extraction regions, the same background regions, and the same screening as for the temporal analysis. For PC mode, however, we further selected only grade 0–4 events in order to improve the spectral resolution. The spectrum was binned in order to ensure a minimum of 20 counts per energy bin, ignoring channels below 0.3 keV. The spectral analysis was performed using `XSPEC` (v11.3). We first considered WT and PC data separately, using the former for the first 2 orbits (3 to 15 ks after the burst) and the latter for the rest of the observation. In both cases, the spectrum was fitted with an absorbed power-law model, yielding good χ^2 values (Table 7.1). Assuming Solar metallicity, the best-fit values for the Hydrogen column density $N_{\rm H}$ and for the photon index Γ did not show significant variations between the first (WT data) and second part (PC data) of the observation. In fact, combin-

	$N_{\rm H}$ (10^{21} cm^{-2})	Γ	χ^2_ν (χ^2/d.o.f.)
XRT (WT)	$1.3^{+0.7}_{-0.6}$	$1.92^{+0.27}_{-0.24}$	1.10 (29.7/27)
XRT (PC)	$1.4^{+0.8}_{-0.7}$	$2.00^{+0.38}_{-0.31}$	1.05 (12.6/12)
XRT (WT+PC)	$1.4^{+0.6}_{-0.5}$	$1.95^{+0.21}_{-0.21}$	1.10 (42.0/38)
XRT (WT)	0.46 (frozen)	1.58 ± 0.12	1.22 (34.1/28)
XRT (PC)	0.46 (frozen)	1.58 ± 0.14	1.41 (19.1/13)
XRT (WT+PC)	0.46 (frozen)	1.61 ± 0.10	1.20 (47.0/39)

Table 7.1: Best-fit spectral parameters for the two segments of the XRT observation (WT and PC data), fitted both separately and together. We report the results either leaving the Hydrogen column density as a free parameter, or freezing it to the Galactic value.

ing the data from the two segments together, we obtained an excellent χ^2 value, indicating that the spectral properties of the afterglow did not change during the observation. Figure 7.4 shows the XRT spectrum (filled circles), together with the best-fit absorbed power-law model (precisely, only data simultaneous to the XMM-*Newton* observation were used for the plot.

To look for the presence of absorbing material in the proximity of the afterglow, we tried to estimate the Galactic Hydrogen column density $N_{\rm H,MW}$ towards the GRB direction. We found three different measurements: Dickey & Lockman (1990) give $N_{\rm H,MW} = 4.6 \times 10^{20}$ cm^{-2}; the Leiden/Argentine/Bonn Galactic H I Survey (Kalberla et al. 2005) provides a lower value, $N_{\rm H,MW} = 3.8 \times 10^{20}$ cm^{-2}; last, the dust maps by (Schlegel et al. 1998) give $A_V = 0.12$ mag, which corresponds to $N_{\rm H,MW} = 2.2 \times 10^{20}$ cm^{-2} after assuming the prescription given by Predehl & Schmitt (1995). While the average of these three independent measurements is $(3.5 \pm 1.7) \times 10^{20}$ cm^{-2}, we conservatively adopted the largest of the above values (4.6×10^{20} cm^{-2}). Stratta et al. (2004) estimated that the typical error affecting the maps by Dickey & Lockman (1990) is 30%, which is not far from the scatter among the three measurements. The best-fit Hydrogen column density derived by the XRT afterglow spectrum is marginally unconsistent with the Galactic value. Fixing $N_{\rm H} = N_{\rm H,MW}$ provided a poor fit ($\chi^2_\nu = 1.20$ for 39 d.o.f.). The probability of such a worsening in the fit is $< 7.5\%$, as estimated by an F-test. Therefore, XRT data marginally suggest the presence of additional absorbing material, likely located in the GRB rest frame. In the next section, we will present further evidence for the presence of excess absorption, based on XMM-*Newton* data with better S/N ratio.

7.4 XMM-*Newton* data analysis and results

The afterglow of GRB 050326 was also observed by XMM-*Newton* as a target of opportunity, starting on 2005 Mar 26 at 18:25 UT (8.5 hr after the burst). The observation lasted for 45.8 ks. Data were collected with the European Photon Imaging Camera (EPIC), which consists of the PN (Strüder et al. 2001) and of the two MOS detectors (Turner et al. 2001). All the cameras were operated in full-frame mode with a thin and medium optical filter on PN and MOS, respectively. A preliminary analysis of these data was presented by De Luca et al. (2005a).

7.4.1 Data and temporal analysis

The appropriate observation data files were retrieved from the XMM Science Archive. The data reduction was performed using the most recent release of the XMM Science Analysis Software (SAS v6.1.0), with the standard pipeline tasks (`epproc` and `emproc` for PN and MOS, respectively). The observation was badly affected by high particle background (soft proton flares), with almost no nominal (quiescent) background time intervals. The back-illuminated PN CCD is particularly sensitive to this background; indeed, more than 25% of the PN observing time was lost due to the detector switching to its counting mode[1]. The afterglow of GRB 050326 (source XMMU J002748.8-712217; Ehle & Perez Martinez 2005) was anyway clearly detected in all cameras. The astrometry of the EPIC images was improved by cross-correlating serendipitous X-ray sources in the field with objects in the USNO-B1 catalog. This yielded the following refined coordinates for the afterglow: $\alpha_{\rm J2000} = 00^{\rm h}27^{\rm m}49\farcs1$, $\delta_{\rm J2000} = -71^\circ22'16\farcs3$, with an 1-$\sigma$ uncertainty of $1\farcs5$. The EPIC and XRT positions differ by $1\farcs7$, and are therefore fully consistent within the uncertainties. The two faint galaxies reported by Pellizza et al. (2006) are $\approx 4''$away from this position, so that these objects are not related to the GRB.

In order to retain a S/N ratio large enough to perform the temporal and spectral analysis, a standard time-filtering approach to screen soft proton flares could not be applied (a high particle flux was present during the whole

[1]The counting mode is activated when the count rate in a quadrant exceeds the telemetry limit (~ 400 count s^{-1} for the PN). In this mode, the informations for individual events of that quadrant are not transmitted to ground.

observation). Thus, source events were extracted with a particularly stringent spatial selection, considering only the innermost portion of the point spread function. We used a circle of 15″ radius (containing ≈ 65% of the EEF). The PSF correction was applied to the flux and spectral measurements by computing the ad-hoc effective area using the SAS task `arfgen`. The error in this procedure is estimated to be at most at the 5% level[2] and it was properly taken into account in the light curve error budget.

Background events were selected from source-free regions within the same CCD chip where the source was imaged. In particular, for the PN data we used 2 boxes of 45″ × 25″ located at the same distance from the readout node as the target; for the MOS we used an annulus centered at the target position with inner and outer radii of 90″ and 180″, respectively. With such a choice, the background amounted to ∼ 13% and ∼ 9% of the counts in the source extraction region for PN and MOS data, respectively, in the 0.3–8 keV range. The overall (background-subtracted) number of source events was 3 990, 1 850 and 1 760 in the PN, MOS1 and MOS2 detectors, respectively.

The background-subtracted count rate clearly showed a declining trend with time. We again fitted the light curve assuming a power law decay. The value of the decay slope α was evaluated independently using PN, MOS1 and MOS2 data, yielding fully consistent results. We therefore repeated the fit using the combined dataset, finding $\alpha = 1.72 \pm 0.09$ in the 0.3–8 keV energy range ($\chi^2_\nu = 1.30$ for 40 d.o.f.). The background-subtracted light curve is shown in Fig. 7.3, together with the XRT light curve, after converting the count rates to fluxes using the best-fit absorbed power-law models described in Sect. 7.3.3 and 7.4.2).

7.4.2 Spectral analysis

Spectra for the source and the background were extracted from the same regions used for the temporal analysis, as described above. Source spectra were rebinned in order to have at least 30 counts per energy bin and to oversample the instrumental energy resolution by a factor 3. Ad-hoc response matrices and effective area files were created with the SAS tasks `rmfgen` and `arfgen`, respectively. The spectral analysis was performed using `XSPEC` (v11.3). The spectra were fitted simultaneously in the 0.3–8 keV band. Since the MOS observation started ≈ 1 hr earlier than the PN, a PN/MOS normalization

[2] See page 9 of `http://xmm.vilspa.esa.es/docs/documents/CAL-TN-0018-2-4.pdf`

factor was introduced in the fit as a further, free parameter. Due to the fading of the source, this also implies that the observed time-averaged flux is expected to be higher in the MOS than in the PN.

An absorbed power-law model reproduced the spectrum quite well ($\chi^2_\nu = 1.17$ for 190 d.o.f.). The best-fit parameter values are reported in Table 7.2 (first row); the MOS-PN normalization factor was 1.08 ± 0.04. Fig. 7.4 shows the spectra collected by the EPIC cameras together with the best-fit model. Both the photon index and the Hydrogen column density are in good agreement with those found by XRT, but are much better constrained. In particular, the value of $N_{\rm H}$ inferred from the fit was significantly larger than the Galactic one $N_{\rm H,MW}$ (Sect. 7.3.3). Moreover fixing $N_{\rm H} = N_{\rm H,MW}$ resulted in a much poorer fit ($\chi^2_\nu = 1.85$ for 191 d.o.f.), and even increasing $N_{\rm H,MW}$ by 30% (see Sect. 7.3.3 and Stratta et al. 2004) the fit was still unacceptable ($\chi^2_\nu = 1.65$ for 191 d.o.f.). A significant improvement was achieved by fixing $N_{\rm H} = N_{\rm H,MW}$ and adding to the spectral model an extra neutral absorber at redshift z with column density $N_{{\rm H},z}$. This yielded $\chi^2_\nu = 1.03$ (189 d.o.f.); the chance probability of such improvement, as estimated by an F-test, was $< 1 \times 10^{-6}$ with respect to the model containing only one absorbing component (with free $N_{\rm H}$). After adding the extra absorption component, the best-fit power law photon index was $\Gamma = 2.03 \pm 0.05$, while the intrinsic gas column density and the redshift were $N_{{\rm H},z} \sim 6 \times 10^{22}$ cm^{-2} and $z \sim 6$, respectively. However, the latter two values are not well constrained, owing to their strong correlation (Fig. 7.5). In any case, the spectral fit allowed us to constrain $N_{{\rm H},z} > 4 \times 10^{21}$ cm^{-2} and $z > 1.5$ (at 90% confidence level for 2 parameters of interest; see inset in Fig. 7.5). We investigated the dependence of these confidence contours on the assumed value of the Galactic column density. By varying $N_{\rm H,MW}$ by 50% (within the range discussed above), we found that the 90% confidence interval on $N_{{\rm H},z}$ varies by 20%, while that on z varies by less than 10%.

The observed (time-averaged) fluxes in the 0.2–10 keV band were 5.1×10^{-13} and 5.5×10^{-13} erg cm^{-2} s^{-1} in the PN and MOS, respectively. The corresponding unabsorbed fluxes were 7.4×10^{-13} and 7.9×10^{-13} erg cm^{-2} s^{-1}.

We also joined together the XRT and XMM-*Newton* dataset, to accumulate the largest possible statistics. The combined joined temporal fit yields a decay index $\alpha = 1.70 \pm 0.05$. In the following, we will adopt this value as the best determination for the temporal decay slope.

In order to search for possible line features in the spectrum (both in emission and in absorption) we divided the 0.4–5 keV energy range into

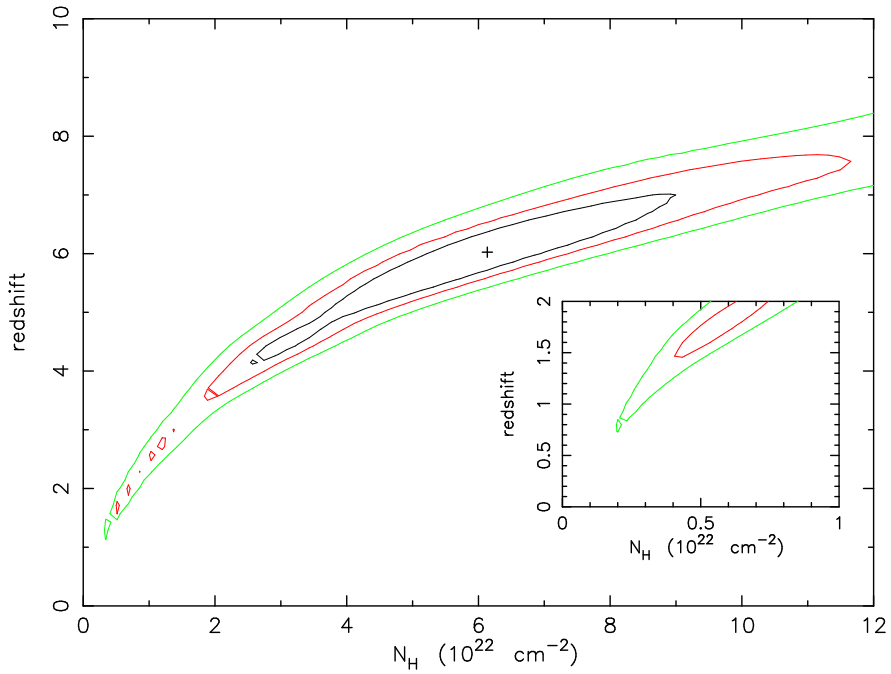

Figure 7.5: Confidence contours (68%, 90% and 99% levels for 2 parameters of interest) for the gas column density $N_{\mathrm{H},z}$ and the redshift z of the intrinsic absorber, as computed from the fit to the EPIC spectra. The Galactic column density was assumed to be $N_{\mathrm{H,MW}} = 4.6 \times 10^{20}$ cm^{-2} (Dickey & Lockman 1990). The inset shows a zoom-in of the low-redshift region.

0.2 keV intervals. For the continuum, we assumed the best-fit absorbed power-law model (including also the rest-frame column density). For each of the intervals, we added a Gaussian line with fixed width (smaller than the instrumental resolution) and central energy free to vary within the selected interval; the normalization could be either positive or negative. We then repeated the exercise with different choices of the energy intervals. We found no significant lines in the 0.4–5 keV range in the combined MOS/PN dataset. The upper limit (3-σ) on the equivalent width of any line is $\sim$ 50 and $\sim$ 250 eV in the 0.4–2 and 2–5 keV energy ranges, respectively.

We also tried to fit the spectra with thermal models (e.g. Reeves et al. 2002; Lazzati 2003). A redshifted, optically thin plasma emission model (MEKAL in `XSPEC`) was used, with the redshift linked to that of the intrinsic absorber. The fit worsened ($\chi^2_\nu \approx 1.4$) with respect to the simple power law model, either fixing the metal abundances to Solar values, or leaving them

Instrument	$N_{\rm H}$ (10^{21} cm^{-2})	Γ	χ^2_ν (χ^2/d.o.f.)
EPIC	$1.3^{+0.1}_{-0.1}$	$2.13^{+0.06}_{-0.06}$	1.17 (222.5/190)
XRT	1.3 (frozen)	$1.96^{+0.29}_{-0.27}$	1.43 (11.4/8)
EPIC + XRT	$1.3^{+0.1}_{-0.1}$	$2.09^{+0.05}_{-0.08}$	1.18 (219.7/197)

Table 7.2: The spectral parameters as measured separately by XMM-*Newton* and XRT, fitting the data both separately and together. For this fit, XRT data were selected from the same time interval covered by the XMM-*Newton* observation. Due to the limited statistics, $N_{\rm H}$ was frozen to the value derived by XMM-*Newton* when fitting XRT data. The errors are at 90% confidence level for a single parameter of interest.

as free parameters.

Finally, we looked for possible spectral evolution with time, using the power law plus redshifted absorber model described above. For this study we divided the data into two subsets with exposure times of $\sim$ 15.8 and $\sim$ 27.6 ks, each subset containing approximately half of the afterglow counts. We then extracted the corresponding spectra for the source and the background. No significant (> 3-σ) variations in the spectral parameters were found (except, of course, for the flux normalization).

7.5 Optical and ultraviolet observations

The UVOT instrument onboard *Swift* observed the field of GRB 050326 together with XRT, starting 54 min after the trigger. In the subsequent orbits, it collected a series of images in its 6 broad-band filters (V, B, U, UVW1, UVM2, and UVW2; Table 7.3). The afterglow was not detected in any of the single or coadded exposures. Summing the images in each of the six filters, we estimated the 3-σ upper limits using the UVOT dedicated software (task `uvotsource`). The counts were extracted from a $6''$ and $12''$ radius aperture for the optical and ultraviolet filters, respectively, after subtracting the background. We then corrected the upper limits for Galactic absorption (Schlegel et al. 1998), assuming the extinction curve of Pei (1992). Our final limits are summarized in Table 7.3. With respect to the original values reported by Holland et al. (2005), our measurements were obtained adopting the most recent on-flight calibration.

The only reported ground-based optical observation for this burst was an R-band upper limit provided by the 0.6m telescope at the Mt. John Obser-

$t - t_0$ (s)	Filter	λ (Å)	$t_{\rm exp}$ (s)	A_λ (mag)	Mag	F_ν (μJy)	$\beta_{\rm OX}$	$F_\nu^{\rm X}/F_\nu^{\rm opt}$
3300	UVW2	1930	10	0.29	> 17.41	< 99.11	< 0.52	$> 23^{+8.9}_{-6.4}$
3306	V	5460	100	0.12	> 18.66	< 107.5	< 0.45	$> 65^{+31}_{-21}$
3350	UVM2	2220	100	0.36	> 18.54	< 34.17	< 0.32	$> 75^{+30}_{-21}$
3470	UVW1	2600	100	0.27	> 18.75	< 27.80	< 0.29	$> 103^{+43}_{-30}$
5219	U	3450	750	0.20	> 19.65	< 11.00	< 0.24	$> 176^{+77}_{-54}$
9390	B	4350	714	0.16	> 20.87	< 17.47	< 0.46	$> 52^{+24}_{-16}$
24840	$R_{\rm MOA}$	6399	600	0.10	> 20.20	< 25.70	< 0.74	$> 10^{+5.0}_{-3.4}$

Table 7.3: Summary of optical and ultraviolet observations. All data but the point in the R band were measured by *Swift*-UVOT. The R-band observations is by Tristram et al. (2005). All measurements were corrected for the Galactic extinction (A_λ, based upon $A_V = 0.123$ mag; Schlegel et al. 1998), assuming the Milky Way extinction curve by Pei (1992). The optical-to-X-ray spectral index is $\beta_{\rm OX} = \log(F_\nu^{\rm opt}/F_\nu^{\rm X})/\log(\nu_{\rm X}/\nu_{\rm opt})$. The X-ray frequency was set to $\nu_{\rm X} = 1.5$ keV, the logarithmic mean of the XRT observing range. The X-ray flux was computed by interpolating the XRT light curve to the time of the optical limit. The last column reports the ratio of the extrapolated X-ray flux to the optical one (assuming no spectral breaks between the two bands; see Fig. 7.7).

vatory (Tristram et al. 2005). This measurement is also listed in Table 7.3.

7.6 Discussion

7.6.1 The X-ray light curve

To date, *Swift* has observed X-ray emission from dozens of GRB afterglows. A systematic analysis of their light curves has evidenced several common features (Nousek et al. 2006; Chincarini et al. 2005). During the first few hundred seconds, a steep decay is often observed ($\alpha \approx 3$–5; Tagliaferri et al. 2005a), usually interpreted as the tail emission from the prompt GRB (e.g. Cusumano et al. 2006a). This phase is followed by a much flatter decline ($\alpha \approx 0$–0.7; e.g. Campana et al. 2005; Nousek et al. 2006), lasting up to 10^3–10^5 s (and in some cases even longer). Then, the light curve steepens again, leading to $\alpha \approx 1$–1.5; this phase was the one seen by *Beppo*SAX, XMM-*Newton* and *Chandra*. At late times, a further steepening is sometimes observed (e.g. Vaughan et al. 2006), likely the signature of a jetted outflow

(Rhoads 1999). In some cases, bumps and flares appear superimposed to the power-law decay, up to several tens of ks (e.g. Piro et al. 2005; Burrows et al. 2005b).

The light curve of GRB 050326 exhibited a different behaviour with respect to that outlined above. Its light curve showed a single, unbroken decay from ≈ 55 min to ≈ 4.2 d. However, our coverage began relatively late, so that we may have missed early deviations from the power law behaviour.

In order to investigate the afterglow early stages and to analyze the connection between the prompt and afterglow emission, we extrapolated the afterglow flux to the time of the prompt emission. We then compared the obtained value with that expected from the prompt emission in the XRT band (0.3–8 keV), computed adopting the Band best-fit model. The result is shown in Fig. 7.3, where the light circles indicate the prompt emission fluxes. Since the GRB spectrum is known in good detail (particularly, since no breaks are expected between the BAT and XRT ranges), the extrapolation process should be quite reliable. As it can be seen, if no temporal breaks were present in the X-ray light curve, the afterglow flux in the X-ray range exceeded the prompt one by a factor of ~ 100 (with a small uncertainty, due to the tiny error in the decay index). We cannot exclude that such emission was present (since we have no prompt observations in the X-ray band), but, if present, the present component would appear as a very bright, soft excess. Such feature would not be unprecedented (Vanderspek et al. 2004; Vetere et al. 2006), but in this case it would likely contaminate the low-frequency end of the BAT spectrum. Moreover, the soft excesses always contained less energy that the GRB proper. Thus, the most conservative hypothesis is to assume that a break was present in the early light curve, or that the afterglow onset was delayed. Indeed, as mentioned above, most of *Swift* afterglows show a shallow decline phase during the first thousands seconds after the GRB. Independently of any extrapolation, we note that GRB 050326 was distinctly different from most bursts observed by *Beppo*SAX, for which the backward extrapolation of the late-time X-ray afterglow roughly matched the prompt emission level in the X-ray range, as measured by the Wide Field Cameras (Frontera et al. 2000).

We also performed a different operation. Using the best-fit X-ray spectrum, we extrapolated the XRT flux to the BAT energy range (20–150 keV), and reported it at the time of the burst using the afterglow decay law. Also in this case, the expected value exceeded the observed prompt emission, but by a smaller factor. This again suggests that a break in the light curve was

present before the beginning of the XRT observation, but the evidence is less compelling. For example, we cannot even exclude that the afterglow spectrum had a break between the XRT and BAT ranges, so that the extrapolation actually overestimated its flux.

7.6.2 Constraints on the afterglow parameters

The properties of the explosion can be inferred in the context of the standard afterglow model (e.g. Mészáros & Rees 1997; Sari et al. 1998). In this context, the observed emission is due to synchrotron radiation from a decelerating relativistic shock, which produces a decaying flux with a power-law spectrum. Depending on the model parameters, definite relations between the spectral and temporal indices α and β are predicted. The combined XMM-*Newton* and *Swift*-XRT data provide $\alpha = 1.70 \pm 0.05$ and $\beta = 1.09 \pm 0.08$. Both values are not unusual among GRB afterglows at comparable epochs (e.g. De Pasquale et al. 2005; Chincarini et al. 2005; Nousek et al. 2006). These numbers are consistent with a spherical outflow expanding inside a homogeneous medium, if the XRT range was between the injection and cooling frequencies (ν_i and ν_c, respectively). In this case, the model prediction is $\alpha = 3\beta/2 = 1.63 \pm 0.12$, in excellent agreement with the measured value $\alpha = 1.70 \pm 0.05$. All other possibilities (a wind-stratified medium, or a different location of the break frequencies) are excluded at > 3.5-σ level. The power-law index of the electron energy distribution is $p = 1 + 4\alpha/3 = 1 + 2\beta$, so that $p = 3.25 \pm 0.06$. Such value is rather high, but not unprecedented.

No break was observed in the X-ray light curve of GRB 050326 between 55 min and ~ 4.2 d after the burst. The condition $\nu_\mathrm{i} < \nu < \nu_\mathrm{c}$ thus held during this time range. While ν_i typically lies below $\sim 10^{15}$ Hz for $t > 1$ hr (e.g. Sari et al. 1998; Panaitescu & Kumar 2000), keeping $\nu < \nu_\mathrm{c}$ up to $t > 4.2$ d requires $n_0 \varepsilon_{\mathrm{B},-2}^{3/2} < 3 \times 10^{-5} E_{\mathrm{iso},54}^{-1/2}$, where $n = n_0 \times 1\ \mathrm{cm}^{-3}$ is the ambient particle density, $\varepsilon_\mathrm{B} = 10^{-2} \varepsilon_{\mathrm{B},-2}$ is the magnetic field energy fraction, and $E_\mathrm{iso} = E_{\mathrm{iso},54} \times 10^{54}$ erg is the (isotropic-equivalent) fireball energy. This condition is difficult to satisfy (e.g. Panaitescu & Kumar 2001a; Yost et al. 2003), so it may be regarded as a problem for the model. We note, however, that for this burst both α and β could be measured with good accuracy, so the consistency between the predicted and observed value of the decay index is remarkable.

The absence of any break also poses some constraints on the geometry of the emission. GRB afterglow light curves often show a late-time steepening,

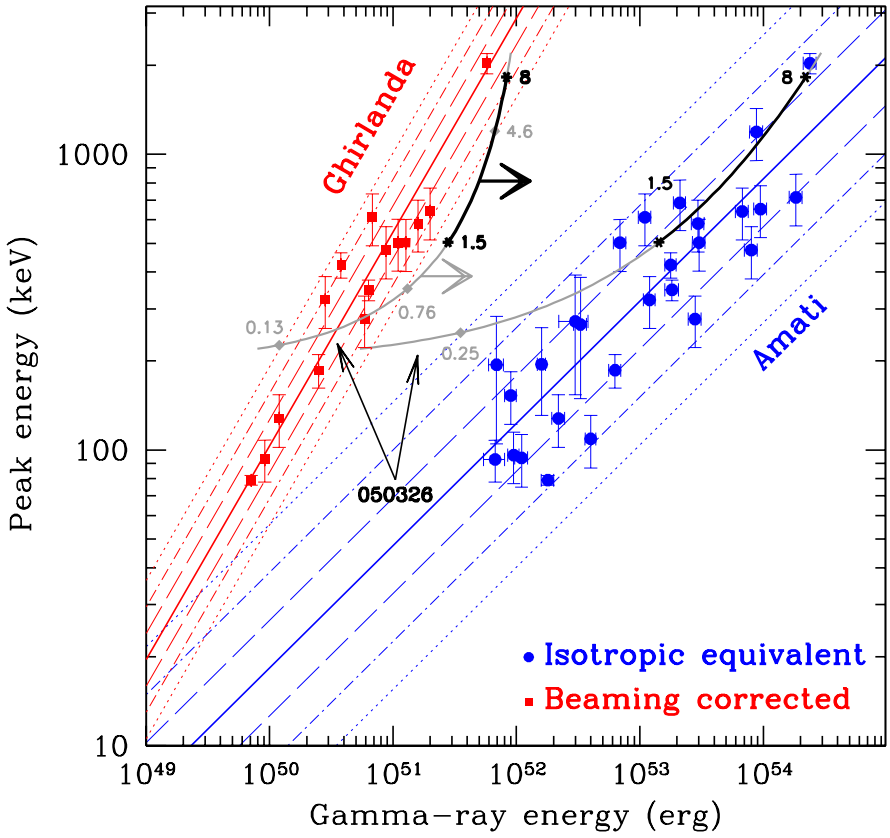

Figure 7.6: Comparison of GRB 050326 with the Amati (right) and Ghirlanda (left) relations (Amati et al. 2002; Ghirlanda et al. 2004). The thick solid curves (black and grey) show the position of GRB 050326 as its redshift varies in the interval $0.1 < z < 10$. The Ghirlanda track is actually a boundary (as the horizontal arrows indicate), since we can infer only a lower limit to the beaming-corrected energy at each redshift. Filled circles and squares indicate the GRBs which define the above two relations, plotted as straight solid lines (together with their 1-, 2- and 3-σ contours: long-dashed, dot-dashed and dotted lines, respectively). Data were taken from Ghirlanda et al. (2004, 2005). Grey diamonds indicate the intersection of the GRB 050326 tracks with the 3-σ contours of the Amati and Ghirlanda relations. These points thus define the 3-σ redshift ranges for which GRB 050326 was consistent with the two relations. In the two GRB 050326 tracks, the region $1.5 < z < 8$ (indicated by the X-ray data) is shown in black, bound by asterisks.

commonly interpreted as the result of a jetted geometry. For GRB 050326, this break likely occurred *after* the end of the *Swift* observations. In fact, breaks earlier than ~ 1 hr are usually due to different reasons (such as the end of the refreshed shock episode; e.g. Zhang et al. 2006). If interpreted as a jet break, a very narrow jet would be implied. Moreover, the decay slope in the monitored time range is quite flat compared with that expected (and usually observed) after jet breaks (e.g. Israel et al. 1999; Harrison et al. 2001; Klose et al. 2004). The measured decay would imply a hard electron distribution ($p < 2$). Using the relations provided by Dai & Cheng (2001), an unreasonably low $p = 4\alpha - 6 = 0.8 \pm 0.2$ would result (with the X-ray band being above ν_c), which would give rise to a spectrum completely inconsistent with the observed one. Assuming ν_c above the observed range would only worsen the situation.

Assuming that the jet break occurred at $t_b \gtrsim 4$ d allows us to put some constraints on the jet opening angle and on the beaming-corrected gamma-ray energy. To this extent, the main obstacle is the lack of a well constrained redshift. Our spectral analysis of the XMM-*Newton* data allowed only to set a broad range $1.5 < z < 8$ (90% confidence level). Using the bolometric fluence $\mathcal{F}$ of the prompt emission, the lower limit on z provides a constraint on the GRB radiated energy:

$$E_{\gamma,\mathrm{iso}} = 4\pi \frac{D_\mathrm{L}^2(z)}{1+z} \mathcal{F} > 1.4 \times 10^{53} \text{ erg}, \tag{7.1}$$

where $D_\mathrm{L} > 3.40 \times 10^{28}$ cm is the luminosity distance. GRB 050326 was therefore quite likely bright in gamma rays compared to other GRBs detected by *Swift* (e.g. Chincarini et al. 2005).

Following Sari et al. (1999), the jet half-opening angle can be constrained as follows:

$$\vartheta_\mathrm{j} > 6.7^\circ \left(\frac{1+z}{2.5}\right)^{-3/8} \left(\frac{E_{\gamma,\mathrm{iso}}}{10^{53} \text{ erg}}\right)^{-1/8} \left(\frac{\eta}{0.2} \frac{n}{1 \text{ cm}^{-3}}\right)^{1/8}, \tag{7.2}$$

where η is the prompt radiative efficiency and we have assumed $t_b > 4$ d. Note that the dependance from the gamma-ray energy and on the other parameters is rather mild. The corresponding beaming-corrected gamma-ray energy is then

$$E_{\gamma,\mathrm{j}} = \frac{\pi}{2} \vartheta_\mathrm{j}^2 E_{\gamma,\mathrm{iso}} \propto \left(\frac{E_{\gamma,\mathrm{iso}}}{1+z}\right)^{3/4} \propto \mathcal{F}^{3/4} \left(\frac{D_\mathrm{L}}{1+z}\right)^{3/2}. \tag{7.3}$$

The quantity $D_{\rm L}/(1+z)$ has only a mild dependence upon z. For the redshift range allowed by our X-ray measurements ($1.5 < z < 8$), we have 1.4×10^{28} cm $< D_{\rm L}/(1+z) < 2.8 \times 10^{28}$ cm, so that $E_{\gamma,{\rm j}} > (3\text{–}8) \times 10^{51}$ erg. This is at the high end of the beaming-corrected gamma-ray energy distribution (Ghirlanda et al. 2004).

Fig. 7.6 shows the position of GRB 050326 in the plane E_γ vs $E_{\rm p}$, to check how it compares with the Amati and Ghirlanda relations (Amati et al. 2002; Ghirlanda et al. 2004). As the redshift varies, the burst position follows the tracks indicated by the thick solid curves (see the figure caption for the details). The Ghirlanda track is actually a boundary, since the lower limit on $t_{\rm b}$ translates into a lower limit for $E_{\gamma,{\rm j}}$ for any given redshift. We can ask for which redshifts GRB 050326 was consistent with the two above relations. Only loose limits are provided by the Amati relation (which has a large dispersion): at the 3-σ level, $z > 0.25$ is implied. The comparison with the Ghirlanda relation is less solid, since further assumptions are needed (such as the ambient particle density and the break time). However, for our fiducial values, we have two allowed ranges: a low-redshift region ($0.1 \lesssim z \lesssim 0.8$), plus a high-redshift solution ($z \gtrsim 4.5$). A lower particle density would move the track towards the left, while a larger jet break time would shift it rightwards.

We note that the only way to make GRB 050326 in agreement with the Ghirlanda relation and simultaneously satisfy our constraints on the X-ray absorption ($z \gtrsim 1.5$) is to require a high redshift for this event, since the low-redshift region is excluded by the fit to the X-ray column density at $> 99\%$ confidence level. Therefore, although our arguments are rather speculative, and would surely need more conclusive data, we regard GRB 050326 as a moderate/high redshift candidate. The lack of a host galaxy inside the XMM error box (Pellizza et al. 2006) is also consistent with a large redshift.

Recently, Liang & Zhang (2005) have presented a model-independent multidimensional correlation between the observed isotropic energy $E_{\gamma,{\rm iso}}$, the rest-frame spectral peak energy $E_{\rm p}$, and the comoving break time $t_{\rm b}/(1+z)$. This relation, in principle, allows to compute $E_{\gamma,{\rm iso}}$ (and z) for a GRB with known $E_{\rm p}$ and $t_{\rm b}$. However, no significant constraints could be inferred in the case of GRB 050326. Moreover, since this relation was derived using the break time as measured in the optical band, its application to X-ray data may not be valid (Liang & Zhang 2005).

7.6.3 Evidence for intrinsic absorption

The presence of intrinsic absorption, besides allowing us to constrain the GRB redshift, has other important consequences. The rest-frame absorbing system has a Hydrogen column density larger than $\sim 4 \times 10^{21}$ cm^{-2}. For moderate redshifts, $N_{\mathrm{H},z}$ would be much larger. Several afterglow observations, both from *Swift* and previous missions, showed evidence for excess X-ray absorption in addition to the Galactic value (e.g. Galama & Wijers 2001; Stratta et al. 2004; De Luca et al. 2005b). Recently, Campana et al. (2006b) showed that about half of *Swift* afterglows have a large rest-frame column density, typical of giant molecular clouds (Reichart & Price 2002). Given the connection between GRB explosion and supernovae (Galama et al. 1998b; Stanek et al. 2003; Hjorth et al. 2003; Malesani et al. 2004), this fact may constitute a powerful way to study the regions where massive star formation takes place in the high-redshift Universe. Lazzati & Perna (2002c) showed that the prompt GRB flux is able to ionize the surrounding medium up to radii as large as ~ 5 pc, therefore leaving no absorbing material. Such process may have been observed in act for GRB 000528 (Frontera et al. 2004). The fact that a large column density was measured in GRB 050326 may imply that the absorbing material was distributed in a wide region ($R \gtrsim 5$ pc), or that the ionizing flux was not large.

For GRB afterglows, comparable absorption in the X-ray range is usually not accompanied by large extinction in the optical band (Galama & Wijers 2001). Only small amounts of dust are usually inferred from the analysis of optical spectra, even when large column densities are observed in the X-ray afterglow. Several explanations were invoked to explain this discrepance, among which the destruction of dust from the burst and/or afterglow photons (Waxman & Draine 2000), a large metal-to-dust ratio in the intervening material (Stratta et al. 2004), or an overabundance of α elements (Watson et al. 2006a). Unluckily, several factors hamper the study of this problem, such as the uncertaintes in the shape and normalization of the extinction curve, the possibility that GRBs occur in special, low-metallicity environments (Fynbo et al. 2003; MacFadyen & Woosley 1999), and in several cases the lack of the redshift determination.

For GRB 050326, no detection in the optical/ultraviolet band could be obtained. Table 7.3 reports the available upper limits to the afterglow flux, from both *Swift*-UVOT and ground-based observations. In Fig. 7.7 we show the optical-to-X-ray spectral energy distribution at different epochs. We com-

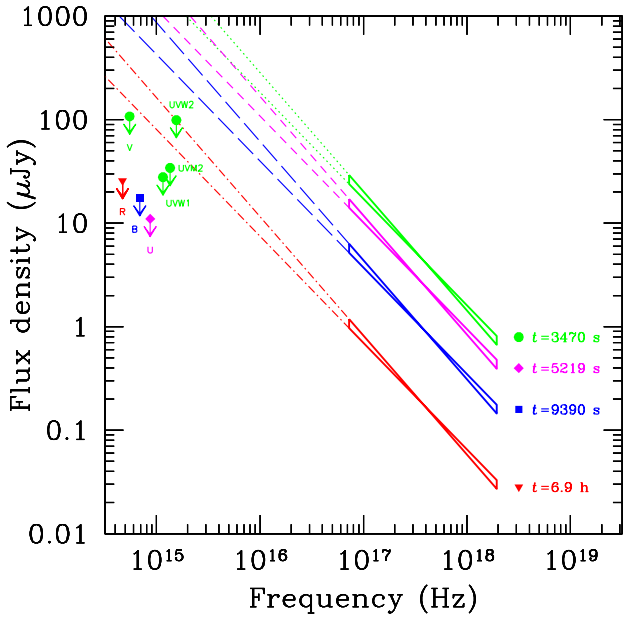

Figure 7.7: Broad-band spectral energy distribution of the afterglow of GRB 050326, computed at different times (which are identified by different symbols). The shape of the X-ray spectrum was assumed to be constant throughout the observation, and the decay law was adopted to report the X-ray flux at the time of the optical measurements.

puted the X-ray flux at the time of each available limit, adopting the decay law measured by *Swift*-XRT and XMM-*Newton*. Furthermore, no spectral evolution was assumed.

As it can be seen, the UVOT limits provide strong constraints, even if they are not particularly deep. In fact, GRB 050326 was bright in X rays (with a flux of $\approx 10^{-10}$ erg cm^{-2} s^{-1}, 1 hr after the GRB). Table 7.3 reports the optical-to-X-ray spectral indices $\beta_{\rm OX}$. For all our measurements, $\beta_{\rm OX} < \beta_{\rm X}$. Moreover, most of them violate the synchrotron limit $\beta_{\rm OX} > 0.5$, which holds for a non-obscured synchrotron spectrum. GRB 050326 can therefore be classified as truly dark, according to the definition proposed by Jakobsson et al. (2004). This limit is quite robust, since no assumptions are made about the position of the synchrotron break frequencies. For this GRB, however, we can go further in this reasoning. Our analysis of the temporal and spectral properties of the afterglow, in fact, indicated that the XRT range was below

the cooling frequency ν_c. Therefore, the extrapolation of the XRT spectrum to the optical domain seems in this case reliable, since no spectral breaks are expected to lie between these two bands. This allows estimating the suppression factor suffered by the optical flux, and is reported in the last column of Table 7.3. Again, large lower limits were found, implying conspicuous rest-frame extinction (up to a factor ~ 100 and more, corresponding to > 5 mag). The presence of the injection frequency ν_i close to or blueward of the optical band may partly explain the flux dearth. However, following the formulation of Panaitescu & Kumar (2000), even choosing rather extreme parameters ($E_{iso} = 10^{54}$ erg, $z = 5$, $\varepsilon_e = \varepsilon_B = 0.1$), ν_i can at most be comparable to the ultraviolet observed frequencies. In particular, at the time of the U-filter measurement, which provides the strongest constraint, ν_i cannot be blueward of this band. So, even if ν_i has some role in this game, it cannot be responsible for the whole suppression of the optical flux. Moreover, low values of ε_B were required to keep the cooling frequency outside the XRT range (see Sect. 7.6.2), so that ν_i was likely at much lower energies than the optical band.

The truly dark nature of this burst allows one of the following two possibilities. The burst may have suffered dust extinction in its host galaxy. The amount of dust is not straightforward to evaluate. The main obstacle is again the lack of the redshift, together with the unkwown shape of the extinction curve. However, our limit that more than 5 mag were missing in the observed U band may roughly correspond to $A_V \gtrsim 2$ mag for $z \sim 1.5$, even if many other solutions are acceptable. The second possibility is that GRB 050326 was at high redshift, as suggested by our analysis of the X-ray spectrum combined with the limits provided by the Ghirlanda relation. In this case, virtually no flux is left blueward of the redshifted Lyman dropout. To suppress the flux in the V band, $z \gtrsim 5$ would be required. However, the combination of a moderate redshift and mild absorption may relax this condition.

7.7 Conclusions

We have presented a detailed analysis of the GRB 050326 prompt and afterglow emission. The combined capabilities of *Swift* (which sampled the light curve for a relatively long time span) and XMM-*Newton* (which ensured a large statistics) allowed to obtain a thorough characterization of the

afterglow properties.

The prompt emission was relatively bright (with a 20–150 keV fluence of $\sim 8 \times 10^{-6}$ erg cm^{-2}). The spectrum was hard (photon index $\Gamma = 1.25 \pm 0.03$), suggesting a peak energy at the high end of the BAT energy range or beyond. Indeed, thanks to the simultaneous detection of this burst by the *Wind*-Konus experiment (Golenteskii et al. 2005a), the prompt spectrum could be fully characterized. The prompt bolometric fluence was $\mathcal{F} \sim 2.4 \times 10^{-5}$ erg cm^{-2} (1–10 000 keV), and the observed peak energy was $E_{\rm p,obs} = 200 \pm 30$ keV.

Due to pointing constraints, XRT and UVOT observations could start only 54 min after the GRB. The X-ray afteglow was quite bright, with a flux of 7×10^{-11} erg cm^{-2} s^{-1} (0.3–8 keV) 1 hr after the GRB. However, no optical counterpart could be detected. The X-ray light curve showed a steady decline, with no breaks or flares. The best-fit power-law decay index was $\alpha = 1.70 \pm 0.05$. Such regular behaviour is different from that usually observed by *Swift*, but this may be the result of the limited time coverage (observations could be carried out only between 54 min and 4.2 d after the burst). Indeed, extrapolation of the afterglow light curve to the time of the prompt emission overpredicts the burst flux, and may suggest a slower decay before the beginning of the XRT observation.

The analysis of the combined XRT and XMM-*Newton* data allowed to characterize in detail the afterglow spectrum. A fit with an absorbed power-law model provided a good description to the data, yielding a photon index $\Gamma = 2.09 \pm 0.08$ and a column density significantly in excess to the Galactic value. The best-fit model was thus computed adding an extra absorption component, leaving its redshift z free to vary. Although both $N_{{\rm H},z}$ and z could not be effectively constrained, a firm lower limit $N_{{\rm H},z} > 4 \times 10^{21}$ cm^{-2} could be set. Therefore, GRB 050326 adds to the growing set of afterglows with large rest-frame column density (Galama & Wijers 2001; Stratta et al. 2004; Campana et al. 2006b). The limits measured in the optical and ultraviolet region by UVOT lie well below the extrapolation of the X-ray spectrum. In particular, they violate the synchrotron limit that the optical-to-X-ray spectral index should be larger than 0.5. This implies a large extinction and/or a high redshift.

The X-ray spectral analysis also allowed us to set the lower limit $z > 1.5$ to the redshift of the absorbing component (and therefore of the GRB). The isotropic-equivalent gamma-ray energy was then $E_{\gamma,{\rm iso}} > 1.4 \times 10^{53}$ erg. The temporal and spectral properties of the afterglow were nicely consistent with

a spherical fireball expanding in a uniform medium, with the cooling frequency above the X-ray range. We could therefore set a lower limit to the jet break time $t_{\rm b} \gtrsim 4$ d. The jet opening angle could be constrained to be $\vartheta_{\rm j} \gtrsim 7^\circ$, with only a weak dependence on the (unknown) fireball energy. The beaming-corrected gamma-ray energy was $E_{\gamma,{\rm j}} = (3\text{–}8) \times 10^{51} (t_{\rm b}/4\ {\rm d})^{3/4}$ erg, independently from the redshift. GRB 050326, thus, released a large amount of gamma rays (only GRB 990123 had a larger energy in the sample of Ghirlanda et al. 2004).

To be consistent with the Ghirlanda relation (Ghirlanda et al. 2004), two redshift ranges are allowed, either at low ($z \lesssim 0.8$) or high ($z \gtrsim 4.5$) redshift. However, to simultaneously satisfy also the limits derived from the X-ray spectral analysis, only the high-redshift region is left. We note that the Ghirlanda relation is still based upon a small sample, so that any inference cannot yet be regarded as conclusive. However, the results from the X-ray spectra, the consistency of the GRB 050326 properties with the Ghirlanda relation, and the strong dearth of optical/ultraviolet afterglow flux, are overall consistent with a moderate/high redshift ($z \gtrsim 4$).

Chapter 8

Conclusions: the SN/GRB connection

The main subjet of this thesis is the SN/GRB connection. In the past years, this reseach field has made big progresses at a surprisingly rapid rate. I try to summarize here the status of the SN/GRB connection, stressing what can be learnt about GRBs and their phsycis.

8.1 Faint and bright gamma-ray bursts

The population of long-duration gamma-ray bursts is currently being thoroughly tested by *Swift*, prosecuting the work of previous missions. At least from a phenomenological point of view, it seems that there are two flavors of long GRBs, roughly denoted as 'bright' and 'faint'. Bright events are preferentially found at large redshifts ($z \gtrsim 0.5$). They have usually bright X-ray afterglows, with more-or-less well defined properties. Their energy is in excess of 10^{51} erg. This dividing line is not well defined, but roughly corresponds to the kinetic energy of a SN. One might speculate that brighter events need some degree of collimation, in order to keep the total energy in the relativistic ejecta comparable to that of the nonrelativistic ones (the SN shells). Estimates of the total energy (non isotropic equivalent) from late-time radio calorimetry also have shown that in many cases the fireball energy is of the order of 10^{51} erg (e.g. Berger et al. 2003b). Bright GRBs follow a few empirical correlations, like the Amati and Ghirlanda relations between the prompt emission peak spectrum and the isotropic and beaming-

corrected energy release, respectively (Amati et al. 2002; Ghirlanda et al. 2004; see however Sakamoto et al. 2006).

On the other hand, a few low-luminosity events are known, starting from the "prototypical" examples GRB 980425 and GRB 031203 (Chapter 2). These have a low redshift ($z \lesssim 0.2$), have weak or absent optical, X-ray and radio afterglows, and in some cases do not satisfy the Amati relation. No clear break signature has been inferred for these events and faint GRBs might be less collimated. Such bursts appear to be very numerous, and the low number of detections is simply due to their faintness, so that we can observe them only from a small volume in the Universe. It is not straightforward to compare the absolute rates of faint and bright events, since they may in principle (and likely do) have different degrees of collimation. In fact, the beaming correction for both bright and faint GRBs is not very well constrained. Current estimates for the beaming factor of bright GRBs vary between ~ 50 and ~ 500, so that the rate is uncertain by an order of magnitude. For faint events, the collimation might quite low (beaming factor of $\sim$ a few). Using the available constraints, the rates of the two groups can be more or less comparable (provided that faint bursts are not much collimated).

The concept of 'faint' GRB is however not so sharply defined. *Swift* is showing that the gap between bright and faint events may be filled with intermediate-type objects (e.g. GRB 060218). The class of X-ray flashes (XRFs) is also likely to contribute to this intermediate population. If XRFs follow the Amati correlation, for a peak energy of the order of a few keV their isotropic energy release is expected to be of the order of 10^{49}–10^{50} erg, akin to that of faint events. XRFs seem to form a low-energy extrapolation of the bright GRB population (they have afterglow with 'normal' properties, they follow the Amati correlation, they are hosted by similar galaxies, and may have similar SN progenitors). Overall, it may well be that the division between faint and bright bursts is only dictated by an observational bias, and that all long GRBs form a continuum.

Among the proposed models to explain the diversity of the two kinds of events, two possibilities have been envisaged. First, faint and bright GRBs may be different objects. Second, faint GRBs may be the result of classical jetted GRBs observed off-axis. I will evaluate both possibilities below. A third solution requires peculiar spectral evolution of these events, which would make us miss part of the emission, so that these bursts would be actually much brighter (Ghisellini et al. 2006). It is not simple, however, to

reconcile the afterglow properties with those of standard GRBs.

8.2 The associated supernovae

The discovery of the SN connection is in principle a very powerful tool to constrain GRB models. Here, there is possibly the biggest surprise. The present data indicate that SNe accompany both faint and bright GRBs. Furthermore, the SNe associated with the two kinds of events can be strikingly similar, as spectacularly demonstrated by the four "golden bursts" GRB 980425, GRB 030329, GRB 031203 and GRB 060218 (GRB 030329 belonging to the bright group). A hypernova with similar properties (both in terms of luminosity, colors and kinetic energy) has been observed beyond doubt in these objects. Albeit there is diversity in the SN population (see Chapters 3, 4, 5), this does not look to be correlated with the properties of the relativistic ejecta. For example, two faint GRBs have the slowest- and the fastest-evolving SN (GRB 031203 and GRB 060218, respectively). The three bursts with deep SN limits (XRF 040703, GRB 060505 and GRB 060614) have different luminosities, and GRB 060614 appears to belong to the bright group (Chapter 5). The distinction between GRBs and XRFs (if real) is also apparently uncorrelated with the SN properties: XRF 029093 and XRF 040701 had a bright hypernova and a deep limit, respectively. Figure 8.1 compares the gamma-ray and SN luminosities for all the bursts with available data (the redshift determination was required for inclusion in the sample). As it can be seen, there is no apparent correlation between the two properties. Moreover, the three objects with no detected SN stand clearly separated from the other cases.

8.3 Off-axis or faint events?

The similarity of the associated SNe have provided strong support for the interpretation of faint GRBs as off-axis events (Yamazaki et al. 2003; Ramirez-Ruiz et al. 2005a). In fact, albeit some asymmetry is present in core-collapse SNe (e.g Wang et al. 2003; Maeda et al. 2006), this is not very pronounced (the angular variation of the emission is at most a factor of ~ 3). On the contrary, the relativistic emission may give rise to strong angular dependance of the emission profile, due to the relativistic light aberration. Far from the

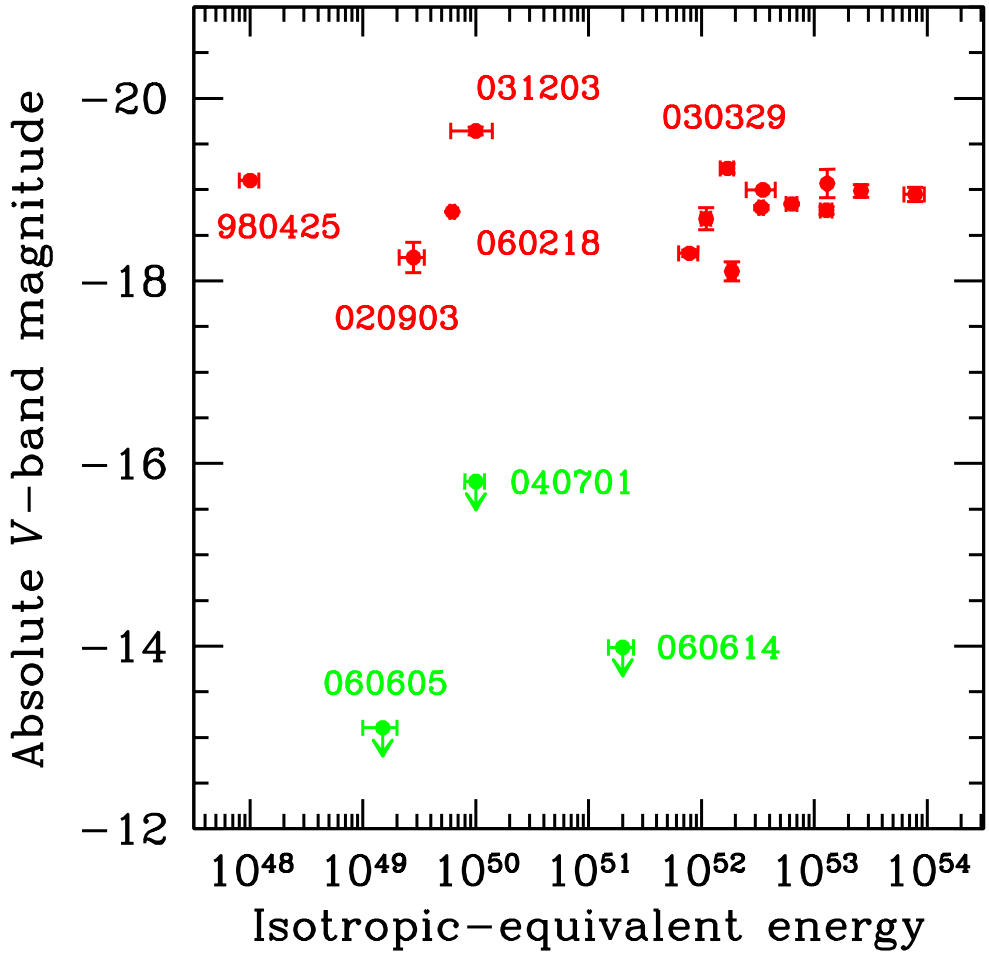

Figure 8.1: Comparison of the peak magnitudes of GRB-associated SNe versus the gamma-ray energy release. $M_V = -19.1$ for SN 1998bw was assumed (from Galama et al. 1998b using the current cosmological parameters). Colors similar to those of SN 1998bw were assumed to compute the V-band magnitudes. Most data come from the light curve fitting performed by Zeh et al. (2004, 2005). Gamma-ray data have been taken from the recent compilation of Amati (2006a). Data for bursts indicated by the labels come from Galama et al. (1998b); Soderberg et al. (2005); Malesani et al. (2004); Ferrero et al. (2006); Lipkin et al. (2004); Della Valle et al. (2006d); Fynbo et al. (2006).

axis, the burst luminosity can be easily lower by a factor 10^3–10^4. Actually, the precise emission depends on the jet angular profile: if there is low-energy material emitted outside the main jet axis (Rossi et al. 2002), its emission may overwhelm the off-beam burst radiation. Therefore, a large spread in the apparent burst energetics can be observed.

Further evidence supporting the off-jet hypothesis comes from the host galaxies of closeby GRBs, which are overall similar to those of bright events (with the caveat of their different redshifts; Sollerman et al. (2005)). Last, the current uncertainties in the rate determination make similar the rate of faint GRBs (*not* corrected for beaming) and that of bright GRBs *after* the beaming correction. This numerical coincidence may suggest that faint GRBs represent the unseen population of off-axis bright bursts. It should be stressed, however, that the uncertainties in the rate determination are still very large. The GRB rate (taking into account the beaming) is about 1% (uncertain by a factor of 3; Della Valle 2006a) of that of type-Ib/c SNe, so that only a small fraction of nearby SNe may host a (likely off-axis) GRB.

There are however also strong arguments against the off-beam hypothesis for faint GRBs. One of the main arguments is that the relativistic aberration effect stops once the fireball becomes nonrelativistic. Such transition has been observed in a few cases (Frail et al. 2000) at radio wavelengths and occurs $\sim$ one year after the GRB (depending on the burst energy and circumburst density). After that time, the GRB emission becomes isotropic, and any observer sees the same luminosity. For an off-axis jet we would than expect to see a rising flux close to this epoch. This has not been observed so far, and very stringent limits have been put for closeby GRBs (Soderberg et al. 2004a,b). Furthermore, no nearby type-Ic SNe (unassociated with a GRB) have shown such behaviour (Soderberg et al. 2004b). To be consistent with bright GRBs, very low densities are implied for these events, forcing us to assume different environments for the two groups.

The energetics of the X-ray afterglow may also be used as a test for the jet model. Figure 8.2 shows the X-ray luminosity (10 hr after the burst) versus the prompt isotropic equivalent energy (from Amati et al. 2006b). Triangles show bright events, while dots show the low-luminosity events. As expected, there is a correlation among these two quantities. Albeit there is large scatter, it is very significant. What is remarkable is that faint burts lie more or less on the extrapolation of the correlation holding for bright bursts alone (dotted line). If faint GRBs are off-axis events, it is not straightforward to let them obey this relation. The X-ray luminosity at 10 hr, due to its low dependance

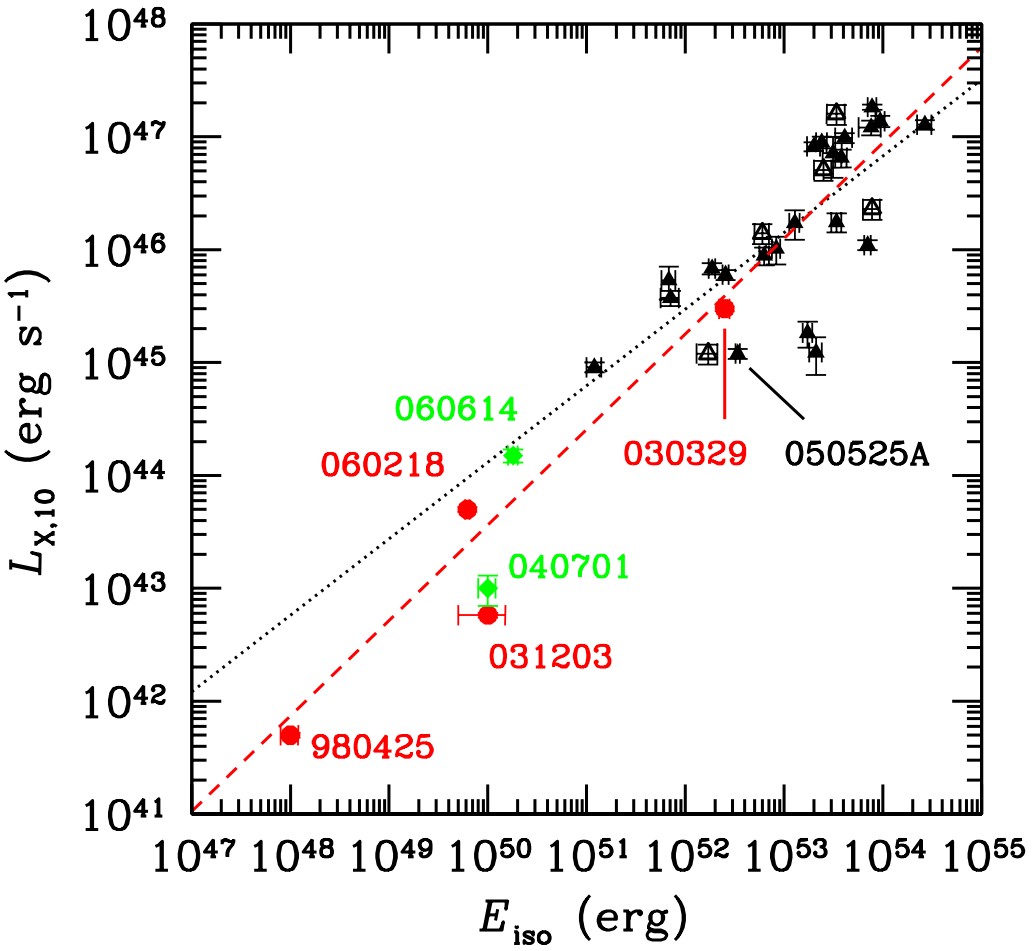

Figure 8.2: 2–10 keV afterglow luminosity at 10 days $L_{X,10}$ versus the isotropic prompt energy release (1–10 000 keV). Triangles represent bursts taken from the samples of Berger et al. (2003c) and Nousek et al. (2006). When available, gamma-ray data were taken from (Amati 2006a) and Nousek et al. (2006). Open triangles represent those *Swift* bursts without measurement of the peak energy, for which a bolometric correction based on an average spectrum was adopted. Other sub-energetic events are included (circles and diamonds); their X-ray luminosities were derived from the X–ray afterglow light curves reported by Kouveliotou et al. (2004), Watson et al. (2004), Campana et al. (2006), and Mangano et al. (2006). The plotted lines are the best fit power-laws obtained excluding (dotted) and including (dashed) sub-energetic GRBs.

from the other parameters, has been used as a proxy to the fireball energy (Freedman & Waxman 2001, but see Granot et al. 2006). For an off-axis jet, the X-ray afterglow at 10 hr is expected to be less de-beamed with respect to the prompt emission, due to the fireball deceleration (the Doppler factor is strongly dependent on Γ), so that we expect off-axis events to be above the relation valid for on-axis events. However, the scatter is large, and more events are needed to populate this plot.

Amati et al. (2006b) have pointed out that, among the faint events, GRB 060218 (Campana et al. 2006) is consistent with the Amati relation (Amati et al. 2002). GRB 980425 and GRB 031203 were outliers to this relation. With a single case, it is difficult to say if this was just a chance coincidence, or if this fact it has a deeper physical meaning. There are however other faint GRBs respecting the Amati relation (such as XRF 020903; Sakamoto et al. 2004). Interestingly, based upon *Wind*/Konus data (Golenetskii et al. 2006), also GRB 060614 looks to lie on the correlation (albeit a more careful analysis of the prompt spectrum is needed to asses this[1]). Adopting $t_{\rm jet} = 1.3$ d (Della Valle et al. 2006d), we infer a half-opening angle of $\approx 12^\circ$, which also makes this burst consistent with the Ghirlanda relation (Ghirlanda et al. 2004). These facts would suggest that the above two intermediate-luminosity GRBs belong to the same group as bright GRBs. Off-axis models are not able to reproduce the Amati relation (Donaghy 2006b).

The fact that faint GRBs are really underenergetic events is not surprising. First, the luminosity function of several kinds of objects peak at low luminosities. Second, the inferred energies for both faint and bright GRBs (after correcting for beaming) are just a fraction of that of a SN. Hypernova ejecta carry more than $\sim 10^{52}$ erg, and also fainter SNe have 10^{51} erg, not to mention the energy released in neutrinos and gravitational waves. A variation in the burst energy would involve only a little fraction of the overall energy budget.

The existence of off-axis bursts, however, is unavoidable if our present understanding of GRBs is correct. The search for these events is thus very

[1]The *Wind*/Konus (Golenetskii et al. 2006) data show that the burst is composed by an initial hard spike with peak energy $E_{\rm p} \approx 300$ keV, followed by a more intense soft episode with unconstrained peak energy and photon index $\Gamma > 2$ (suggesting $E_{\rm p} \lesssim 20$ keV. From these data the flux-weighted peak energy is $E_{\rm p} \approx 60$ keV, with an error of $\sim 50\%$. Preliminary analysis of BAT spectra shows that $E_{\rm p} \lesssim 30$ keV (Mangano et al. 2006). The allowed range for being consistent with the updated Amati relation (Amati 2006a) is 10 keV $\lesssim {\rm E_p} < 100$ keV (2-σ level; Amati et al. 2006b).

important. Some authors have pointed out a handful of nearby SNe as candidate off-axis events (Granot & Ramirez-Ruiz 2004; Mazzali et al. 2005), but these suggestions are far from being solid. I think that a clear detection of an off-axis GRB is among the most important observational advances to be achieved in GRB field. The more direct way would be to discover rising lightcurves at radio or optical frequencies ("orphan afterglows"), or possibly to detect superluminal expansion of the ejecta associated to some nearby SN.

8.4 Short gamma-ray bursts

The study of short gamma-ray bursts has just begun. The first data have suggested a rich variety of features. Short GRBs arise from diverse environments. The first short GRB identified galaxy was a bright elliptical, a fact somehow expected having in mind a binary merger origin. However, the second identified galaxy was of a different kind (see Chapter 6), with significant star formation. Now the currently known host population is equally split among early- and late-type galaxies, though the number of known events is still small.

The offset distribution of short GRB counterparts can provide a very important clue to their origin. Remarkably, at least two of the short GRB counterparts have exploded outside their parent galaxies. Again, a binary merger origin is capable to explain this feature. Such systems can in fact receive a large kick velocity due to the SN explosions, and since a long delay can be expected between the binary formation and its coalescence, large distances can be travelled. In this respect, the small offset found between the optical counterparts of GRB 050709 (Chapter 6) and GRB 051221A and their host galaxy centers would be consistent with the younger ages of the stellar populations (both hosts show active star formation). However, this simple argument may not hold if the binary is bound to the galaxy via gravitational interaction. For example, GRB 050724 exploded well inside its host galaxy, even if its stellar population was quite old.

It would be very interesting, in this respect, to measure directly the peculiar velocity of a short GRB. This is in principle possible through spectroscopy, by comparing the afterglow redshift with that of the parent galaxy. To date, no direct spectroscopic observation could be achieved for a short GRB afterglow (all redshifts were measured for the host galaxies). However, this may turn out difficult to perform in practice, since short GRB after-

glows are faint, and particularly those outside their host galaxies. Further, for GRBs exploding out of their galaxies only very weak absorption lines are expected. Nonetheless, this is a possibility worth being explored.

Current data are indicating that the progenitor systems of short GRBs explode with a significant delay after their formation. This lag seems to be strongly variable. Binary merging systems fit in this view, but this is not the only possibility. A different solution may be the collapse of a neutron star to a black hole due to accretion from a companion star. The lag would be in this case tied to the time needed to reach the maximum stable mass for a neutron star.

Direct spectroscopy of afterglows may allow getting some indirect information on the progenitor, through the study of the burst environment. Such analyses have provided important clues for long GRB afterglows, and they may be relevant also for the short ones. The ISM surrounding merging objects is not expected to be particularly dense. However, in the collapsing neutron star scenario, the situation may be more favorable. For example, it would be possible to detect the signature of the wind from the secondary star.

The next few years will likely provide us with new clues and new surprises. As the number of known events will grow, we will be able to build meaningful distributions of the observed properties, and to compare them to model predictions. Should the binary merger scenario be confirmed, further clues to the system composition could be drawn. For example, systems containing a black hole may have different behaviours with respect to binary neutron stars. It is of the primary importance to collect the largest possible observational material.

From a different point of view, it is remarkable that both the prompt and the afterglow emission are overall similar between long and short GRBs. Thus, despite the very different environmental conditions, there seems to be an underlying similar physical mechanism. Likely, both kind of explosions witness the formation of a stellar-mass black hole, with the formation of a relativistic outflow powered by accretion. It looks then that the understanding of GRBs may have wider implications for the physics of other systems with jets, like Galactic superluminal sources and possibly AGNs.

8.5 Future prospects

The GRB field has now reached some degree of maturity. There is a general framework with well supported observational evidence. Likely, the next frontier in GRB studies is the full exploitation of their potential to probe the far Universe. Their value is still larger once their strict connection with the star formation is considered. The existence of GRBs at large redshift has been demonstrated by the discovery of GRB 050904 at $z = 6.295$ and several other events at $z > 4$. Albeit the fraction of high-redhisft objects in the gamma-ray bursts sample is much larger than for any other class of objects (AGN, galaxies), the complexity of discovering high-redshift counterparts and measuring their redshifts has been an issue up to now. However, it seems that the GRB community has trained, and things may improve in the next few years.

The big, critical issue which still threaten the possibility of using GRBs as unbiased probes of the star formation is to understand which kind of conditions are necessary for their production. There is now some evidence that GRB host galaxies are different from other star forming system. Albeit the impact of selection effects has not been fully evaluated yet, it looks that the critical parameter is the metallicity (see Chapter 1). The collapsar model explicitely favors GRB production in low-metallicity systems. Interestingly, this may actually *favor* the production of GRBs at high redshifts, where the metallicity is much lower than at $z = 0$. On the other hand, a low metallicity is more likely to be found in low-mass (and luminosity) galaxies. This is consistent with the average low brightness of GRB hosts. This offers the unique opportunity to study very faint systems, which would be otherwise very difficult to probe. Host galaxies as faint as $V \sim 30$ have a measured redshift thanks to a GRB exploding inside them.

GRB afterglows also allow probing the chemical composition, the excitation state, and the dynamical conditions of the gas in star-forming regions. The information coming from both optical and X-ray observations can be coupled effectively, thus allowing to draw a complete picture of the different gas components (hydrogen, metals, dust). These observations cannot be achieved using AGN absorption spectra, since star forming regions are compact, and the probability of being on the sightline to a quasar are very small. On the other hand, GRB explosions are located just inside the star forming regions, so that they are very well suited to study the conditions in star-formation sites.

However, in order to exploit effectively GRBs as cosmological probes, we are forced to reach a full understanding of the GRB production mechanism. The theoretical modelling has found viable solutions to yield successful GRB explosions, but these need to be thoroughly tested before being applied to the far Universe. Nearby GRBs offer the opportunity to study in detail the environment where GRBs were born, and this can provide a critical test to models.

Bibliography

Akerlof, C., Balsano, R., Barthelmy, S., et al. 1999, Nature, 398, 400

Alard, C. 2000, A&AS, 144, 363

Alard, C., & Lupton, R. H. 1998, ApJ, 503, 325

Amati, L., Frontera, F., Tavani, M., et al. 2002, A&A, 390, 81

Amati, L. 2006a, MNRAS, 372, 233

Amati, L., Della Valle, M., Frontera, F., Malesani, D., Guidorzi, C., Montanari, E., & Pian, E. 2006b, A&A, submitted (astro-ph/0607148)

Antonelli, L. A., Piro, L., Vietri, M., et al. 2000, ApJ, 545, L39

Barth, A. J., Sari, R., Cohen, M. H., et al. 2003, ApJ, 584, L47

Barthelmy, S., Chincarini, G., Burrows, D. N., et al. 2005a, Nature, 438, 994

Barthelmy, S., Gehrels, N., Norris, J., & Sakamoto, T. 2005b, GCN Circ. 4401

Band, D., Matteson, J., Ford, L., et al. 1993, ApJ, 413, 281

Band, D., Cummings, J., Perri, M., et al. 2005, GCN Circ. 3466

Belczyński, K., & Kalogera, V. 2001, ApJ, 550, 183

Belczyński, K., Bulik, T., & Rudak, B. 2002, ApJ, 571, 394

Belczynski, K., Perna, R., Bulik, T., Kalogera, V., Ivanova, V., & Lamb, D. Q. 2006, ApJ, 648, 1110

Berger, E., Kulkarni, S. R., Bloom, J. S., et al. 2002, ApJ, 581, 981

Berger, E., Cowie, L. L., Kulkarni, S. R., Frail, D. A., Aussel, H., & Barger, A. J. 2003a, ApJ, 588, 99

Berger, E., Kulkarni, S. R., Pooley, G., et al. 2003b, Nature, 426, 154

Berger, E., Kulkarni, S. R., & Frail, D. A. 2003c, ApJ, 590, 379

Berger, E., Kulkarni, S. R., Fox, D. B., et al. 2005a, ApJ, 634, 501

Berger, E., Price, P. A., Cenko, S. B., et al. 2005b, Nature, 438, 988

Berger, E., Penprase, B. E., Cenko, S. B., Kulkarni, S. R., Fox, D. B., Steidel, C. C., & Reddy, N. A. 2006, ApJ, 642, 979

Bersier, D., Rhoads, J. E., Fruchter, A. S., et al. 2004, GCN Circ. 2544

Blake, C. H., Bloom, J. S., Starr, D. L., et al. 2005, Nature, 435, 181

Blanton, M. R., Hogg, D. W., Bahcall, N. A., et al. 2003, ApJ, 592, 819

Bloom, J. S., Kulkarni, S. R., Djorgovski, S. G., et al. 1999, Nature, 401, 453

Bloom, J. S., Kulkarni, S. R., & Djorgovski, S. G. 2002a, AJ, 123, 1111

Bloom, J. S., Kulkarni, S. R., Price, P. A., et al. 2002b, ApJ, 572, L45

Bloom, J. S., Frail, D. A., & Kulkarni, S. R. 2003a, ApJ, 594, 674

Bloom, J. S., Prochaska, J. X., Pooley, D., et al. 2006a, ApJ, 638, 354

Bloom, J. S., Perley, D. A., Chen, H.-W., et al. 2006b, ApJL, in press (astro-ph/0607223)

Blustin, A. J., Band, D., Barthelmy, S., et al. 2006, ApJ, 637, 901

Boër, M., Atteia, J. L., Damerdji, Y., Gendre, B., Klotz, A., & Stratta, G. 2006, ApJ, 638, L71

Brown, P. J., Holland, S. T., Mangano, V., Parsons, A. M., & Gehrels, N. 2006, GCN Circ. 5262

Bosnjak, Z., Celotti, A., Ghirlanda, G., Della Valle, M., & Pian, E. 2006, A&A, 447, 121

Burrows, D. N., Hill, J. E., Nousek, J. A., et al. 2005a, Space Sci. Rev., 120, 165

Burrows, D. N., Romano, P., Falcone, A., et al. 2005b, Science, 309, 1833

Burrows, D. N., Grupe, D., Capalbi, M., et al. 2006, ApJ, submitted (astro-ph/0604320)

Butler, N., Sakamoto, T., Suzuki, M., et al. 2005, ApJ, 621, 88

Caldwell, N., McLeod, B., Garnavich, P., & Stanek, K. Z. 2002, GCN Circ. 1759

Cameron, P. B., & Frail, D. A. 2005, GCN Circ. 3495

Campana, S., Antonelli, L. A., Chincarini, G., et al. 2005, ApJ, 625, L23

Campana, S., Mangano, V., Blustin, A. J., et al. 2006a, Nature, 442, 1008

Campana, S., Romano, P., Covino, S., et al. 2006b, A&A, 449, 61

Cappellaro, E., Patat, F., Mazzali, P. A., et al. 2001, ApJ, 549, L215

Cardelli, J. A., Clayton, G. C., & Mathis, J. S. 1989, ApJ, 345, 245

Castro-Tirado, A. J., Castro-Cerón, J. M., Gorosabel, J., et al. 2002, A&A, 393, L55

Castro-Tirado, A. J., de Ugarte-Postigo, A., Gorosabel, J., et al. 2005, A&A, 439, L15

Chincarini, G., Moretti, A., Romano, P., et al. 2005, astro-ph/0506453

Christensen, L., Hjorth, J., & Gorosabel, J. 2005, A&A, 425, 913

Cimatti, A., Daddi, E., Mignoli, M., et al. 2002, A&A, 381, L68

Cobb, B. E., Baylin, C. D., van Dokkum, P. G., Buxton, M. M., & Bloom, J. S. 2004, ApJ, 608, L93

Cobb, B. E., & Baylin, C. D. 2006a, GCN Circ. 5282

Cobbe, B. E., Bailyn, C. D., van Dokkum, P. G., & Natarajan, P. 2006, ApJ, 651, L85

Colgate, S. A. 1968, Canadian J. Phys., 46, 476

Corsi, A., & Piro, L. 2006, A&A, 458, 741

Costa, E., Frontera, F., Heise, J., et al. 1997, Nature, 387, 783

Covino, S., Lazzati, D., Ghisellini, G., et al. 1999, A&A, 348, L1

Covino, S., Malesani, D., Israel, G. L., et al. 2006, A&A, 447, L5

Crew, G. B., Villasenor, J., Vanderspek, R., et al. 2002, GCN Circ. 1734

Crew, D. B., Lamb, D. Q., Richter, G. R., et al. 2003, ApJ, 599, 387

Cummings, J., Barthelmy, S., Barbier, L., et al. 2005, GCN Circ. 3145

Cusumano, G., Mangano, V., Angelini, L., et al. 2006a, ApJ, 639, 316

Cusumano, G., Mangano, V., Chincarini, G., et al. 2006b, Nature, 440, 164

Dai, Z. G., & Chen, K. S. 2001, ApJ, 558, L109

Della Valle, M., Malesani, D., Benetti, S., et al. 2003a, A&A, 406, L33

Della Valle, M., Malesani, D., Benetti, S., Testa, V., & Stella, L. 2003b, IAU Circ. 8197

Della Valle, M. 2006, procs. of Gamma Ray Burst in the Swift Era (astro-ph/0604110)

Della Valle, M, Malesani, D., Bloom, J. S., et al. 2006b, ApJ, 642, L103

Della Valle, M., Malesani, D., Benetti, S., Chincarini, G., Stella, L., & Tagliaferri, G. 2006c, IAUC 8696

Della Valle, M., Chincarini, G., Panagia, N., et al. 2006, Nature, in press (astro-ph/0608322)

De Luca, A., Götz, D., & Campana, S. 2005a, GCN Circ. 3293

De Luca, A., Melandri, A., Caraveo, P., et al. 2005b, A&A, 440, 85

De Pasquale, M., Piro, L., Perna, R., et al. 2003, ApJ, 592, 1018

De Pasquale, M., Piro, L., Gendre, B., et al. 2005, A&A, 455, 813

Dermer, C. D., & Atoyan, A. 2006, ApJ, 643, L13

Devillard, N. 1997, The Messenger, 87, 19

Dickey, J. M., & Lockman, F. J., 1990, ARA&A, 28, 215

Djorgovski, S. G., Kulkarni, S. R., Bloom, J. S., Goodrich, R., Frail, D. A., Piro, L., & Palazzi, E. 1998, ApJ, 508, L17

Donaghy, T. Q., Lamb, D. Q., Sakamoto, T., et al. 2006a, ApJ, submitted (astro-ph/0605570)

Donaghy, T. Q. 2006b, ApJ, 645, 436

Dressler, A., & Gunn, J. E. 1983, ApJ, 270, 7

Dutra, C. M., Ahumada, A. V., Clariá, J. J., Bica, E., & Barbuy, B. 2003, A&A, 408, 287

Ehle, M., & Perez Martinez, R. 2005, GCN Circ. 3149

Eichler, D., Livio, M., Piran, T., & Schramm, D. N. 1989, Nature, 340, 126

Eldridge, J. J., Genet, F., Daigne, F., & Mochkovitch, R. 2006, MNRAS, 367, 186

Ellison, S., Vreeswijk, P. M., Ledoux, C., et al. 2006, MNRAS, 372, L38

Esin, A., & Blandford, R. 2000, ApJ, 534, L151

Falcone, A. D., Burrows, D. N., Lazzati, D., et al. 2006, ApJ, 641, 1010

Fan, Y. Z., Piran, T., & Xu, D. 2006, JCAP, 09, 013

Fenimore, E. E., Ramirez-Ruiz, E., & Wu, B. 1999a, ApJ, 518, L73

Ferrero, P., Kann, D. A., Zeh, A., et al. 2006, A&A, 457, 857

Filippenko, A. V., Richmond, M. W., Branch, D., et al. 1992, AJ, 104, 1543

Filippenko, A. V., Barth, A. J., Matheson, J., et al. 1995, ApJ, 450, L11

Fishman, G. J., & Meegan, C. A. 1995, ARA&A, 33, 415

Fiore, F., Brusa, M., Cocchia, F., et al. 2003, A&A, 409, 79

Fiore, F., D'Elia, V., Lazzati, D., et al. 2005, ApJ, 624, 853

Foley, R. J., Papenkova, M. S., Swift, B. J., et al. 2003, PASP, 115, 1220

Foley, R. J., Chen, H.-W., Bloom, J. S., & Prochaska, J. X. 2005, GCN Circ. 3483

Ford, L. A., Band, D. L., Matteson, J. L., et al. 1995, ApJ, 439, 307

Fox, D. W., & Price, P. A. 2002, GCN Circ. 1731

Fox, D. W., Yost, S., Kulkarni, S. R., et al. 2003a, Nature, 422, 284

Fox, D. W., Price, P. A., Soderberg, A. M., et al. 2003b, ApJ, 586, L5

Fox, D. B., Frail, D. A., Cameron, P. B., et al. 2005a, GCN 3585

Fox, D. B., Frail, D. A., Price, P. A., et al. 2005b, Nature, 437, 845

Frail, D. A., Kulkarni, S. R., Nicastro, L., Feroci, M., & Taylor, G. B. 1997, Nature, 389, 261

Frail, D. A., Waxman, E., & Kulkarni, S. R. 2000, ApJ, 537, 191

Frail, D. A., Kulkarni, S. R., Sari, R., et al. 2001, ApJ, 562, L55

Frail, D. A. 2003, GCN Circ. 2473

Freedman, D. L., & Waxman, E. 2001, ApJ, 547, 922

French, J., Melady, G., Hanlon H., Jelínek, M., & Kubánek, P. 2006, GCN Circ. 5257

Fryer, C. L., & Heger, A. 2005, ApJ, 623, 302

Frontera, F., Amati, L., Costa, E., et al. 2000, ApJ, 127, 59

Frontera, F., Amati, L., Lazzati, D., et al. 2004, ApJ, 614, 301

Fruchter, A. S., Thorsett, S. E., Metzger, M. R., et al. 1999, ApJ, 519, L13

Fruchter, A. S., Levan, A., Vreeswijk, P. M., Holland, S. T., & Kouveliotou, C. 2002, GCN Circ. 1781

Fruchter, A. S., Levan, A., Strolger, L., et al. 2006, Nature, 441, 463

Fukugita, M., Shimasaku, K., & Ichikawa, T. 1995, PASP, 107, 945

Fynbo, J. U., Jensen, B. L., Gorosabel, J., et al. 2001, A&A, 369, 373

Fynbo, J. P. U., Jakobsson, P., Møller, P., et al. 2003, A&A, 406, L63

Fynbo, J. P. U., Sollerman, J., Hjorth, J., et al. 2004, ApJ, 609, 962

Fynbo, J. P. U., Watson, D., Thöne, C., et al. 2006, Nature, in press (astro-ph/0608313)

Galama, T. J., Groot, P. J., van Paradijs, J., et al. 1998a, ApJ, 497, L13

Galama, T. J., Vreeswijk, P. M., van Paradijs, J., et al. 1998b, Nature, 395, 670

Galama, T. J., & Wijers, R. A. M. J. 2001, ApJ, 549, L209

Gal-Yam, A., Ofek, E. O., & Shemmer, O. 2002, MNRAS, 332, L73

Gal-Yam, A., Moon, D. S., Fox, D. W., et al. 2004, ApJ, 609, L59

Gal-Yam, A., Fox, D. W., Price, P. A., et al. 2006, Nature, in press (astro-ph/0608322)

Garnavich, P. M., Stanek, K. Z., Wyrzykowski, L., et al. 2003, ApJ, 582, 924

Garnavich, P. M., Pahre, M., Noriega-Crespo, A., et al. 2005, GCN Circ. 3532

Gehrels, N., Chincarini, G., Giommi, P., et al. 2004, ApJ, 621, 558

Gehrels, N., Sarazin, C. L., O'Brien, P. T., et al. 2005, Nature, 437, 851

Gehrels, N., et al. 2006, Nature, submitted

Germany, L. M., Reiss, D. J., Sadler, E. M., Schmidt, B. P., & Stubbs, C. W. 2000, ApJ, 533, 320

Ghirlanda, G., Celotti A., & Ghisellini, G. 2002, A&A, 393, 409

Ghirlanda, G., Ghisellini, G., & Lazzati, D. 2004, ApJ, 616, 331

Ghirlanda, G., Ghisellini, G., Lazzati, D., & Firmani, C. 2005, Il nuovo cimento, 28, 303

Ghirlanda, G., Ghisellini, G., & Firmani, C. 2006, New J. Phys, 6, 123.

Ghisellini, G., Celotti, A., & Lazzati, D. 2000, MNRAS, 313, L1

Ghisellini, G., Ghirlanda, G., Mereghetti, S., Bosnjak, Z., Tavecchio, F., & Firmani, C. 2006, MNRAS, in press (astro-ph/0605431)

Golenteskii, S., Aptekar, R., Mazets, E., et al. 2005a, GCN Circ. 3152

Golenetskii, S., Aptekar, R., Mazets, E., Pal'shin, V., Frederiks, D., & Cline, T. 2005b, GCN Circ. 3474

Golenetskii, S., Aptekar, R., Mazets, E., Pal'shin, V., Frederiks, D., & Cline, T. 2006, GCN Circ. 5264

Gonzalez, M. M., Dingus, B. L., Kaneko, Y., Preece, R. D., Dermer, D. D., & Briggs, M. S.; 2003, Nature, 424, 749.

Gorosabel, J., Castro-Tirado, A. J., Guziy, S., et al. 2006, A&A, 450, 87

Götz, D., Mereghetti, S., Beck, M., Borkowski, J., & Mowlavi, N. 2003, GCN Circ. 2459

Götz, D., Mereghetti, S., Mowlavi, N., Shaw, S., Beck, M., Borkowski, J., & Lund, N. 2005, GCN Circ. 3472

Granot J., & Ramirez-Ruiz, E. 2004, ApJ, 609, L9

Granot, J., Königl, A., & Piran, T. 2006, MNRAS, 370, 1946

Greiner, J., Klose, S., Reinsch, K., et al. 2003, Nature, 426, 157

Grimm, H.-J., Gilfanov, M., & Sunyaev, R., 2003, MNRAS, 339, 793

Guetta, D., Perna, R., Stella, L., & Vietri, M. 2004, ApJ, 615, L73

Guetta, D., & Piran, T. 2005, A&A, 435, 421

Guetta, D., & Piran, T. 2006, A&A, 453, 823

Haislip, J., Nysewander, M., Reichart, D., et al. 2006, Nature, 440, 181

Hamuy, M., Pinto, P. A., Maza, J., et al. 2001, ApJ, 558, 615

Hamuy, M. 2003, in Core Collapse of Massive Stars, ed. C. Fryer (Dordrecht: Kluwer)

Harkness, R. P., Wheeler, J. C., Margon, B., et al. 1987, ApJ, 317, 355

Harrison, F. A., Yost, S. A., Sari, R., et al. 2001, ApJ, 559, 123

Heise, J. 2003, in AIP Conf. Ser. 662, Gamma-ray Burst and Afterglow Astronomy 2001, ed. G. R. Ricker & R. K. Vanderspek (New York: AIP), 229

Hill, J. E., Burrows, D. N., Nousek, J. A., et al. 2004, Proc. SPIE, 5165, 175

Hjorth, J., Sollerman, J., Møller, P., et al. 2003, Nature, 423, 847

Hjorth, J., Watson, D., Fynbo, J. P. U., et al. 2005a, Nature, 437, 859

Hjorth, J., Sollerman, J., Gorosabel, J., et al. 2005b, ApJ, 630, L117

Hoge, J., Willott, C., Grimes, J., Tilanus, R., & Moriarty-Schieven, G. 2002, GCN Circ. 1742

Holland, S. T., Bersier, D., Bloom, J. S., et al. 2004, AJ, 128, 1955

Holland, S. T., Still, M., Landsman, W., et al. 2005, GCN Circ. 3150

Humphrey, P. J., Fabbiano, G., Elvis, M., Church, M. J., & Bałucińska-Church, M., 2003, MNRAS, 344, 134

Hurley, K., Dingus, B. L., Mukherjee, R., et al. 1994, Nature, 372, 652

Hurley, K., Berger, E., Castro-Tirado, A. J., et al. 2002, ApJ, 567, 447

Hurley, K., Boggs, S. E., Smith, D. M., et al. 2005, Nature, 434, 1098

Israel, G. L., Marconi, G., Covino, S., et al. 1999, A&A, 348, L5

Iwamoto, K., Nomoto, K., Höflich, P., et al. 1994, ApJ, 437, L115

Iwamoto, K., Mazzali, P. A., Nomoto, K., et al. 1998, Nature, 395, 672

Iwamoto, K., Nakamura, T., Nomoto, K., et al. 2000, ApJ, 534, 660

Jakobsson, P., Hjorth, J., Fynbo, J. P. U., et al. 2004, ApJ, 617, L21

Jakobsson, P., Levan, A., Fynbo, J. P. U., et al. 2006, A&A, 447, 897

Jensen, B. L., Jörgensen, U. G., Hjorth, J., et al. 2005, GCN Circ. 3589

Kalberla, P. M. W., Burton, W. B., Hartmann, D., et al. 2005, ApJ, 440, 775

Kawabata, K. S., Deng, J., Wang, L., et al. 2003, ApJ, 593, L19

Kawai, N., Kosugi, G., Aoki, K., et al. 2006, Nature, 440, 184

Kennicutt, R. C. Jr 1998, ARA&A, 36, 189

King, A., O'Brien, P. T., Goad, M. R., et al. 2005, ApJ, 630, L113

Klebesadel, R. W., Strong, I. B. & Olson, R. A. 1973, ApJ, 182, L85

Klose, S., Greiner, J., Rau, A., et al. 2004, AJ, 128, 1942

Klotz, A., Boer, M., & Atteia, J.-L. 2003, A&A, 404, 815

Klotz, A., Boër, M., Atteia, J. L., Stratta, G., Behrend, R., Malacrino, F., & Damerdji, Y. 2005, A&A, 439, L35

Kouveliotou, C., Meegan, C. A., Fishman, G. J., et al. 1993, ApJ, 413, 101

Kouveliotou, C., Woosley, S. E. Patel, S. K., et al. 2004, ApJ, 608, 872

Kulkarni, S. R., Frail, D. A., Wieringa, M. H., et al. 1998, Nature, 395, 663

Lamb, D. Q., Ricker, G. R., Atteja, J.-L., et al. 2003, procs. of Gamma-Ray Bursts in the Afterglow Era - Thirs Workshop

Lamb, D. Q., Donaghy, T. Q., & Graziani, C. 2004, NewA Rev., 48, 423

La Parola, V., Mangano, V., Fox, D., et al. 2006, A&A, 454, 753

Lazzati, D., Ramirez-Ruiz, E., & Ghisellini, G. 2001, A&A, 379, L39

Lazzati, D., Covino, S., & Ghisellini, G. 2002, MNRAS, 330, 583

Lazzati, D., Rossi, E., Covino, S., Ghisellini, G., & Malesani, D. 2002, A&A, 396, L5

Lazzati, D., & Perna, R. 2002c, MNRAS, 330, 383

Lazzati, D. 2003, A&A, 399, 913

Lazzati, D., Covino, S., Gorosabel, J., et al. 2004, A&A, 422, 121

Lazzati, D., Ghirlanda, G., & Ghisellini, G. 2005, MNRAS, 362, L8

Lee, M. G., Kim, E., Kim, S. C., et al. 1995, JKAS, 28, 31

Le Floc'h, E., Duc, P.-A., Mirabel, I. F., et al. 2003, A&A, 400, 499

Le Floc'h, E., Charmandaris, V., Forrest, W. J., Mirabel, I. F., Armus, L., & Devost, D. 2006, ApJ, 642, 636

Levan, A., Nugent, P., Fruchter, A., et al. 2005, ApJ, 624, 880

Li, W., Filippenko, A. V., Chornock, R., & Jha, S. 2003, apj, 586, L9

Liang, E. P. 1997, ApJ, 491, L15

Liang, E., & Zhang, B. 2005, ApJ, 633, 611

Liang, E., Zhang, B., & Dai, Z. G. 2006, ApJL, submitted (astro-ph/0605200)

Lipkin, Y. M., Ofek, E. O., Gal-Yam, A., et al. 2004, ApJ, 606, 381

Lithwick, Y., & Sari, R. 2001, ApJ, 555, 540

Lyutikov, M. 2006, New J. Phys., 8, 119

MacFadyen, A. I., & Woosley, S. E. 1999, ApJ, 524, 262

MacFadyen, A. I., Ramirez-Ruiz, E., & Zhang, W. 2005, astro-ph/0510192

Maeda, K., Nakamura, T., Nomoto, K., Mazzali, P. A., Patat, F., & Hachisu, I. 2002, ApJ, 565, 405

Maeda, K., Mazzali, P. A., & Nomoto, K. 2006, ApJ, 645, 1331

Malesani, D., Tagliaferri, G., Chincarini, G., et al. 2004, ApJ, 609, L5

Mangano, V., Holland, S. T., et al. 2006, to be submitted

Mannucci, F., Maiolino, R., Cresci, G., et al. 2003, A&A, 401, 519

Margutti, R., Chincarini, G., & Fugazza, D. 2006, procs. of *Swift* and GRBs: Unveiling the relativistic Universe

Markwardt, C., Barthelmy, S., Barbier, L., et al. 2005, GCN Circ. 3143

Mazzali, P. A., & Lucy, L. B. 1993, A&A, 279, 447

Mazzali, P. A., Deng, J., Maeda, K., et al. 2002, ApJ, 572, L61

Mazzali, P. A., Maeda, K., Kawabata, K., et al. 2005, Science, 308, 1284

Mazzali, P. A., Deng, J., Pian, E., et al. 2006, ApJ, 645, 1323

McCracken, H. J., Radovich, M., Betin, E., et al. 2003, A&A, 410, 17

McEnery, E. 2002, GCN Circ. 1740

McKenzie, E. H., & Schaefer, B. E. 2000, PASP, 111, 964

Medvedev, M. V. 2000, ApJ, 540, 704

Mereghetti, S., & Götz, D. 2003a, GCN Circ. 2460

Mereghetti, S., Götz, D., Borkowski, J., Walter, R., & Pedersen, H. 2003b, A&A, 411, L291

Mészáros. P., & Rees, M. J. 1993, ApJ, 405, 278

Mészáros. P., & Rees, M. J. 1997, ApJ, 476, 232

Mészáros, P. 2006, Rep. Prog. Phys., 69, 225

Metzger, M. R., Djorgovski, S. G., Kulkarni, S. R., Steidel, C. C., Adelberger, K. L., Frail, D. A., Costa, E., & Frontera, F. 1997, Nature, 387, 879

Mirabal, N., Bonfield, D., & Schawinski, K. 2005, GCN Circ. 3488

Mirabal, N., Halpern, J., An, D., Thorstensen, J. R., & Terndrup, D. M. 2006, ApJ, 643, L99

Modjaz, M., Stanek, K. Z., Garnavich, P. M., et al. 2006, ApJ, 645, L21

Montanari, E., Frontera, F., Guidorzi, C., & Rapisarda, M. 2005, ApJ, 625, L17

Moretti, A., Campana, S., Lazzati, D., & Tagliaferri, G., 2003, ApJ, 588, 696

Moretti, A., Campana, S., Romano, P., et al. 2005a, GCN Circ. 3147

Moretti, A., Campana, S., Mineo, T., et al. 2005b, Proc. SPIE, 5898, 360

Moretti, A., Perri, M., Capalbi, M., et al. 2006a, A&A, 448, L9

Moretti, A., De Luca, A., Malesani, D., et al. 2006b, A&A, 451, 777

Nakar, E., Piran, T., & Granot, J. 2003, New Astr., 8, 495

Nakar, E., Gal-Yam, A., & Fox, D. W. 2006, ApJ, 650, 281

Nakar, E., Gal-Yam, A., Piran, T., & Fox, D. W. 2006, ApJ, 640, 849

Nardini, M., Ghisellini, G., Ghirlanda, G., Tavecchio, F., Firmani, C., & Lazzati, D. 2006, A&A, 451, 821

Nava, L., Ghisellini, G., Ghirlanda, G., Tavecchio, F., & Firmani, C. 2005, A&A, 450, 471

Nomoto, K., Maeda, K., Mazzali, P. A., Umeda, H., Deng, J., & Iwamoto, K. 2004, in Core Collapse of Massive Stars, ed. C. Fryer (Dordrecht: Kluwer)

Norris, J. P., Scargle, J. D., & Bonnell, J. T. 2001, in Gamma-Ray Bursts in the Afterglow Era, ed. E. Costa, F. Frontera, & J. Hjorth (Berlin: Springer), 40

Nousek, J. A., Kouveliotou, C., Grupe, D., et al. 2006, ApJ, 642, 389

Nysewander, M. C., Reichart, D. E., Park, H.-S., et al. 2006, ApJ, 651, 994

O'Brien, P. T., Willingale, R., Osborne, J., et al. 2006, ApJ, 647, 1213

Paczíński, B. 1998, ApJ, 494, L45

Panagia, N. 2003 in Supernovae and Gamma-Ray Bursters, ed. K. W. Weiler (Springer-Verlag, Berlin) 598, 113

Panaitescu, A., & Kumar, P. 2000, ApJ, 543, 66

Panaitescu, A., & Kumar, P. 2001a, ApJ, 560, L49

Panaitescu, A., Kumar, P., & Narayan, R. 2001b, ApJ, 561 L171

Panaitescu, A., Mészáros, P., Burrows, D., Nousek, J., Gehrels, N., O'Brien, P., & Willingale, R. 2006a, MNRAS, 369, 2059

Pandey, S. B., Anupama, G. C., Sagar, R., Bhattacharya, D., Castro-Tirado, A. J., Sahu, D. K., Parihar, P., & Prabhu, T. P. 2003a, A&A, 408, L21

Pandey, S. B., Anupama, G. C., Sagar, R., Bhattacharya, D., Sahu, D. K., & Pandey, J. C. 2003b, MNRAS, 340, 375

Park, H. S., Williams, G., & Barthelmy, S. 2002, GCN Circ. 1736

Parsons, A., Cummings, J., Gehrels, N., et al. 2006, GCN Circ. 5252

Pastorello A., Zampieri, L., Turatto, M., et al. 2004, MNRAS, 347, 74

Patat, F., Cappellaro, E., Danziger, J., et al. 2001, ApJ, 555, 900

Pe'er, A., Mészáros, P., & Rees, M. J. 2006, ApJ, 642, 995

Pei, Y. C. 1992, ApJ, 395, 130

Pellizza, L. J., Duc, P.-A., Le Floc'h E., & Mirabel, I. F. 2006, GCN Circ. 5270

Perna, R., & Belczyński, K. 2002, ApJ, 570, 252

Perna, R., Armitage, P. J., & Zhang, B. 2006, ApJ, 636, L29

Petrovic, J., Langer, N., Yoon, S.-C., & Heger, A. 2005, A&A, 435, 247

Pian, E., Amati, L., Antonelli, L. A., et al. 2000, ApJ, 536, 778

Pian, E., Mazzali, P. A., Masetti, N., et al. 2006, Nature, 442, 1011

Piran, T., & Shemi, A. 1993, ApJ, 403, L67

Piran, T. 1999, Phys. Rep., 314, 575

Piro, L., Amati, L., Antonelli, L. A., et al. 1998, A&A, 331, L41

Piro, L., Garmire, G., Garcia, M., et al. 2000, Science, 290, 955

Piro, L., De Pasquale, M., Soffitta, P., et al. 2005, ApJ, 623, 314

Preece, R. D., Briggs, M. S., Mallozzi, R. S., Pendleton, G. N., Paciesas, W. S. & Band, D. L. 2000, ApJS, 126, 19

Predehl, P., & Schmitt, J. H. M. M. 1995, A&A, 293, 889

Price, P. A., Kulkarni, S. R., Schmidt, B. P., et al. 2003, ApJ, 584, 931

Price, P. A., Roth, K., & Fox, D. W. 2005a, GCN Circ. 3605

Price, P. A., Jensen, B. L., Jörgensen, U. G., et al. 2005b, GCN Circ. 3612

Price, P. A., Cowie, L. L., Minezaki, T., et al. 2006, ApJ, 645, 851

Price, P. A., Berger, E. & Fox, D. B. 2006, GCN Circ. 5275

Prochaska, J. X., Chen, H. W., Hurley, K., Bloom, J. S., Graham, J. R., & Vacca, W. D. 2003, GCN Circ. 2475

Prochaska, J. X., Bloom, J. S., Chen, H.-W., et al. 2004, ApJ, 611, 200

Prochaska, J. X., Chen, H.-W., & Bloom, J. S. 2006, ApJ, 648, 95

Quimby, R. M., Rykoff, E. S., Yost, S. A., et al. 2005, ApJ, 640, 402

Ramirez-Ruiz, E., Granot, J., Kouveliotou, C., Woosley, S. E., Patel, S. K., & Mazzali, P. A. 2005, ApJ, 625, L91

Ramirez-Ruiz, E., García-Segura, G., Salmonson, J. D., & Pérez-Rendón, B. 2005b, ApJ, 631, 435

Rees, M. J., & Mészáros, P. 1994, ApJ, 430, L93

Reeves, J. N., Watson, D., Osborne, J. P., et al. 2002, Nature, 416, 512

Reichart, D. E. 1999, ApJ, 521, L111

Reichart, D. E. 2001, ApJ, 554, 643

Reichart, D. E., & Price, P. A. 2002, ApJ, 565, 174

Rhoads, J. E. 1999, ApJ, 525, 737

Richmond, M. W., Van Dyk, S. D., Ho, W., et al. 1996, AJ, 111, 327

Rigon, L., Turatto, M., Benetti, S., et al. 2003, MNRAS, 340, 191

Rol, E., & Strom, R. 2002, GCN Circ. 1777

Rol, E., Schady, P., Hunsberger, S., et al. 2005, GCN Circ. 3186

Romaniello, M., Panagia, N., Scuderi, S., & Kirshner, R. P. 2002, ApJ, 123, 915

Roming, P. W. A., Kennedy, T. E., Mason, K. O., et al. 2005a, Space Sci. Rev., 120, 95

Roming, P. W. A., Schady, P., Fox, D. B., et al. 2005b, ApJ, in press (astro-ph/0509273)

Roming, P. W. A., Vanden Berk, D., Palshin, V., et al. 2006, ApJ, 651, 985

Rossi, E., Lazzati, D., & Rees, M. J. 2002, MNRAS, 332, 945

Rykoff, E., Yost, S. A., & Swan, H. 2005a, GCN Circ. 3465

Rykoff, E., Yost, S. A., Swan, H., & Quimby, R. 2005b, GCN Circ. 3468

Sahu, K. C., Livio, M., Petro, L., et al. 1997, Nature, 387, 476

Sakamoto, T., Lamb, D. Q., Graziani, C., et al. 2004, ApJ, 602, 875

Sakamoto, T., Lamb. D. Q., Graziani, C., et al. 2005, ApJ, 629, 311

Sakamato, T., Barbier, L., Barthelmy, S. D., et al. 2006, ApJ, 636, L73

Santos-Lleo, M., & Calderon, P. 2003, GCN Circ. 2464

Sari, R., Piran, T., & Narayan, R. 1998, ApJ, 497, L17

Sari, R., Piran, T., & Halpern, J. P. 1999, ApJ, 519, L17

Sari, R., & Esin, A. A. 2001, ApJ, 548, 787

Sazonov, S. Y., Lutovinov, A. A., & Sunyaef, R. A. 2004, Nature, 430, 646

Schaefer, B. E., Gerardy, C. L., Hoflich, P., et al. 2003, ApJ, 588, 387

Schaefer, B. E., & Xiao, L. 2006, ApJL, submitted (astro-ph/0608441)

Schlegel, D. J., Finkbeiner, D. P., & Davis, M. S. 1998, ApJ, 500, 525

Schmidt, B. P., Kirshner, R. P., Leibundgut, B., Wells, L. A., Porter, A. C., Ruiz-Lapuente, P., Challis, P., & Filippenko, A. V. 1994, ApJ, 434, L19

Schmidt, M. 1999, apj, 523, L117

Schmidt, B. P., Peterson, B., & Lewis, K. 2006, GCN Circ. 5258

Šimon, V., Hudec, R., Pizzichini, G., & Masetti, N. 2001, A&A, 377, 450

Soderberg, A. M., Kulkarni, S. R., Berger, E., et al. 2004a, Nature, 430, 648

Soderberg, A. M., Frail, D. A., & Wieringa, M. H. 2004b, ApJ, 607, L13

Soderberg, A. M., Kulkarni, S. R., Fox, D. B., et al. 2005, ApJ, 627, 877

Soderberg, A. M., Kulkarni, S. R., Nakar, E., et al. 2006a, Nature, 442, 1014

Soderberg, A. M., Berger, E., Kasliwal, M., et al. 2006b, ApJ, 650, 261

Sollerman, S., Ostlin, G., Fynbo, J. P. U., Hjorth, J., Fruchter, A., & Pedersen, K. 2005, New Astr., 11, 103

Sollerman, J., Jaunsen, A. O., Fynbo, J. P. U., et al. 2006, A&A, 454, 503

Spergel, D. N., Verde, L., Peiris, H. V., et al. 2003, ApJS, 148, 175

Stanek, K. Z., Matheson, T., Garnavich, P. M., et al. 2003, ApJ, 591, L17

Stanek, K. Z., Garnavich, P. M., Nutzman, P. A., et al. 2005, ApJ, 626, L5

Stanek, K. Z., Gnedin, O. Y., Beacom, J. F., et al. 2006, ApJ, submitted (astro-ph/0604113)

Stratta, G., Fiore, F., Antonelli, L. A., Piro, L., & De Pasquale, M. 2004, ApJ, 608, 846

Stritzinger, M., Hamuy, M., Suntzeff, N. B., et al. 2002, AJ, 124, 2100

Strüder, L., Briel, U., Dennerl, K., et al. 2001, A&A, 365, L18

Tagliaferri, G., Covino, S., Fugazza, D., Chincarini, G., Malesani, D., Della Valle, M., & Stella, L. 2004, IAU Circ. 8308

Tagliaferri, G., Goad, M., Chincarini, G., et al. 2005a, Nature, 436, 985

Tagliaferri, G., Antonelli, L. A., Chincarini, G., et al. 2005b, A&A, 443, L1

Tagliaferri, G., Malesani, D., Vergani, S., et al. 2006, procs. of *Swift* and GRBs: Unveiling the relativistic Universe

Tanvir, N., Barnard, V. E.., Blain, A. W., et al. 2004, MNRAS, 352, 1073

Tanvir, N., Chapman, R., Levan, A., & Priddey, R. 2005, Nature, 438, 991

Taylor, G. B., Frail, D. A., Berger, E., & Kulkarni, S. R. 2004, ApJ, 609, L1

Testa, V., Fugazza, D., Della Valle, M., et al. 2003, GCN Circ. 1821

Thomsen, B., Hjorth, J., Watson, D., et al. 2004, A&A, 419, L21

Thóne, C., Fynbo, J. P. U., Jensen, B. L., Hjorth, J., Xu, D., Joergensen, U. G., & Woller, K. 2006, GCN Circ. 5272

Tominaga, N., Deng, J., Mazzali, P. A., Maeda, K., Nomoto, K., Pian, E., Hjorth, J., & Fynbo, J. P. U. 2004, ApJ, 612, L105

Tristram, P., Jelínek, M., de Ugarte-Postigo, A., et al. 2005, GCN Circ. 3151

Tueller, J., Antonelli, L. A., Barthelmy, S., et al. 2005, GCN Circ. 3005

Turatto, M., Benetti. S., Cappellaro, E., et al. 1996, MNRAS, 283, 1

Turner, M. J. L., Abbey, A., Arnaud, M., et al. 2005, A&A, 365, L27

Usov, V. V. 1992, Nature, 357, 472

Vanderspek, R., Sakamoto, T., Barraud, C., et al. 2004, ApJ, 617, 1251

van Paradijs, J., Groot, P. J., Galama, T., et al. 1997, Nature, 386, 686

van Paradijs, J., Kouveliotou, C., & Wijers, R. A. M. J. 2000, ARA&A, 38, 379

Vaughan, S., Willingale, R., O'Brien, P. T., et al. 2004, ApJ, 603, L5

Vaughan, S., Goad, M. R., Beardmore, A. P., et al. 2006, ApJ, 638, 920

Vestrand, W. T., Woźniak, P. R., Wren, J. A., et al. 2005, Nature, 435, 178

Vetere, L., Massaro, E., Costa, E., Soffitta, P., & Ventura, G. 2006, A&A, 447, 499

Vietri, M., & Stella, L. 1998, ApJ, 507, L45

Vietri, M., Ghisellini, G., Lazzati, D., Fiore, F., & Stella, L. 2001, ApJ, 550, L43

Villasenor, J., Lamb, D. Q., Ricker, G. R., et al. 2005, Nature, 437, 855

Vreeswijk, P. M., Smette, A., Fruchter, A. S., et al. 2006, A&A, 446, 145

Wang, L., & Wheeler, J. C. 1998, ApJ, 504, L87

Wang, L., Baade, D., Höflich, P., & Wheeler, J. C. 2003, ApJ, 592, 457

Watson, D., Vaughan, S., Willingale, R., et al. 2004, ApJ, 605, L97

Watson, D., Fynbo, J. P. U., Ledoux, C., et al. 2006a, ApJ, in press (astro-ph/0510368)

Watson, D., Reeves, J. N., Hjorth, J., et al. 2006b, ApJ, 637, L69

Watson, D., Hjorth, J., Jakobsson, P., Xu, D., Fynbo, J. P. U., Sollerman, J., Thone, C. C., & Pedersen, K. 2006c, A&A, 454, L123

Waxman, E., & Draine, B. T. 2000, ApJ, 537, 796

Wijers, R. A. M. J., Vreeswijk, P. M., Galama, T. J., et al. 1999, ApJ, 523, L33

Woosley, S. E. 1993, ApJ, 405, 273

Woosley, S. E., Eastman, R. G., & Schmidt, B. P. 1998, ApJ, 516, 788

Woosley, S.E., Zhang, W. & Heger, A. 2003, in Gamma-Ray Burst and Afterglow Astronomy 2001: A Workshop Celebrating the First Year of the HETE Mission, eds G. R. Ricker & R. Vanderspek, 662, 185 (AIP, New York)

Woosley, S., & Bloom., J. S. 2006, ARA&A, in press

Woosley, S., & Heger, A. 2006, ApJ, 637, 914

Woźniak, P., Vestrand, W. T., Starr, D., et al. 2002, GCN Circ. 1757

Yamazaki, R., Yonetoku, D., & Nakamaura, T. 2003, ApJ, 594, L79

Yoon, S.-C., & Langer, N. 2005, A&A, 443, 643

Yoshii, Y., Tomita, H., Kobayashi, Y., et al. 2003, ApJ, 592, 467

Yost, S. A., Harrison, F. A., Sari, R., & Frail, D. A. 2003, ApJ, 597, 459

Zeh, A., Klose, S., & Hartmann, D. H. 2004, ApJ, 609, 952

Zeh, A., Klose, S., & Hartmann, D. H. 2005, procs. of the 22nd Texas Symposium on Relativistic Astrophysics

Zerbi, F. M., Chincarini, G., Covino, S., et al. 2003, GCN Circ. 2471

Zhang, B., & Mészáros, P. 2004, Int. Journ. Mod. Phys. A, 15, 2385

Zhang, B., & Kobayashi, S. 2005, ApJ, 628, 315

Zhang, B., Fan, Y. Z., Dyks, J., Kobayashi, S., Mészáros, P. Burrows, D. N., Nousek, J. A., & Gehrels, N. 2006, ApJ, 642, 354